

AN ABSTRACT OF THE DISSERTATION OF

Alison C. Iles for the degree of Doctor of Philosophy in Zoology presented on November 7, 2012.

Title: Bridging environmental physiology and theoretical ecology in climate change research: Temperature effects on species interactions and community structure

Abstract approved:

Bruce A. Menge

Most climate change predictions focus on the response of individual species to changing local conditions and ignore species interactions, largely due to the lack of a sound theoretical foundation for how to incorporate species interactions into climate change models. Much of the variability in species interaction strengths may be governed by fundamental constraints on physiological rates, possibly providing a framework for including species interactions into climate change models. Metabolic rates, ingestion rates and many other physiological rates are relatively predictable from body size and body temperature due to constraints imposed by the physical and chemical laws that govern fluid dynamics and the kinetics of biochemical reaction times. My dissertation assesses the usefulness of this framework by bridging the fields of environmental physiology and theoretical ecology and exploring the community-level consequences of physiological constraints.

In Chapter 2, I incorporated temperature and body size scaling into the biological rate parameters of a series of realistically structured trophic network models. The relative magnitude of the temperature scaling parameters affecting consumer energetic costs (metabolic rates) and energetic gains (ingestion rates) determined how consumer energetic efficiency changed with temperature. I systematically changed consumer energetic efficiency and examined the sensitivity of network stability and species

persistence to various temperatures. I found that a species' probability of extinction depended primarily on the effects of organismal physiology (body size and energetic efficiency with respect to temperature) and secondarily on the effects of local food web structure (trophic level and consumer generality). This suggests that physiology is highly influential on the structure and dynamics of ecological communities.

If consumer energetic efficiency declined with temperature, that is, energetic costs increased faster with temperature than energetic gains, the simulated networks had greater stability at lower temperatures. The opposite scenario resulted in greater stability at higher temperatures. This inverted response formed the research question for Chapter 3: How does consumer energetic efficiency change with temperature? Existing evidence was scarce but suggestive of decreasing consumer energetic efficiency with increasing temperature. I tested this hypothesis on seven rocky intertidal invertebrate species by measuring the relative temperature scaling of their metabolic and ingestion rates as well as consumer interaction strength under lab conditions. Energetic efficiencies of these rocky intertidal invertebrates declined and species interaction strengths tended to increase with temperature. Thus, in the rocky intertidal, the mechanistic effect of temperature would lower community stability at higher temperatures.

Chapter 4 tests if the mechanistic effect of temperature on ingestion rates and species interaction strengths seen in the lab is apparent under field conditions. Bruce Menge and I related bio-mimetic estimates of body temperatures to estimates of *per capita* mussel ingestion rates and species interaction strengths by the ochre sea star *Pisaster ochraceus*, a keystone predator of the rocky intertidal. We found a strong, positive effect of body temperature on both *per capita* ingestion rates and interaction strengths; however, the effects of season and the unique way in which *P. ochraceus* regulates body temperatures were also apparent, leaving room for adaptation and acclimation to partially compensate for the mechanistic constraint of body temperature.

Community structure of the rocky intertidal is associated with environmental forcing due to upwelling, which delivers cold, nutrient rich water to the near shore environment. As upwelling is driven by large-scale atmospheric pressure gradients, climate change has the potential to affect a wide range of significant ecological processes through changes in water temperature. In Chapter 5, my coauthors and I identified long-

term trends in the phenology of upwelling events that are consistent with climate change predictions: upwelling events are becoming stronger and longer. As expected, longer upwelling events were related to lower average water temperatures in the rocky intertidal. Furthermore, recruitment rates of barnacles and mussels were associated with the phenology of upwelling events. Thus climate change is altering the mode and the tempo of environmental forcing in nearshore ecosystems, with ramifications for community structure and function.

Ongoing, long-term changes in environmental forcing in rocky intertidal ecosystems provide an opportunity to understand how temperature shapes community structure and what the ramifications of climate change are. My dissertation research demonstrates that the effect of temperature on organismal performance is an important force structuring ecological communities and has potential as a tractable framework for predicting the community level effects of climate change.

© Copyright by Alison C. Iles
November 7, 2012
All Rights Reserved

Bridging environmental physiology and theoretical ecology in climate change research:
Temperature effects on species interactions and community structure

by
Alison C. Iles

A DISSERTATION

submitted to
Oregon State University

in partial fulfillment of
the requirements for the
degree of

Doctor of Philosophy

Presented November 7, 2012
Commencement June 2013

Doctor of Philosophy dissertation of Alison C. Iles presented on November 7, 2012.

APPROVED:

Major Professor, representing Zoology

Chair of the Department of Zoology

Dean of the Graduate School

I understand that my dissertation will become part of the permanent collection of Oregon State University libraries. My signature below authorizes release of my dissertation to any reader upon request.

Alison C. Iles, Author

ACKNOWLEDGEMENTS

My mentor and advisor, Bruce Menge, has been nothing but supportive and enthusiastic as I navigated my way through grad school. I'm extremely grateful for his willingness to let me chase after whatever ideas I had brewing, his patience with my ever changing research "plans", and his understanding when life happens. Bruce is an always available, bottomless resource of intertidal natural history and ecological knowledge, with a passion for research that is inspiring. I hope to be a student of his for many years to come. Thanks also to Jane Lubchenco for helping to get me started and for making me so proud and heartened by her hard work and perseverance in D.C.

Many thanks for the guidance of my committee members, especially Eric Berlow, whose imagination and creativity always keeps me thinking; Sally Hacker for her thoughtful words of advice; Dave Lytle for his valuable perspective on my work; Jessica Miller for her advice in experimental design in the cold rooms at the Hatfield Marine Science Center (HMSC); and to Elizabeth Borer for helping to get my adventures in modeling off the ground.

My graduate studies were largely supported by teaching assistantships from the Department of Zoology. I am very grateful for the Zoology department faculty and staff; particularly Tara Bevandich, Torri Givigliano, Traci Durrell-Khalife, Sally Hacker and Mike Blouin, for helping me navigate the paper work and deal with the graduate school on countless occasions. I was also supported through generous research assistantships from Bruce, a post-graduate scholarship from the National Science and Engineering Research Council of Canada, two research grants from the Zoology graduate student research funds, a Mamie Markham award from HMSC, discretionary research funds provided by Bruce and Jane, and travel and lodging awards to attend courses organized by the Partnership for Interdisciplinary Studies of Coastal Oceans (PISCO), a long-term ecological consortium which is partially funded by the David and Lucile Packard Foundation and the Gordon and Betty Moore Foundation.

A huge part of graduate school for me is the friendship and support from fellow grads, particularly my academic siblings: Margot Hessing-Lewis, Dafne Eerkes-Medrano, office mates Sarah Close and Joe Tyburczy, Jeremy Rose, Luis Vinuezza,

Davon Callander, and the current life of the lab: Allie Barner, Liz Cerny-Chipman, Chenchen Shen, and Jessie Reimer. I am also grateful for my friendships with grads from other labs: Phoebe Zarnetske, Jay Zarnetske, Kate Boersma, Paul Bradley, Lindsay Biga, Mike Bogan, Orissa Moulton, Elise Vaccaro, Julia Buck, Angela Brandt, Catherine Searle, and many, many others.

Thanks to all Lubmenges over the last five years. Much appreciation goes to Tarik Gouhier, who taught me a lot and has always been encouraging; Jerod Sapp and Mike Frenock for generously querying the PISCO databases for me; my Work Study students, Melissa Prechtl and Kyle Jones, for processing the bulk of my field samples; Cindy Kent and Kathleen Norris for keeping my paperwork in line; Kirsten Grorud-Colvert to whom I will be forever grateful for that lamb costume, so cute; and the many lab techs (a.k.a. dudes) for putting up with this stude and helping me figure out so many random but necessary things: Kim Page-Albins, Ruth Milston-Clements, Lindsay Hunter, Camryn Pennington, Angela Johnson, Megan Poole, Erin Richmond, Mae Nobel, Becky Focht, Jonathan Robinson, and Ryan Craig.

My work benefitted a great deal from the generous assistance of many other people, including Uli Brose for help with the ATN model, Brian Helmuth's lab for help developing the bio-mimetic temperature loggers, HMSC staff for help building the system of space buckets, and Dave Schiel's lab at the University of Canterbury for help navigating New Zealand's import/export protocols.

Finally, I am grateful for my friends and family for keeping me grounded and filling my life with love and joy. I dedicate my dissertation to James, Eleanor and the bump. Thank you, James, for all the things you do for me and Eleanor. I don't know where I would be without you, but definitely not defending my dissertation because there is no way this could happen without you!

CONTRIBUTION OF AUTHORS

Dr. Bruce A. Menge provided the predation rate data, the intertidal recruitment data and the temperature data analyzed in Chapters 4 and 5 and contributed to the interpretation of these analyses. Tarik C. Gouhier contributed the wavelet analyses, including all of Appendices C and D, and the analysis of upwelling event percentiles of Chapter 5. Julia S. Stewart, Alison J. Haupt and Margaret C. Lynch assisted with the initial conceptual development, exploratory analyses and writing of Chapter 5.

TABLE OF CONTENTS

	<u>Page</u>
CHAPTER 1: General Introduction	1
CHAPTER 2: Effects of Temperature on Community and Population Stability in Allometric Trophic Network Models.....	7
2.1 Introduction	8
2.2 Methods	10
2.2.1 ATN model overview	10
2.2.2 Food web structure	10
2.2.3 Trophic levels and body masses	11
2.2.4 Allometric and temperature scaled consumer-resource dynamics	12
2.2.5 Producer-nutrient model	14
2.2.6 ATN Model evaluation	15
2.2.7 ATN Model simulations	16
2.2.8 Statistical analyses	17
2.3 Results	17
2.4 Discussion	19
2.4.1 Conclusions	24
CHAPTER 3: Temperature Effects on the Energetic Efficiency and Species Interaction Strength of Rocky Intertidal Invertebrate Consumers	32
3.1 Introduction	32
3.2 Methods	35
3.2.1 Metabolic rate trials	35
3.2.2 Ingestion rate trials	36
3.2.3 Statistical analyses	38
3.3 Results	40
3.4 Discussion	41
3.4.1 Conclusions	44
CHAPTER 4: A Field Test of the Mechanistic Effect of Body Temperature on Species Interaction Strength.....	57
4.1 Introduction	58
4.2 Methods	60

TABLE OF CONTENTS (continued)

	<u>Page</u>
4.2.1 Field data	60
4.2.2 Calculations	62
4.2.3 Statistical analyses.....	63
4.3 Results	64
4.4 Discussion	65
CHAPTER 5: Climate-Driven Trends and Ecological Implications of Event-Scale Upwelling in the California Current System	72
5.1 Introduction	73
5.2 Methods	78
5.2.1 Regional upwelling index dataset.....	78
5.2.2 Trends in the annual number, duration and magnitude of upwelling events	78
5.2.3 Trends in the intra-annual distribution of event duration and magnitude	79
5.2.4 Determining the temporal trends in the raw upwelling time series.....	80
5.2.5 Intertidal water conditions in response to upwelling events.....	80
5.2.6 Response of intertidal ecosystem productivity to upwelling.....	82
5.2.7 Effects of upwelling events on recruitment to the intertidal	82
5.3 Results	84
5.3.1 Trends in the annual number, duration and magnitude of upwelling events	84
5.3.2 Trends in the intra-annual distribution of event duration and magnitude	84
5.3.3 Intertidal water conditions in response to upwelling events.....	85
5.3.4 Effects of upwelling events on recruitment to the intertidal	86
5.4 Discussion	87
5.4.1 Temporal trends and climate change hypotheses	88
5.4.2 Intertidal water temperature response to upwelling conditions.....	88
5.4.3 Effects of upwelling events on recruitment	90
5.4.4 Broader impacts	92
CHAPTER 6: General Conclusion	103
Bibliography	106
APPENDICES	117

LIST OF FIGURES

<u>Figure</u>	<u>Page</u>
2.1 Sensitivity of time window for evaluating population stability.....	26
2.2 Average web robustness and intrinsic population stability.....	27
2.3 Interactive effect of CTI, temperature, body mass and trophic level on a species probability of extinction.....	28
2.4 Effect of consumer generality of probability of extinction.....	29
2.5 Effect of consumer Hill exponent on probability of extinction	30
2.6 Relative contribution of variables and model terms to the model of a species probability of extinction.....	31
3.1 Metabolic rates as a function of water temperature and body mass	51
3.2 Ingestion rates as a function of water temperature and body mass.....	53
3.3 Interaction strength as a function of water temperature and body mass.....	55
4.1 <i>P. ochraceus</i> body mass distributions.....	71
5.1 Map of the study region	95
5.2 Temporal trends in the intra-annual distribution of upwelling event durations.....	96
5.3 The effect of daily upwelling conditions on daily rocky intertidal water temperatures	98
5.4 Pairwise wavelet coherence analysis of daily upwelling and temperature	99
5.5 Correlation analyses of barnacle and mussel recruitment with upwelling event conditions.....	101

LIST OF TABLES

<u>Table</u>	<u>Page</u>
3.1 Intertidal consumer ingestion rate experimental trials.....	46
3.2 UTD models for lab measurements of metabolic rate, ingestion rate and species interaction strength,.....	47
3.3 Optimal models for lab measurements of metabolic rate, ingestion rate and species interaction strength.....	49
3.4 Consumer thermal impact estimates	50
4.1 UTD models for field measurements of <i>P. ochraceus</i> ingestion rate and species interaction strength.....	69
4.1 Optimal models for field measurements of <i>P. ochraceus</i> ingestion rate and species interaction strength.....	70
5.1 Temporal Trends in Upwelling Events	94

LIST OF APPENDICES

<u>Appendix</u>	<u>Page</u>
Appendix A – An evaluation of the temperature scaling equations of Chapter 2	118
Appendix B – Robust linear regression analysis for the estimation of the coefficients of the UTD models from Chapter 3	121
Appendix C – Wavelet analysis tutorial	132
Background	132
Wavelet theory	134
Bivariate extensions of wavelet analysis.....	139
An example of wavelet analysis.....	143
Appendix D – Wavelet analysis of temporal trends in upwelling and temperature along the California Current system	153
Appendix E – Temporal trends in the annual mean and intra-annual distribution of upwelling events along the California Current system	167
Sensitivity analysis of annual temporal trends in upwelling events.....	167
Temporal trends in the intra-annual distribution of upwelling events	169
Appendix F – Chlorophyll-a and nutrient analysis	183

LIST OF APPENDIX FIGURES

<u>Figure</u>	<u>Page</u>
B1 Metabolic rates as a function of water temperature and body mass.....	126
B2 Ingestion rates as a function of water temperature and body mass	128
B3 Interaction strength as a function of water temperature and body mass	130
C1 Analysis of time series with classical power spectrum methods and wavelets.....	145
C2 The effect of scale on wavelet analyses	147
C3 Wavelet analysis example	149
C4 Examples of pairwise cross-wavelet and wavelet coherence analyses	151
D1 Wavelet analysis of 6-hour upwelling time series	157
D2 Temporal trends in scale-averaged wavelet power	159
D3 Wavelet analysis of daily intertidal temperature time series	161
D4 Pairwise cross-wavelet analysis of daily upwelling and temperature time series....	163
D5 Scale-averaged wavelet power for daily upwelling and temperature time series	165
E1 Minimum duration effect on trends in the number of upwelling events	171
E2 Minimum duration effect on trends in the mean duration of upwelling events	173
E3 Minimum duration effect on trends in the mean magnitude of upwelling	175
E4 Minimum duration effect on trends in the total magnitude of upwelling.....	177
E5 Trends in the intra-annual distribution of upwelling event mean magnitude.....	179
E6 Trends in the intra-annual distribution of upwelling event total magnitude	181
F1 Upwelling event frequency and duration of local chlorophyll-a and nutrient levels	183

LIST OF APPENDIX TABLES

<u>Table</u>	<u>Page</u>
A1 Coefficients for the mass-specific metabolic and ingestion rate UTD models.....	120
B1 Coefficients for the metabolic and ingestion rate UTD models.....	123
B2 Consumer thermal impact estimates	125

DEDICATION

To my growing family: James, Eleanor and the bump.

Bridging environmental physiology and theoretical ecology in climate change research: Temperature effects on species interactions and community structure

CHAPTER 1: General Introduction

Earth's average surface temperature is currently increasing at 0.2 °C per decade with the rate of warming projected to increase, resulting in a 2-4 °C rise over the next century (IPCC 2007). Extensive and consistent evidence shows that climate change effects already permeate many aspects of terrestrial and aquatic ecological communities, causing shifts in species ranges, phenology, morphology, reproduction, population sizes, and extinction risks (reviewed in Walther *et al.* 2002; Parmesan 2006; IPCC 2007). The scope of the majority of these studies is at the species-level and most climate change predictions also focus on the response of individual species to changing local conditions. This approach has been repeatedly criticized for considering species in isolation and ignoring species interactions, which can have striking consequences for species abundances (Davis *et al.* 1998a; Davis *et al.* 1998b; Tylianakis *et al.* 2008; Gilman *et al.* 2010; Walther 2010; Woodward *et al.* 2010; Zarnetske *et al.* 2012). Experimental manipulations in which entire communities were slowly warmed suggest that community-level effects of temperature have strong influences on population dynamics, population persistence and ecosystem functioning. In these systems, communities became less stable at higher temperatures and differential survival of trophic levels altered the balance between producers and consumers (Petchey *et al.* 1999; Voigt *et al.* 2003; Hawkins *et al.* 2009; Beveridge *et al.* 2010a; Beveridge *et al.* 2010b).

Understandably, the reason why species interactions have been ignored comes from the fact that ecological networks are complex, with hundreds of species interacting in many different ways (Walther *et al.* 2002), and from the lack of a strong, tested theoretical foundation for incorporating the myriad of species interactions into climate change models (Gilman *et al.* 2010). However, a great deal of the variability in community structure and dynamics may be governed by relatively predictable

bioenergetic constraints affecting the strength of species interactions and the flows of energy through food webs (Berlow *et al.* 2009; Woodward *et al.* 2010). Many physiological rates are predictable from body size and body temperature due to constraints imposed by the physical and chemical laws that govern rates of resource uptake and distribution and the kinetics of biochemical reaction times. Examples include body size and temperature effects on metabolism (Gillooly *et al.* 2001), larval development (O'Connor *et al.* 2007), autotroph production and respiration (Lopez-Urrutia *et al.* 2006), and many more (see reviews by Dell *et al.* 2011; Somero 2011). Community-level processes, including ingestion rates and the *per capita* strength of species interactions, are the end result of a series of physiological processes occurring at the organismal-level (Woodward *et al.* 2010). These include foraging activity levels, prey handling times and digestion rates, all of which are influenced by temperature and body size (Sanford 1999, 2002a, b; Yee & Murray 2004; Pincebourde *et al.* 2008a, b; Yamane & Gilman 2009; Rall *et al.* 2010; Englund *et al.* 2011; Vucic-Pestic *et al.* 2011). If bioenergetic constraints account for a large amount of the variation in species interaction strength, then they could form the basis of a simplified framework for including species interactions in climate change models based solely on body size and body temperature information (Berlow *et al.* 2009; Woodward *et al.* 2010). However, the community-level influences of these bioenergetic constraints are only starting to be explored.

My dissertation bridges the fields of environmental physiology and theoretical ecology by exploring the community-level consequences of bioenergetic constraints on species interactions due to body size and temperature. I initially used dynamic modeling of food webs to explore how these bioenergetic constraints might manifest at the community level (Chapter 2). Here I incorporated temperature and body size scaling into the biological rate parameters (including metabolic rate, ingestion rate and autotroph production rate) of a series of realistically structured trophic networks of 30 interacting species. For each network, I systematically changed the ambient temperature of the model and the temperature scaling parameters affecting consumer metabolic rate and ingestion rate and analyzed effects at the species level and at the network level.

At the species level, I used statistical models to characterize a species' probability of extinction as a function of several species attributes, such as energetic efficiency, body mass, trophic level, vulnerability (the number of consumers), generality (the number of resources), Hill exponent (the shape of the functional response), and predator interference coefficient (the degree to which individuals of that species interfere with each other's consumption activities). The results indicate that the relative effects of physiology (body size and energetic efficiency) are more important than the effect of local food web structure (trophic level and generality) and both of these were overwhelmingly more influential than the random effects of the network structure. Thus, the bioenergetic effects of body size and temperature were highly influential on species persistence; however, local community structure also influenced the effect that temperature had by either limiting the flow of energy up the food web and imposing additional energetic constraints on higher trophic species, or by mitigating the negative effects of temperature with stabilizing species interactions.

At the network level, the relative scaling of consumer metabolic rates (energetic losses) and ingestion rates (energetic gains) determined whether consumer energetic efficiencies would increase or decrease with temperature, which had implications for the stability of the network. If consumer energetic efficiency declined with temperature (the consumer's energetic costs increased faster with temperature than its energetic gains), then the community was more stable at lower ambient temperatures. If ambient temperatures were increased, then more species would go extinct and average community stability would decline. The opposite scenario of increasing consumer energetic efficiency with temperature resulted in greater average community stability at higher temperatures.

This inverted response begs the question: How does consumer energetic efficiency change with temperature? Existing measurements of the relative temperature scaling of metabolic and ingestion rates have only been published from one forest floor invertebrate community of spiders and beetles, in which consumer energetic efficiencies decline with temperature (Rall *et al.* 2010; Vucic-Pestic *et al.* 2011). Thus, according to

the model results of Chapter 2, the community level consequences of warming in this forest floor community would be a loss of species from the system. A loss of species at warmer temperatures has also been observed in freshwater microcosm communities of bacteria and protists and grassland mesocosms communities of invertebrates that have been experimentally warmed (Petchey *et al.* 1999; Voigt *et al.* 2003; Beveridge *et al.* 2010a; Beveridge *et al.* 2010b), suggesting that other ecological communities may also have species whose energetic efficiencies decline with temperature.

In Chapter 3, I tested this prediction on a suite of species from Oregon's rocky intertidal invertebrate community. The rocky intertidal is an ideal system to test bioenergetic constraints on community structure and dynamics because all the species are ectotherms, they are easily accessible and manipulated at low tide and are relatively easy to maintain in a lab environment. I measured the relative temperature and body size scaling of metabolic rates (using oxygen consumption as a proxy) and ingestion rates of preferred prey under controlled lab conditions. The results show that consumer basal metabolic rates (energetic costs) were more sensitive to temperature than ingestion rates (energetic gains). As predicted from the model results of Chapter 2, and in concordance with measurements on terrestrial invertebrates, rocky intertidal invertebrates exhibited declining energetic efficiency with temperature.

Many exothermic species have the capacity to compensate for these bioenergetic constraints by behaviorally adapting to abiotic conditions. If such idiosyncratic mechanisms are strong, they would limit the usefulness of general constraints for predicting the community-level effects of climate change. In Chapter 4, Bruce A. Menge and I used long term predation rate data to test if the bioenergetic effects of temperature and body size observed in the lab are apparent under field conditions. We related field measurements of *per capita* mussel predation rates by several populations of the ochre sea star *Pisaster ochraceus*, a keystone predator of the rocky intertidal, to temperature and body size. We used two different estimates of temperature: mean daily water temperatures and a bio-mimetic estimate of *P. ochraceus* body temperatures. Whereas mean daily water temperature is only an accurate estimate of *P. ochraceus* body

temperature at high tide, the bio-mimetic temperature logger approximates both high and low tide body temperatures. The results supported the mechanistic effect of body temperature on *per capita* ingestion rates and species interaction strengths. However, seasonal effects and the effects of the unique method in which *P. ochraceus* regulates its body temperature were also apparent, leaving some room for adaptation and acclimation to compensate for this bioenergetic constraint.

Another reason why the rocky intertidal is an ideal system for testing the usefulness of this simplified, bioenergetic framework for including species interactions into climate changes models is because the community structure has been repeatedly associated with environmental forcing due to upwelling (Menge & Olson 1990; Menge *et al.* 1997a; Menge *et al.* 1997b; Menge *et al.* 2003; Menge *et al.* 2011b). Upwelling is the main factor driving water temperatures by delivering deep, cold, nutrient rich water to the nearshore environment (Huyer 1983). As upwelling is driven by large-scale atmospheric pressure gradients, climate change has the potential to affect a wide range of significant ecological processes through changes in water temperature. Chapter 5 (Iles *et al.* 2012) examines how the upwelling regime has changed over the last half century in relation to climate change predictions and how these changes may influence the community structure of the rocky intertidal. My coauthors and I identified long-term trends in the frequency, duration, and strength of upwelling events and related the trends to water temperature and mussel and barnacle recruitment rates. Our results showed that upwelling events have become less frequent, stronger, and longer in duration, changes which are consistent with climate change predictions (Bakun 1990; Bakun *et al.* 2010). As expected, longer upwelling events were related to lower average water temperatures in the rocky intertidal. However, upwelled water is not only low in temperature, but is also high in nutrients and low in dissolved oxygen, which contributes to the hypoxia observed along the Oregon coast over the last ten years (Grantham *et al.* 2004; Chan *et al.* 2008). Furthermore, these upwelled waters are high in dissolved carbon dioxide and low in pH, which is physiologically stressful for the many intertidal species with carbonate body parts (Feely *et al.* 2008). Thus climate change is altering the mode and

the tempo of environmental forcing in nearshore upwelling ecosystems in many ways beyond temperature effects, with potentially severe and discontinuous ramifications for ecosystem structure and function.

My dissertation research demonstrates that the mechanistic effect of body temperature and body size on organismal performance is an important force structuring ecological communities and may be a useful generalization for modeling the community level effects of climate change. My results largely provide support for the influence of temperature as a dominant abiotic force structuring ecological communities, including 1) that a suite of species from the same environment exhibited a similar change in energetic efficiencies with changing temperature, 2) that the effects of body temperature on ingestion rates and species interactions strengths were apparent from field data, and 3) that organismal-level attributes, including how a species energetic efficiency scaled with body size, accounted for most of the variability in simulated community data. This view of how environmental forcing influences community structure through bioenergetics has potential as a baseline model for predicting community level effects of climate change.

CHAPTER 2: Effects of Temperature on Community and Population Stability in Allometric Trophic Network Models

ABSTRACT

Most research on the effects of climate change focuses on individual species rather than entire community assemblages due to the complex structure and chaotic dynamics of communities. Here I explore how bioenergetic effects of temperature at the organismal level manifest at the community level when embedded in simulations of trophic species interaction networks. I show that despite the random structures of the species interaction networks and the chaotic nature of the simulations, the results are consistent with expectations from first principles and previous work on model systems of only two interacting species. I incorporated theoretical equations for how metabolic (energetic costs) and ingestion (energetic gains) rates scale with temperature and body size into dynamic models of 500 realistic 30-species networks. By systematically changing ambient temperatures, and the parameters governing how metabolic and ingestion rates scale with temperature, I was able to characterize the effects on community stability, population stability and understand how individual species attributes affected a species probability of extinction. The relative temperature scaling of metabolic and ingestion rates reversed the effect that increasing temperatures had on network robustness and population stability. The probability of a species going ‘extinct’ depended largely on organismal-level attributes of body size and energetic efficiency at particular temperatures and secondarily on local network structure, specifically trophic level and consumer generality. The influence of the random network structure was relatively minor. The methodology used here is useful for identifying the relative influence of factors at different levels of biological organization and for setting a mechanistic baseline, upon which additional complexity can be built, towards identifying which species are likely to be vulnerable to climate change.

2.1 INTRODUCTION

Predictions of climate change effects on species abundances and distributions typically focus on individual species in isolation. However, species interactions have an important influence on species distributions, abundances and the stability of entire communities and thus should not be ignored (Tylianakis *et al.* 2008; Araujo *et al.* 2011; Urban *et al.* 2011). The presence or absence of links between species determines the structure of community networks and the strength of these interactions influence how energy flows through the network. The structure and dynamics of these networks ultimately impacts community stability and species persistence in the face of environmental disturbance and stress (de Ruiter *et al.* 1995; McCann *et al.* 1998; Emmerson & Raffaelli 2004; Thebault & Loreau 2005; Navarrete & Berlow 2006; Rooney *et al.* 2006; Goudard & Loreau 2008). For instance, webs with higher connectance, or a greater number of interactions between species, have greater stability and lower probabilities of secondary extinctions (Dunne *et al.* 2002). The challenge is now to develop a strong theoretical foundation for climate influences on both species interactions and the flow of energy through communities, which will help clarify the implications of climate change for community structure and stability (Tylianakis *et al.* 2008; Gilman *et al.* 2010).

Due to the complexity of ecological networks, directly measuring the strength of species interactions is often difficult (Berlow *et al.* 2004; Wootton & Emmerson 2005). Despite this, there are constraints on the effects of environmental temperature at the physiological level that can help elucidate the important mechanisms affecting species interaction strengths and community level patterns (Berlow *et al.* 2009). Environmental temperature is often identified as the most important abiotic factor directly influencing species performance and, indirectly, the strength of species interactions. For instance, in ectotherms, the scaling of metabolic rate with temperature due to the kinetics of biochemical reactions is well established (Gillooly *et al.* 2001) and sets the baseline energetic costs per unit biomass. In fact, temperature is the most important factor dictating per unit biomass metabolic rates (Brown *et al.* 2004). Increased energetic costs

of higher temperatures are at least somewhat offset by increased ingestion rates, thus influencing the strength of consumer interactions with their resources (Vasseur & McCann 2005). These general constraints on species energetic gains and losses influence energy flow through community networks, but are only just beginning to be explored.

A consumer's energetic efficiency is defined as the ratio of energy gain through ingestion to energy lost through metabolism and represents the amount of energy available for growth and reproduction (Rall *et al.* 2010; Vucic-Pestic *et al.* 2011; Sentis *et al.* 2012). The effect of temperature on a consumer's energetic efficiency depends on the relative temperature scaling of the consumer's ingestion and metabolic rates. If consumer metabolic rates increase faster (more slowly) with temperature than ingestion rates, then energetic efficiencies decline (increase) with temperature. Of the handful of studies that have measured consumer energetic efficiency, Rall *et al.* (2010) and Vucic-Pestic *et al.* (2011) found that it decreased with temperature in several species of beetles and spiders, however Sentis *et al.* (2012) found for a ladybeetle species that it increased to an optimum and the decreased at higher temperatures.

Vasseur & McCann (2005) incorporated temperature dependency of consumer metabolism and ingestion rates into a model of a simple consumer-resource system. The general effect of temperature on the system depended on how the consumer's energetic efficiency changed with temperature, or how metabolic and ingestion rates scaled with temperature relative to one another. If the energetic efficiency of the consumer declined with warming, population stability increased (Vasseur & McCann 2005). However, greater energetic costs relative to energetic gains may increase the risk of starvation and extinction of the consumer (Rall *et al.* 2010). Alternatively, if energetic efficiency increases with warming, then the consumer has a larger impact on its prey and system stability declines (Vasseur & McCann 2005). Thus, the effects of temperature in a simple consumer-resource system depend on the parameters affecting temperature scaling of energetic costs and energetic gains.

While Vasseur and McCann (2005) modeled a system with 2 interacting species, it is unknown how this mechanism affects the structure and dynamics of entire

community networks. Here I use a network approach that incorporates temperature scaling of energetic costs and energetic gains to explore community-level consequences of environmental temperature. To do this, I incorporated the Arrhenius temperature dependence equations for metabolic and ingestion rates developed by Vasseur and McCann (2005) for a simple predator-prey system into an allometrically-scaled multi-species food web model. So-called Allometric Trophic Network (ATN) models have been useful previously for investigating community level effects of body size structure (Yodzis & Innes 1992; Brose *et al.* 2006b; Berlow *et al.* 2009). I used simulations of many random webs to visualize the consequences of differences in the temperature scaling differences of metabolic rates (energetic losses) and ingestion rates (energetic gains) along a range of ambient temperatures. The outcome of this theoretical analysis provides valuable insight into the relative influence of organismal traits versus network structure. I discuss the usefulness of such baseline, mechanistic models for predicting when and where species are likely to be vulnerable to climate change.

2.2 METHODS

2.2.1 ATN model overview

The Allometric Trophic Network (ATN) model used in these simulations was developed based on previously published models (Brose *et al.* 2006b; Berlow *et al.* 2009). The ATN model was built in a 4-step process: (1) the niche model (Williams & Martinez 2000) determines the food web structure, (2) the trophic levels and body masses of the species are then calculated based on the food web structure, (3) the parameters of the dynamic consumer-resource model are calculated based on allometric and temperature scaling relationships or are randomly parameterized, and (4) the producer-nutrient component of the model is randomly parameterized.

2.2.2 Food web structure

I used the niche model (Williams & Martinez 2000) to generate the structure of the model food webs, the properties of which compare well with empirical food webs

(Dunne *et al.* 2004; Williams & Martinez 2008). This model assumes that direct interactions between species are only trophic. The omission of other non-trophic interactions might be an over simplification, but we are just beginning to understand the network structure of non-trophic interactions (Kefi *et al.* 2012).

The niche model is based on algorithms that arrange trophic links, L , among species with species richness, S , and connectance, $C = L/S^2$, as input parameters. All species are assigned a ‘niche value’, n_i , drawn uniformly from the interval $(0, 1)$. Species i consumes all species whose niche values fall in a range, r_i , that is placed uniformly by drawing the center, c_i , of the range from the uniform interval $(r_i/2, n_i)$. The size of r_i is assigned by using a beta function to randomly draw values from the interval $(0, 1)$ whose expected value is $2C$ and then multiplying that value by n_i (whose expected value is 0.5) to match the C of the empirical web being modeled (Williams & Martinez 2000). Primary producers are those species whose feeding range does not encompass the niche value of other species, thus they do not consume other species. Only webs with at least 15% of species as primary producers were accepted. Species that were completely disconnected from the other species in the web or that were trophically identical were eliminated and replaced until the web was free of such species.

2.2.3 Trophic levels and body masses

The food web matrix created by the niche model is used to calculate species trophic levels as one plus the average trophic level of their prey, assuming that consumers feed evenly on multiple resources. Because of looping, prey trophic levels can depend on consumer trophic levels, particularly for cannibals (Williams & Martinez 2004). Thus, I followed an analysis which utilizes the theory of Markov chains and produces a continuous measure of trophic level from the food web matrix (Levine 1980).

The body masses of all basal species were set to one and the body masses of each consumer was calculated by randomly sampling predator-prey body-mass ratios, Z , from a log-normal distribution (mean=3.60, SD=3.57). This distribution matched a weighted mean and standard deviation of body-mass ratios found in natural ecosystems (Brose *et*

al. 2006a) and was consistent with previous findings that high body mass ratios stabilize complex food webs (Brose *et al.* 2006b). The body mass of each consumer, M_C , depends on its trophic level, TL , as:

$$M_C = Z_C^{TL-1} \quad (1)$$

This methodology assumes that consumer body size is constant and non-adaptive. Many species have indeterminate adult body sizes and exhibit plasticity under different conditions (e.g. Iles & Rasmussen 2005). Since the effect of body size on biochemical reaction rates is much larger than the effect of temperature, this important omission warrants further investigation but is beyond the scope of this study. The model also assumes that the body sizes of producers are all the same, which is reasonable for pelagic systems where the majority of producers are single celled phytoplankton but is inappropriate for almost every other ecosystem.

2.2.4 Allometric and temperature scaled consumer-resource dynamics

ATN models follow the bioenergetic approach of Yodzis and Innes (1992), where the change in relative, dimensionless biomass densities, B_i , of S species with respect to time, t , is described by S coupled ordinary differential equations for consumers (eqn. 2a) and primary producers (eqn. 2b).

$$B'_i(t) = \sum_{j \in R_i} x_i y_i B_i F_{ij} e_{ij} - \sum_{j \in C_i} x_j y_j B_j F_{ji} - x_i B_i \quad (2a)$$

$$B'_i(t) = r_i G_i(N) B_i - \sum_{j \in C_i} x_j y_j B_j F_{ji} - x_i B_i \quad (2b)$$

The biomass density of consumer species i (eqn. 2a) equals the energetic gains from consumption of i 's set of resource species, R_i , minus the energetic losses due to consumption from i 's set of consumer species, C_i , and energetic losses due to i 's mass and temperature-specific metabolic rate, x_i . For primary producer species (eqn. 2b), biomass density equals energetic gains due to a growth, G_i , which is a saturating function based on the most limiting nutrient (details below), minus energetic losses due to consumption from i 's set of consumer species, C_i , and due to i 's mass and temperature-specific metabolic rate, x_i . In these equations, r_i is the mass and temperature-specific maximum growth rate of the primary producers, y_i is consumer's maximum ingestion rate relative to

its metabolic rate, e_{ij} is i's assimilation efficiency when consuming species j, which was set to 0.85 for carnivores and 0.45 for herbivores (Yodzis & Innes 1992), and F_{ij} is the functional response describing the fraction of i 's maximum rate of ingestion accounted for when ingesting species j :

$$F_{ij} = \frac{\omega_{ij}B_j^h}{B_0^h + cB_iB_0^h + \sum_{k=R_i} \omega_{ik}B_k^h} \quad (3)$$

Where ω_{ij} denotes the resource preference of i for species j , B_0 is the half-saturation density, h is the Hill exponent and c quantifies predator interference. I set uniform relative ingestion rates for consumers with n resources ($\omega_{ij} = 1/n$, $B_0 = 0.5$), which assumes that consumers have no prey preference and feed on all resources according to their relative biomass. The Hill exponent, h , regulates the shape of the functional response from Holling Type II to Holling Type III. Predator interference, c , quantifies the degree to which individuals within the same species interfere with each other's consumption activities. For each consumer-resource species interaction in the food web models, I used random, normally distributed Hill exponents (mean = 1.5, SD = 0.25) and predator interference coefficient (mean = 0.5, SD = 0.25).

Following the approach of Vasseur and McCann (2005), the effect of temperature is incorporated into the dynamic ATN model through its effects on mass-specific production rates, R_P , metabolic rates, $X_{C,P}$, and ingestion rates, Y_C , of consumers, c , and producers, p , as:

$$R_P = a_{r(T_0)} M_p^{-0.25} e^{E_r(T-T_0)/kTT_0} \quad (4a)$$

$$X_{C,P} = a_{x(T_0)} M_c^{-0.25} e^{E_x(T-T_0)/kTT_0} \quad (4b)$$

$$Y_C = a_{y(T_0)} M_c^{-0.25} e^{E_y(T-T_0)/kTT_0} \quad (4c)$$

Where M_i is species i 's body size, and the intercepts of the allometric relationships ($a_{i(T_0)}$) are empirically derived constants representing the maximum sustainable rates (physiological maxima measured at temperature T_0). The effect of temperature in these equations is derived from the Arrhenius equation, where the proportion of molecules with sufficient kinetic energy to activate a reaction is expressed as the activation energy (eV),

E , divided by the temperature (K), T , and modified by the Boltzmann's constant ($k = 8.62 \cdot 10^{-5}$ eV K $^{-1}$) (Brown *et al.* 2004). Please see Appendix A for the full details of how these equations were evaluated.

The time scale of the model system is defined by setting the mass-specific growth rate of the basal populations to unity. Then, to bring the rest of the rates to the same scale, the rate of mass-specific consumer metabolism is normalized by the time scale and the mass-specific ingestion rates are normalized by the metabolic rates:

$$r_i = R_P/R_P = 1 \quad (5a)$$

$$x_i = \frac{X_{C,P}}{R_P} = \frac{a_x}{a_r} \left(\frac{M_{C,P}}{M_P} \right)^{-0.25} e^{-(E_r - E_x)(T - T_0)/kTT_0} \quad (5b)$$

$$y_i = \frac{Y_C}{X_C} = \frac{a_y}{a_x} e^{(E_y - E_x)(T - T_0)/kTT_0} \quad (5c)$$

Thus, through the temperature dependencies of metabolic rates and ingestion rates, the difference in activation energies governs the effect temperature has on a system of interacting species. In equation 5c, the difference between the activation energies of ingestion rate and metabolic rate, $E_y - E_x$, is termed the consumer thermal impact (CTI) of the system (Vasseur & McCann 2005). When CTI is negative, consumer energetic efficiency declines with temperature, when CTI is positive, consumer energetic efficiency increases with temperature. The activation energy of production rate, E_r , was set to 0.5 for all simulations based on calculations for marine and freshwater unicellular algae (Vasseur & McCann 2005). The allometric normalization constants evaluated at $T_0 = 20^\circ\text{C}$ were set to the following for all simulations: $a_r = 0.386$ (Vasseur & McCann 2005), $a_x = 0.12$ (for consumers; see Appendix A), $a_x = 0.189$ (for primary producers; Brown *et al.* 2004), and $a_y = 1.3$ (see Appendix A).

2.2.5 Producer-nutrient model

The nutrient-dependent growth rate of the primary producers, G_i , follows a well-established nutrient intake model (Tilman 1977; Brose *et al.* 2005; Brose 2008; Berlow *et al.* 2009), where growth is a saturating function of the most limiting nutrient:

$$G_i(N) = \text{MIN} \left(\frac{N_1}{K_{li} + N_1}, \frac{N_2}{K_{li} + N_2} \right) \quad (6)$$

Where MIN is the minimum operator and K_{li} is the half saturation density of primary producer i for nutrient l . The half saturation densities for both nutrients were selected for each primary producer from a uniform interval (0.1, 0.2). Producer nutrient-intake efficiencies decrease with higher half saturation densities. Thus, this term helps define the competitive hierarchy among the producers since the model assumes that all producers have the same growth rate and effectively compete for two possible limiting nutrients. The dynamic variation in the concentration of the limiting nutrient, N_l , is given by:

$$N'_l(t) = D(S_l - N_l) - \sum_{i=1}^n (c_{li}r_i G_i(N)B_i) \quad (7)$$

Where, D is the turnover rate, S_l is the supply concentration of nutrient l and removal depends on the current concentration in the system, N_l , and the total absorption rate of all the primary producers in the system multiplied by c_{li} , the content of nutrient l in the biomass of species i . In all simulations the turnover rate ($D = 0.25$) was kept constant, relative to the time scale of the producer growth rate ($r_i = 1$). The supply concentrations of both nutrients was also constant ($S_1 = S_2 = 1$), however the first nutrient was the one most in demand as it had the highest content in the biomass of the primary producers ($c_{1i} = 1$, $c_{2i} = 0.5$).

2.2.6 ATN Model evaluation

I ran several evaluations of the model to choose how long to run the simulations and over what time period to calculate community and population stability. Most extinctions occur within the first 2000 time steps, thus, I measured community stability as web robustness, or the percentage of species remaining at $t = 2,000$ (Brose *et al.* 2006b; Heckmann *et al.* 2012). Longer time series ($t = 5,000$) had the same qualitative results, except with lower overall robustness. To measure population stability, I used the coefficient of variation (CV) of species' biomass densities from $t = 50$ to 350, which measures population stability before equilibrium is reached and is akin to the non-equilibrium state of natural ecosystems (Brose *et al.* 2006b; Berlow *et al.* 2009). An analysis of 10 random webs showed that biomass densities at $t = 50$ was sufficiently

removed from initial biomass densities to be uncorrelated (p -values ranged from 0.1-0.8). The length of the time-averaged window was determined by evaluating the point at which mean biomass densities stopped changing. A window length of 300 time steps was long enough to incorporate at least a full cycle of most population fluctuations (Fig. 2.1). Numerical integration of equations 2a-b and 5 used the Runge-Kutta method with adaptive step sizes and the simulations were implemented in Matlab 7.8.0 (MathWorks R2011b).

2.2.7 ATN Model simulations

I ran two sets of simulations. The objective of the first set was to evaluate the effect of CTI on general web robustness and population stability and the second set was to evaluate how species attributes affected the probability of extinction. In the first set of simulations, I generated 100 food webs with a set species richness $S = 30$ and food web connectance $C = 0.15$. For each food web realization, I evaluated community and population stability at different activation energies for metabolic and ingestion rates, $0 \leq E \leq 1.2 \text{ eV}$ with $\Delta E = 0.3 \text{ eV}$, and temperatures from $0 \leq T \leq 30 \text{ }^{\circ}\text{C}$, $\Delta T = 3 \text{ }^{\circ}\text{C}$. The activation energy of producer production rates, E_r was set to 0.6. Initial biomass densities were selected randomly and uniformly from the interval (0.05, 1) and initial nutrient concentrations were constant ($N_1 = N_2 = 1$). Any species with a biomass density less than the extinction threshold $B_{ext} < 10^{-30}$ at the end of the simulation was considered ‘extinct’. Lower extinction thresholds produced qualitatively the same results with higher persistence.

In the second set of simulations to evaluate how species attributes affect the probability of extinction, I generated 500 food webs with the same parameter values as before except that each species was assigned its own random activation energies for metabolic and ingestion rates, $0.2 \leq E \leq 1 \text{ eV}$, resulting in a continuous range of CTI values (-0.8, 0.8). The ambient temperature of each simulation was randomly selected between 0 and 40 $^{\circ}\text{C}$. For each web realization, I recorded the web number and the ambient temperature of the simulation, and for each consumer species I recorded whether

or not it went extinct, its CTI, body mass, trophic level, vulnerability (i.e. the number of consumers it has), generality (i.e. the number of resources it has), Hill exponent (which regulates the shape of the functional response from Holling Type II to Holling Type III), and predator interference coefficient (which quantifies the degree to which individuals of that species interfere with each other's consumption activities).

2.2.8 Statistical analyses

To analyze the effects of all these variables, and many of their interactions, on a species probability of extinction, I used a generalized linear mixed model (GLMM) with a binomial distribution for the response variable (whether or not a species went extinct). I incorporated the web number as a random factor, since species from the same web depend on one another and are thus highly likely to influence each other's extinction probability. Body size was log transformed to improve the distribution and all the predictor variables were centered before analysis. Pearson's correlation coefficients were calculated for all pairs of predictor variables to check for collinearity. All correlated variables were retained in the analysis since the strongest correlation was between log body size and trophic level ($r = 0.35$).

Traditional methods to assess effect size typically use the coefficient of determination (R^2) to understand the percent of the variation in the data accounted for by a variable. However, calculating R^2 values are inappropriate for binomial regression models. However, model comparisons using the change in AICc due to the influence of a variable represents the comparative statistical contribution of a variable to model fit, or the relative information lost by removing a variable. I used AICc model comparisons of the final model to models in which each variable or interaction term was sequentially removed.

All analyses were conducted in R 2.14.1 (The R Foundation for Statistical Computing 2011) and followed statistical methods outlined in Zuur *et al.* (2009).

2.3 RESULTS

When the CTI is negative (i.e., when consumer energetic efficiency declines with temperature), increasing temperatures are destabilizing at both the community and population levels. At low temperatures, robustness is high and the coefficient of variation in population biomass densities is low (Fig. 2.2). As temperatures increase, this relatively stable system becomes more and more unstable. Population stability declines as the variability of population densities increases. As the model system becomes destabilized, mathematical extinctions occur and web robustness declines. The opposite occurs when CTI is positive (i.e. when consumer energetic efficiency increases with temperature), in which case increasing temperatures are stabilizing at both the community and population levels.

The GLMM analysis of which species attributes contribute to the probability of extinction indicated a strong 4-way interaction between CTI, temperature, body mass and trophic level (1 df, $X^2 = 114.61, p = 2.2\text{E-}16$; Table 1, Fig. 2.3). For all body masses and for all trophic levels, there was a clear and consistent interaction between CTI and temperature that mimics the pattern observed from the first round of simulations. When CTI is negative, probabilities of extinction are low at low temperatures but as temperature increases, the probability of extinction increases. The opposite occurs when CTI is positive; probabilities of extinction are high at low temperature and decrease as the temperature increases (compare subplots horizontally in Fig. 2.3). Species with smaller body masses consistently had higher probabilities of extinction than species with larger body masses under all the combinations of parameter values tested. Species with larger body masses were also not as sensitive to how CTI affected their probability of extinction (compare across colored lines in all subplots of Fig. 2.3). At higher trophic levels, the effect of body size becomes more pronounced, as the spread between small and large-bodied species widens (compare subplots vertically in Fig. 2.3). For large-bodied species (blue and purple lines in Fig. 2.3), the probability of extinction goes down as trophic level increases. However, for average and small-bodied species (green, orange and red lines in Fig. 2.3), the probability of extinction increases with trophic level.

More generalized species with greater numbers of resources to rely on exhibited a lower probability of extinction than specialized species ($1 \text{ df}, X^2 = 68.72, p < 2.2 \text{ E-16}$; Fig. 2.4). There was no effect of species vulnerability (the number of consumers a species has) on the probability of extinction and this term was dropped from the model ($1 \text{ df}, X^2 = 1.49, p = 0.22$). However, species vulnerability was negatively correlated with species generality ($r = -0.26$), thus there is minor collinearity between these variables.

For the parameters affecting each species' functional response, the Hill exponent, h , had an interactive effect with body mass on the probability of extinction ($1 \text{ df}, X^2 = 4.51, p = 0.03$; Fig. 2.5). Large-bodied consumers exhibited a greater probability of extinction with more of a type III functional response while small-bodied consumers showed a greater probability of extinction with a type II functional response. The parameter controlling the extent of predator interference within a species, c , did not have a systematic effect on species persistence and was dropped from the GLMM ($1 \text{ df}, X^2 = 2.42, p = 0.1198$).

To assess the effect size of the different variables, I used delta AICc comparisons between the final model and models where each variable (Fig. 2.6a), or each term of the model (Fig. 2.6b) was sequentially removed. The relative statistical contribution of body mass far surpassed that of temperature and CTI, which were in turn relatively more important for model fit than trophic level or generality with variability in the hill coefficient being the least influential (Fig. 2.6a). The relative statistical contribution of the statistically significant model terms (Fig. 2.6b) indicates that the main effect of body size has a greater influence than any of the interaction terms in which body size is also influential. The interaction between CTI and temperature is the next most influential term. The random effect of the web a species came from is relatively minor.

2.4 DISCUSSION

Incorporating temperature scaling into ATN models demonstrates that the influence of temperature on per unit biomass rates of metabolism and ingestion can have implications for community stability. Moreover, the relative influence of temperature

depends on species body size, energetic efficiency, and to a lesser degree, trophic level and generality. However, the relative effects of species attributes (body size, energetic efficiency) are collectively more important to the final model fit than the effects of local food web structure (trophic level, generality) and both of these are overwhelmingly more influential than the random effects of the network structure. Thus, the results are consistent with expectations from first principles and analyses of simple systems of two interacting species despite the chaotic and random network structure imposed in these analyses.

Increasing temperatures were destabilizing for simulations in which consumer energetic efficiencies decline with temperature (i.e. a negative CTI), which mimics observations of community stability from empirical studies where species were more likely to go extinct in warmed communities (Petchey *et al.* 1999; Voigt *et al.* 2003). Most lab measurements of CTI corroborate this, showing that consumer energetic efficiencies tend to decrease with temperature for various terrestrial arthropods (Rall *et al.* 2010; Vucic-Pestic *et al.* 2011) and rocky intertidal marine invertebrates (Iles *in prep*). The model simulations also indicate that at high ambient temperatures, populations whose energetic efficiencies increase with temperature (i.e. those with a positive CTI) would be more likely to persist. Such species may be found in warmer habitats. There is very little support for this hypothesis, but Sentis *et al.* (2012) found increasing energetic efficiencies with temperature for a ladybeetle, *Coleomegilla maculata lengi*, which increased up to an optimum at ~30°C and then decreased thereafter, likely due to catabolism. Although this is just one study, this result may indicate adaptation, or acclimation, to high ambient temperatures, especially considering this lab population of *C. maculata* was reared at a relatively high ambient temperature (24°C) and tested along a much higher range of temperatures (14 - 33°C) compared to the terrestrial arthropods (8 – 22°C) and marine invertebrates (5 – 17°C) tested. If the energetic efficiencies of species are adapted to their local climate, then entire community assemblages living under similar abiotic conditions are likely to exhibit similar scaling of metabolic and ingestion rates. Thus, more

empirical measurements of energetic efficiency from diverse habitats and climates are necessary to assess the real world importance of this finding.

In the simulations, the influence of temperature and CTI on a species' probability of extinction was dramatically lower for large-bodied species. This effect of body size stems from the underlying expressions for mass-specific metabolic and ingestion rates, which scale with body size as $M^{-0.25}$ (Equations 4a-c, Gillooly *et al.* 2001; Brown *et al.* 2004). Although larger organisms require more resources, they operate more efficiently, requiring fewer resources on a per mass basis than smaller organisms (Brown *et al.* 2004). Since the effect of body size is multiplied by the effect of temperature, per unit biomass rates of metabolism and ingestion become less sensitive to temperature as body size increases. Consequently, species with larger body sizes at any given trophic level were less susceptible to temperature fluctuations. Previous simulations of ATN models have shown that incorporating body size scaling means that consumers tend to have lower per unit biomass rates of metabolism and ingestion relative to their resources, which effectively decreases per unit biomass species interaction strengths and increases food web stability (Yodzis & Innes 1992; Brose *et al.* 2006b). In natural systems, such a disproportionate effect of temperature on small bodied species would provide added selection pressure for predators to be larger than their prey.

The effect of trophic level in the simulations suggests that in real systems, small-bodied consumers at higher trophic levels would be more vulnerable to temperature fluctuations and would thus experience greater selection pressure on traits affecting body size, energetic efficiency, or reproductive rates. In particular, parasites, parasitoids and other infectious agents, which typically occupy high trophic levels and have small body sizes, have been shown to reproduce at higher rates and exhibit higher energetic efficiencies (Lafferty *et al.* 2008a; Hechinger *et al.* 2011) and are quite vulnerable to ecosystem disturbance (Lafferty *et al.* 2008b; Wood *et al.* 2010). Furthermore, parasites only fit into the common macro-ecology scaling rule for abundance as a function of body size and temperature unless trophic level is taken into account (Hechinger *et al.* 2011). Experimental studies manipulating temperature on entire communities have generally

found that upper trophic levels are more sensitive to climate change. For example, in communities of aquatic microorganisms held in microcosms that were slowly warmed, species went extinct disproportionately from top trophic levels (Petchey *et al.* 1999). Similarly, Voigt *et al.* (2003) found that climate accounted for a greater amount of explained variance in abundance of higher trophic levels in a grassland community of invertebrate consumers. Due to the space requirements of large-bodied species and handling species of dramatically different body sizes, these manipulative experimental studies typically use organisms that are relatively small. This logistical limitation may unintentionally limit the size structure of the experimental community (i.e. predators are relatively small) and bias results towards greater extinction rates of top trophic levels.

That large-bodied consumers at higher trophic levels would be less vulnerable to temperature fluctuations due to the overwhelming influence of body mass on metabolic rates, would be difficult to test. Not only because of the aforementioned logistical difficulties of experimenting with large-bodied species, but also because the confounding effects of other mechanisms that disproportionately affect large-bodied, top-trophic position species but were not incorporated into the ATN model. Most notably, large-bodied animals tend to have lower population densities, slower population growth rates, and occupy habitat at a greater spatial scales (Burness *et al.* 2001). This makes them more vulnerable to demographic and genetic variability with a reduced capacity to recover from disturbances or habitat loss (Karlsson *et al.* 2007). The ATN model is not spatially explicit and thus does not take into account the greater space requirements of larger species or allow species to disperse to or between more favorable habitats. Although the ATN model includes a minimum biomass density in the simulations, below which a species was considered mathematically extinct, it does not include a minimum density of individuals which would take into account body size and the minimum population size for maintaining long-term population viability. Finally, the ATN models do not include the ability of species to adapt to their environment and large bodied species with small population sizes and long generation times tend to adapt slower than small bodied species.

The results of the simulations support the hypothesis that specialized species should be more sensitive than generalists to climate change since the loss of a key prey could be catastrophic for a specialist but a generalist has other resources to draw from (Gilman *et al.* 2010). This result is also consistent with network analyses by Araujo *et al.* (2011) in which poorly connected species were most exposed to the effects of climate change. Furthermore, network robustness is known to increase with connectivity, which increases the proportion of generalists (Dunne *et al.* 2002). From the perspective of species interaction strength, consumers with multiple resources had no prey preference in the simulations and fed in proportion to the biomass densities of their resources. Thus the average per unit biomass interaction strength of a consumer would decrease when it had more resources to draw from, increasing the probability of persistence of species with more resources. This supports findings from marine communities in which highly connected species tended to have weak effects on average (O'Gorman *et al.*) and the species involved in strong interactions were more likely to have additional, stabilizing, weak interactions as well (Bascompte *et al.* 2005).

There are many limitations and assumptions of these simulations. The ATN model system represents closed communities, in which species cannot disperse to better suited habitats and they either go extinct or persist. Species cannot adapt to their environmental conditions, nor do they have any ability to acclimate. This is important because for many organisms with indeterminate growth, temperature is often a major factor affecting adult body sizes and the effect of body size outweighs the effect of temperature. Furthermore, many organisms exhibit phenotypic plasticity with regard to metabolism. At times of resource scarcity or under stressful environmental conditions, many species can lower their metabolic rates and resource requirements by entering a low energy use torpor or diapause (Fly *et al.* 2012). Non-trophic interactions are not included, yet can account for much of the complexity of ecological networks (Kefi *et al.* 2012). Particular non-trophic interactions may be very influential; For instance some species ameliorate of stressful environmental conditions for others. Endotherms are in a different metabolic class, with very different coping mechanisms for preventing heat loss or heat

gain as environmental temperatures change (Burness *et al.* 2001). Finally, there are many other ways, besides temperature changes, in which climate change will affect organism performance, such as changes to precipitation patterns and ocean acidification. Thus, there are many more additional complexities and countervailing mechanisms missing from these simulations. Incorporating these complexities into such simulations would give insight into their relative importance. Developing these models further will also help identify influential factors that are easy to measure in the real world (e.g. body size) to make predictions for when and where species are likely to be vulnerable to climate change. Where the model predictions deviate from trends seen in empirical observations or experimental manipulations of warmed communities is also informative for what mechanisms are missing from the models and where the knowledge gaps lie.

2.4.1 Conclusions

The simulations presented here put the physiological effects of temperature at the organismal level into a trophic network context. The results provide insights into the mechanistic basis of temperature on community level patterns of stability and provide predictions for how vulnerable species are likely to be to climate change. Exothermic consumers in cooler habitats are likely to exhibit declining energetic efficiency and be vulnerable to warming, whereas exothermic consumers in warm environments would benefit from increasing energetic efficiency, which reflects existing but limited empirical measurements. Temperature changes are likely to have a greater influence on small-bodied consumers, particularly those at higher trophic levels such as parasites, and contribute to the observed size structure of ecological communities.

Despite these insights learned from incorporating temperature scaling of fundamental biological rates into trophic networks, the analysis also reveals the relatively minor importance of trophic network structure in comparison to particular species attributes and local food web structure for understanding species extinction probabilities. Of course, it is only after characterizing the general, bioenergetic constraints that species face and putting them in the network context that we are able to assess the relative

influence of different factors at different levels of biological organization. The approach used here helps characterize general bioenergetic constraints and set a baseline for predicting when and where species are likely to be vulnerable to climate change.

ACKNOWLEDGEMENTS

I thank B. Menge for advice and support throughout my PhD. I also thank E. Berlow, J. Bolte, U. Brose, and S. Hacker and for much needed help and advice; T. Gouhier for statistics mentoring and coding assistance; M. Frenock and J. Sapp for computer and database help; and A. Barner, E. Berlow, L. Cerny-Chipman, S. Close, J. Henderson, B. Menge, C. Shen, and J. Reimer for reviewing drafts of this Chapter. Funding was provided by a National Science and Engineering Research Council of Canada pre-doctoral fellowship and the Partnership for Interdisciplinary Studies of Coastal Oceans (PISCO), a long-term ecological consortium which is partially funded by the David and Lucile Packard Foundation and the Gordon and Betty Moore Foundation.

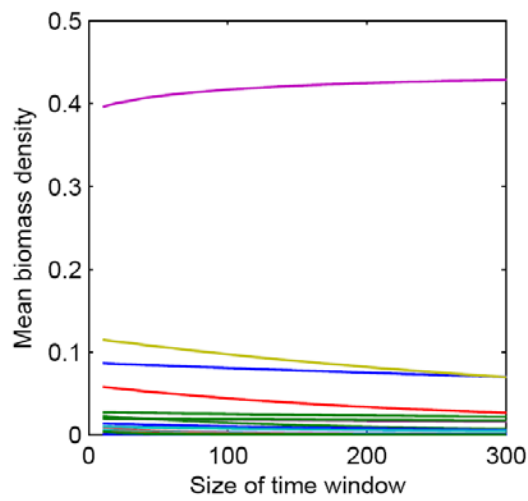


Figure 2.1 To determine the size of the time window over which to evaluate population stability, I plotted the mean biomass density (mass/area) depending on the size of the time window, or the number of time steps starting after time step 50. The different colors represent different species in the model.

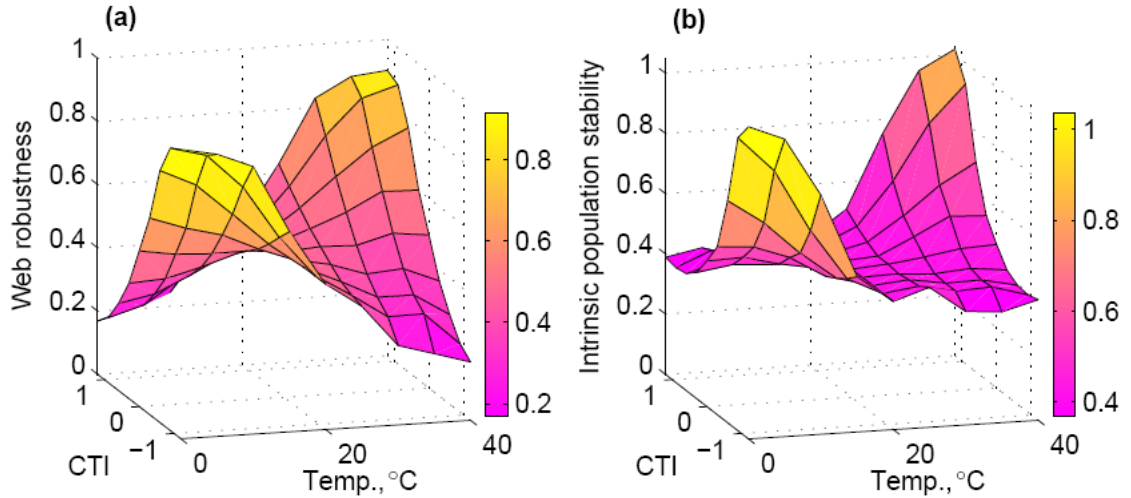


Figure 2.2 Average web robustness (a; the proportion of species persisting in the web), and intrinsic population stability (b; the inverse of variability in biomass density over time) over 100, 30-species simulated food webs evaluated at different combinations of Consumer Thermal Impact ($CTI = E_y - E_x$) and ambient temperature. Higher values, or more yellow on the color bar spectrum, are indicative of greater community (a) and population (b) stability. The axes of invariance are found at $CTI = 0$ eV and temperature = 20°C. These are the values where the intercepts of the temperature dependent functions for metabolic and ingestion rates are defined.

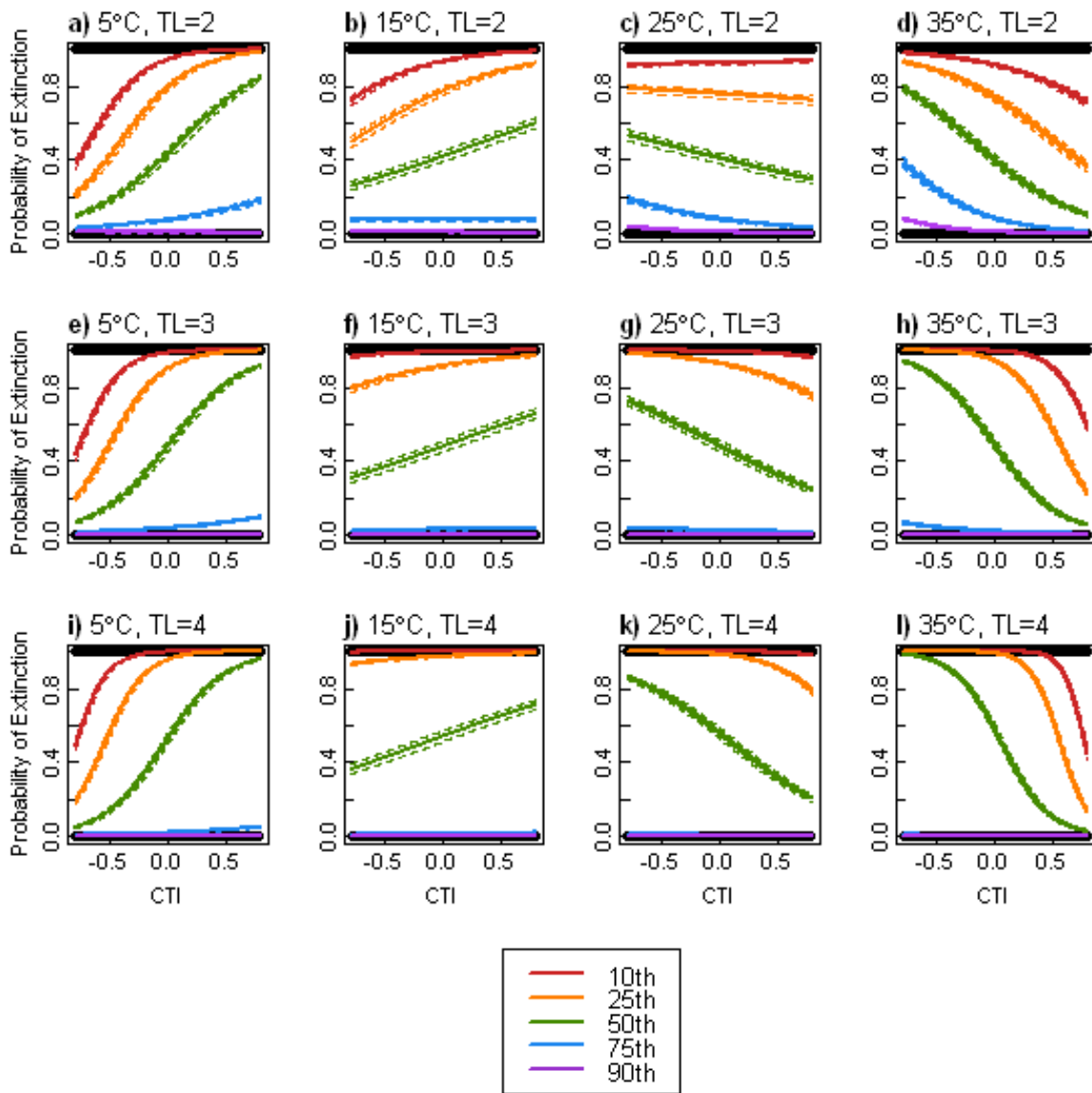


Figure 2.3 The effect of CTI on the probability of a species extinction at four ambient temperatures: 5, 15, 25 and 35°C and trophic levels 2, 3 and 4. The effect is plotted separately for various percentiles of body mass (see legend). The solid lines represent the GLMM-predicted values for the ‘population of webs’ at that particular combination of set temperature, trophic level and body mass; the dashed lines encompass the 95th percentile of the variation between the 500 webs analyzed.

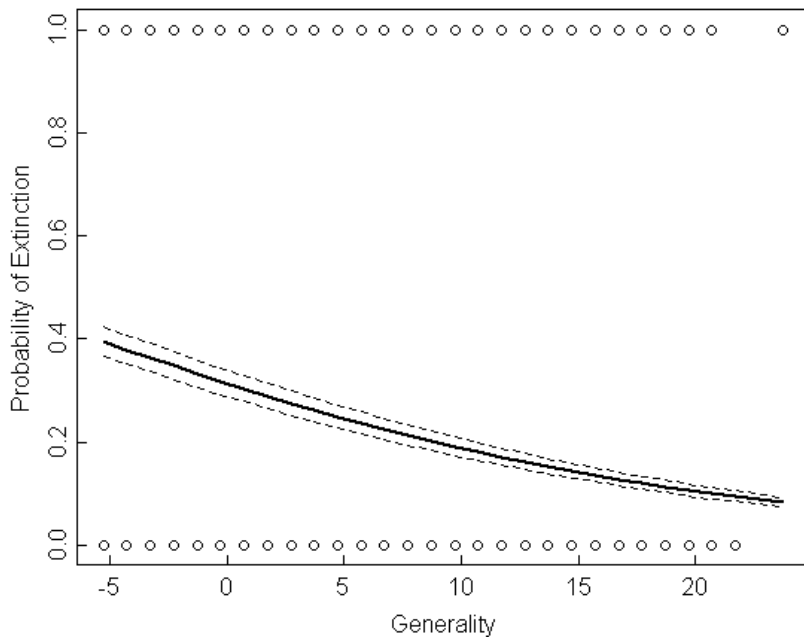


Figure 2.4 The effect of consumer (centered) generality on GLMM-predicted probabilities of extinction. The thick line in the middle represents the predicted values for the ‘population of webs’; the two dashed lines encompass the 95th percentile of the variation between the 500 webs analyzed.

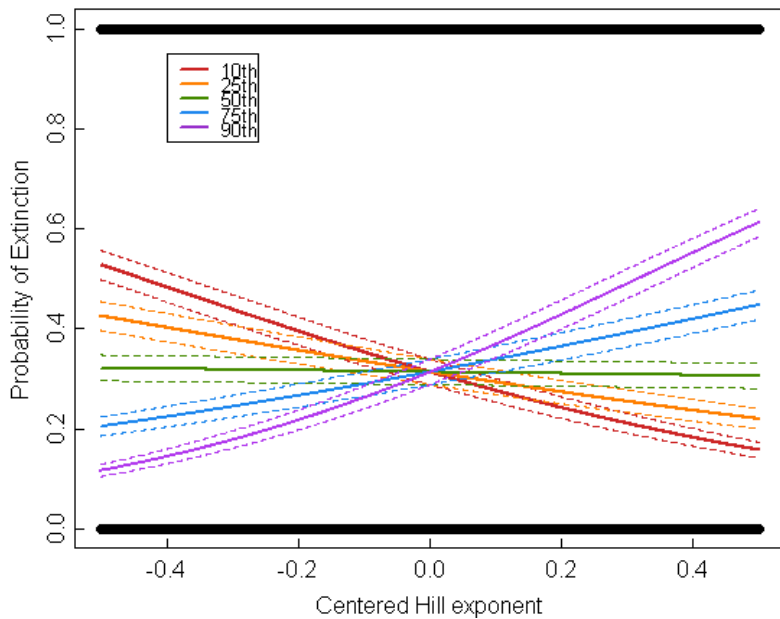


Figure 2.5 The effect of consumer (centered) Hill exponents on GLMM-predicted probabilities of extinction. The effect is plotted separately for various percentiles of body mass (see legend). The solid lines represent the predicted probability of extinction for a species of a particular body mass for the ‘population of webs’; the two dashed lines encompass the 95th percentile of the variation between the 500 webs analyzed.

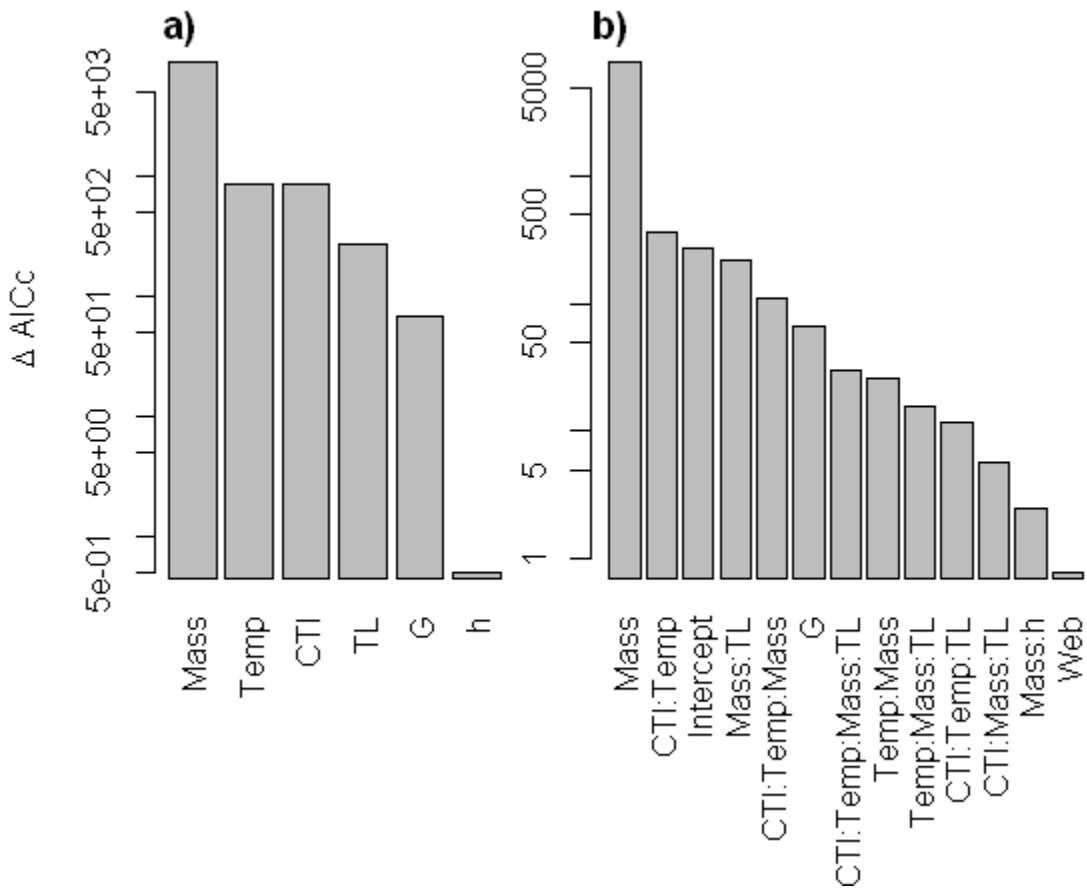


Figure 2.6 The relative contribution of a) the total effect of each variable, and b) the effect of each statistically significant model term to a species probability of extinction. The effect of each variable or term on model fit was assessed by the change in the corrected Akaike information criterion, ΔAIC_c , after that variable or term was removed from the model.

CHAPTER 3: Temperature Effects on the Energetic Efficiency and Species Interaction Strength of Rocky Intertidal Invertebrate Consumers

ABSTRACT

Predicting the effects of climate change on ecological communities requires a fundamental understanding of how environmental factors influence both physiological and interspecific processes. Specifically, the net impact of temperature on community structure depends on the relative response of physiological energetic costs (basal metabolism) and interspecific gains (ingestion) that mediate the flow of energy throughout a food web. However, the relative scaling of metabolic and ingestion rates with temperature have never been measured for an entire ecological assemblage and it is not known how, and to what extent, they differ. To investigate the relative influence of these processes, I measured the temperature scaling of basal metabolic and ingestion rates for a suite of rocky intertidal species using a multiple regression experimental design. I compared oxygen consumption rates (as a proxy for basal metabolic rate) and ingestion rates by estimating the temperature scaling parameter (E_A ; the activation energy) of the ‘universal temperature dependence’ (UTD) model, a theoretical model derived from first principles of biochemical kinetics and allometry. The results show that consumer basal metabolic rates (energetic costs) were more sensitive to temperature than ingestion rates (energetic gains). Thus, as temperature increased, metabolic rates tended to increase faster relative to ingestion rates and energetic efficiency declined. Metabolic and ingestion rates largely scaled in accordance with the UTD model; however, convex curvature was evident in several cases. These results highlight the relative importance of physiological processes for forecasting temperature effects on ecological communities and the importance of measuring the effects of environmental factors in ways that can be easily incorporated into community models.

3.1 INTRODUCTION

With mounting evidence of climate change, ecologists face the challenge of forecasting impacts on ecological communities (Helmuth et al. 2006). In particular, the influence of environmental temperature at the community level may be significant. Environmental temperature affects virtually all biochemical and physiological rates of ectotherms and is thus highly influential on their distribution and abundance (Somero 2002; Pörtner & Peck 2010; Somero 2011). At the organismal level, the first principles of thermodynamics are quite successful in relating environmental temperature to body temperature in ectotherms (Helmuth 1998; Denny & Harley 2006; Szathmary *et al.* 2009). Physiological responses to changing body temperatures are well understood, with effects on metabolism (Gillooly *et al.* 2001), larval development (O'Connor *et al.* 2007) and autotroph production and respiration (Lopez-Urrutia *et al.* 2006), to name just a few (see reviews by Dell *et al.* 2011; Somero 2011). Although the direct effects of temperature on the strength of species interactions (i.e. attack rates, maximum ingestion rates) is becoming increasingly recognized (Sanford 1999, 2002a, b; Yee & Murray 2004; Pincebourde *et al.* 2008a, b; Yamane & Gilman 2009; Rall *et al.* 2010; Englund *et al.* 2011; Vucic-Pestic *et al.* 2011), little is understood about how these underlying physiological mechanisms manifest at the community level. Freshwater microcosm experiments on bacteria-protist communities (Petchey *et al.* 1999; Beveridge *et al.* 2010a; Beveridge *et al.* 2010b) suggest that the effects of temperature, through changes in species interaction strengths and the flow of energy through food webs, has strong influences on population dynamics, population persistence and ecosystem functioning. Thus, understanding the temperature responses of the processes that mediate the flow of energy through food webs is critical for forecasting the impact of temperature on ecological communities.

Several general theoretical models have explored the effects of temperature on community structure by incorporating temperature dependency into consumer metabolism and ingestion rates (Vasseur & McCann 2005; Rall *et al.* 2010), herbivore metabolism and autotroph production rates (O'Connor *et al.* 2011), and consumer attack rates and handling times (Petchey *et al.* 2010). Collectively, these modeling exercises

confirm that the rate at which these processes scale *relative* to one another is extremely important for predicting ecosystem responses to temperature change. For instance, if consumer energetic efficiencies decline with warming (*i.e.* metabolic rates increase faster with warming than ingestion rates), it increases population stability but also increases the risk of starvation and extinction of top trophic levels (Vasseur & McCann 2005; Rall *et al.* 2010). Alternatively, if ingestion outpaces metabolism in response to warming, then consumers have a larger impact on their resources and system stability declines (Vasseur & McCann 2005). Thus, to understand temperature effects at the ecosystem level, we need to determine if there are systematic differences in how physiological responses scale with temperature. Identifying these general, species-independent effects of temperature on the flow of energy through food webs would significantly increase our ability to predict how food web structure and functioning may shift under climate change.

My main objective was to investigate the temperature scaling of metabolic and ingestion rates for several key rocky intertidal species in ways that can easily be incorporated into community models. Specifically, I asked:

How sensitive are metabolic and ingestion rates of rocky intertidal invertebrates to water temperature?

Does the relative sensitivity of metabolic and ingestion rates to temperature vary across species or do all show similar patterns?

What are the implications for food web models and for predicting climate change impacts on ecosystems?

Metabolic and ingestion rates have rarely been measured on the same species, except collectively for a group of spider and beetle species from a terrestrial forest floor community, in which metabolic rates were more sensitive to temperature than ingestion rates (Rall *et al.* 2010; Vucic-Pestic *et al.* 2011). In freshwater microcosm communities of eukaryotic microorganisms that were warmed at 2 °C per week (or approximately 0.1–0.2 °C per generation), warming greatly increased extinction rates of top consumers and increased the dominance of lower trophic levels (Petchey *et al.* 1999). These microcosm results are consistent with theoretical model predictions (Vasseur & McCann 2005) only

when consumer metabolic rate increases faster with warming than ingestion rate. Thus, I hypothesized that for all species metabolic rates would be more sensitive to temperature than ingestion rates and predicted I would find higher activation energy estimates for metabolic rates. My results support this hypothesis and in the discussion section I talk about possible causes of this trend and consequences in the face of climate change.

3.2 METHODS

All measurements of metabolic and ingestion rates took place at the Hatfield Marine Science Center (HMSC; Newport, Oregon, USA). The animals and algae were collected from two rocky intertidal field sites along the Oregon coast, Fogarty Creek ($44^{\circ} 50' 24''$ N, $124^{\circ} 3' 36''$ W) and Yachats Beach ($44^{\circ} 19' 12''$ N, $124^{\circ} 7' 12''$ W). During collection, I ensured that the individuals selected for experimentation were evenly distributed along the entire range of body sizes encountered at the field sites. The species included a classic keystone predator, the sea star *Pisaster ochraceus* and its main prey *Mytilus californianus* (Conrad), a mussel which is a dominant competitor for space and a foundation species in the mid zone of the intertidal; two secondary predators, the whelks *Nucella ostrina* (Gould) and *N. canaliculata* (Duclos) and two of their preferred prey, the mussel *Mytilus trossulus* (Gould) and the barnacle *Balanus glandula* (Darwin), and two common grazers of the kelp *Saccharina sessilis* (Kuntze), the urchin *Strongylocentrotus purpuratus* (Stimpson) and the chiton *Katharina tunicata* (Wood). Because *B. glandula* could not be collected non-destructively, I bolted 10 X 10 cm PVC plates covered in Safetywalk® antislip tape to intertidal rocks, to which barnacles readily settled (Farrell *et al.* 1991; Menge *et al.* 2011b).

3.2.1 Metabolic rate trials

I used an experimental regression study design to measure how oxygen consumption rates (as a proxy for metabolic rate) scale with body mass and temperature for *P. ochraceus*, *M. californianus*, *M. trossulus*, *S. purpuratus*, *K. tunicata*, *N. ostrina*, and *N. canaliculata*. Oxygen measurements were made using a Fibox 3 fiber-optic

oxygen meter (PreSens, Precision Sensing GmbH, Germany) and oxygen sensitive spots. The oxygen sensitive spots were mounted inside clear, airtight containers (respirometers) of various sizes to accommodate the different body sizes of the species being measured. Individual organisms were sealed underwater into a respirometer and checked to ensure there were no trapped air bubbles. The water was aerated and sterilized with a UV filter for at least 18 hours prior to each trial. For each trial, I took 3-5 oxygen measurements of each respirometer over a 3-4 hour period. I repeated these oxygen consumption trials at various water temperatures ranging from ~5-20 °C. I maintained stable water temperatures by keeping the respirometers in water baths of the same temperature, removing them briefly from the cold room to make oxygen concentration measurements.

Measurements were made using the default setting of the oxygen meter (% air saturation) and were converted to $\mu\text{mol/L}$ with atmospheric pressure readings from the HMSC weather station and the average summertime salinity of HMSC seawater (34 ppt). Due to the low solubility of O_2 in water, aquatic animals come to hypoxic conditions relatively faster than air breathing animals in traditional respirometers, which can considerably change their metabolism (Lamprecht *et al.* 1999). Thus, I calculated the rate of change of O_2 concentration ($\mu\text{mol O}_2 \cdot \text{L}^{-1} \cdot \text{s}^{-1}$) only over the period of time in which the animals were experiencing normoxia ($>110 \mu\text{mol O}_2 \cdot \text{L}^{-1}$). I converted the oxygen consumption rate into energetic equivalents of metabolism ($\text{J} \cdot \text{s}^{-1}$) by assuming an oxycaloric equivalent of 0.44 ($\text{J} \cdot \mu\text{mol} \cdot \text{O}_2^{-1}$), which represents the catabolism of a mixed metabolic substrate dominated by proteins but also containing carbohydrates and lipids (Lauff & Wood 1996; Hand & Kemp 1999).

3.2.2 Ingestion rate trials

I used an experimental regression study design to measure how ingestion rates scale with body mass and temperature for various consumer-resource species interactions. The details of each ingestion rate experimental trial can be found in Table 3.1. The experimental system consisted of 65, 19 L buckets, each with an air hose and air stone, insulated with reflective bubble insulation (Reflectix Inc., Markleville, Indiana,

USA) and plumbed with flow-through seawater. To help prevent escape, the experimental animals and algae were confined to smaller plastic containers with mesh sides within the buckets, except for the *P. ochraceus* trial, in which the animals were placed directly in the buckets. The system was housed within a cold room with the thermostat set to 5 °C. To vary the water temperatures among the buckets, I used 7.5 and 15 W aquarium heaters (Hydor Mini Heaters, Hydor USA Inc., Sacramento, CA, USA) to randomly assign 0 W, 7.5 W, 15 W, 22.5 W or 30 W of heat to each bucket. Although the variation in water temperature was created with distinct levels, as in an ANOVA design, I instead used temperature as a continuous variable, measured every other day with a digital handheld thermometer (Model HH-22A, Omega Engineering Inc., Stamford, CT, USA) and averaged over the course of each experiment. This is because there were many factors affecting the final water temperature of each bucket, including variation in air temperature around the cold room and the randomly assigned temperatures of neighboring buckets. However, the variability of within bucket water temperature was low, with a pooled standard deviation of 0.62 °C, as measured every 30 minutes by iButton temperature loggers (Maxim Integrated Products, Inc., Sunnyvale, California, USA) placed in 12 haphazardly chosen buckets.

The ingestion rate trials were run consecutively from June through September, 2010. The duration of each trial depended on the fastest rate at which the resources were being consumed so that no individual consumer exhausted its resource (Table 3.1). For the trials using *B. glandula* as the resource, I randomly assigned one barnacle plate per container, as the number of barnacles that settled on each plate varied. Each experimental trial included 5 consumer-free controls, one for each wattage level, which showed that resource mortality was negligible. For the trials using *S. sessilis* as the resource, the percent biomass loss from the controls was taken into account when calculating urchin and chiton consumption rates. Other than the controls, each container contained one consumer which was weighed at the start of each trial.

For every combination of consumer j and resource i, I calculated the ingestion rate J_{ij} ($\text{J}\cdot\text{s}^{-1}$) as:

$$J_{ij} = (N_e M_i \varepsilon) / t \quad (1)$$

where N_e is the number of prey eaten (1 for *S. sessilis*), M_i is the estimated shell-free wet mass (g) of an averaged length prey item based on length-mass relationships for each prey species (ACI, unpublished data) or the wet mass (g) of *S. sessilis* eaten, and t is time in seconds. The energy content of the resources, ε , was set to 6173 and 5751 J·g⁻¹ of ash free wet mass for *Mytilus* spp. and *B. glandula*, respectively (B. A. Menge, unpublished data), and 3122 J·g⁻¹ for *S. sessilis* (Paine & Vadas 1969). I calculated the *per capita* strength of the interaction between each consumer, j , and resource, i , as the absolute value of the log response ratio (Berlow *et al.* 1999; Rall *et al.* 2010):

$$\alpha_{ij} = \left| \frac{\ln \left(\frac{N_i - N_e}{N_i} \right)}{t} \right| \quad (2)$$

where t (days) is the experimental duration, N_i is the initial prey abundance and N_e is the number of prey eaten.

3.2.3 Statistical analyses

The metabolic rate and ingestion rate data were first analyzed using the ‘universal temperature dependence’ (UTD) model, a theoretical model derived from first principles of biochemical kinetics and allometry (Gillooly *et al.* 2001; Brown *et al.* 2004). The UTD model characterizes the effects of temperature and body mass on metabolic rate (Gillooly *et al.* 2001) and has been extended to other biological rates, including ingestion rate and species interaction strength (Rall *et al.* 2010; Vucic-Pestic *et al.* 2011). Under the UTD, per capita rates of metabolism, I_j (J·s⁻¹), ingestion, J_{ij} (J·s⁻¹), and interaction strength, α_{ij} , of ectothermic organisms depend jointly on body mass, M (g), and environmental temperature, T (K) as:

$$I_j = i_0 M_j^{b_I} e^{-E_I/kT} \quad (3a)$$

$$J_{ij} = j_0 M_j^{b_J} e^{-E_J/kT} \quad (3b)$$

$$e^{\alpha_{ij}} = \alpha_0 M_j^{b_\alpha} e^{-E_\alpha/kT} \quad (3c)$$

where b is an allometric exponent, E (eV) is the activation energy, k is Boltzmann's constant (8.62×10^{-5} eV·K $^{-1}$) and i_0 and j_0 are normalization constants. Taking the natural logarithm of both sides of equations 3a-c, results in the form of the multiple linear regression UTD models used to estimate the scaling coefficients of the continuous variables (1) body mass [$\ln(M)$], and (2) water temperature ($\frac{1}{kT}$) and the normalization constants for each species:

$$\ln(I_j) = b_I \ln(M_j) - E_I \left(\frac{1}{kT} \right) + \ln(i_0) \quad (4a)$$

$$\ln(J_{ij}) = b_J \ln(M_j) - E_J \left(\frac{1}{kT} \right) + \ln(j_0) \quad (4b)$$

$$\alpha_{ij} = b_\alpha \ln(M_j) - E_\alpha \left(\frac{1}{kT} \right) + \ln(\alpha_0) \quad (4c)$$

Zero values in the ingestion rate data set were omitted in order to log transformation the data. A completely inactive consumer (the individuals with zero ingestion) is also an indication of an injured organism that has gone into a state of torpor, thus including zero values in the ingestion rate data may bias the results. Data for water temperatures > 17 °C were excluded as such temperatures are outside the ranges of normal water temperatures these organisms experience in their natural habitat. Regression diagnostics were performed on all models including tests for normality and constant variance of residuals. The residuals of several models were non-normally distributed due to influential outliers and curvature in the data. Because linear least squares is not robust to influential outliers and the accurate estimation of regression parameters was the primary objective, I also estimated the UTD model parameters using the Huber method for robust linear regression (see Appendix A). To address the curvature in the data, I considered optimal models including interaction and quadratic terms for body mass and temperature. I tested whether these optimal models were a statistically superior fit to the data by assessing the change in Akaike's Information Criteria (ΔAIC).

The activation energies, E , are a measure of the temperature dependency of metabolic and ingestion rates. The difference between them ($E_J - E_I$), is the 'consumer thermal impact' (CTI), which describes how the impact of a consumer on its resource changes with temperature (Vasseur & McCann 2005). A positive CTI means that

ingestion rate outpaces metabolic rate as temperatures increase. A negative CTI means that a consumer's metabolic demands increase faster than it can compensate with increased ingestion. To test for systematic differences between metabolic and ingestion rates across species, I performed a paired, two-tailed *t*-test. I used MATLAB 7.13 (MathWorks R2011b) for data processing and R 2.13.2 (The R Foundation for Statistical Computing 2011) for all statistical analyses.

3.3 RESULTS

Metabolic rates, ingestion rates and species interaction strengths tended to increase with temperature and body mass in accordance with the UTD model (Table 3.2, Figs. 3.1-3.3); however, ingestion rate and interaction strength decreased with body size for the *N. canaliculata* – *B. glandula* interaction and convex curvature was evident in several models, indicating that the UTD model is inappropriate in some cases. The range of each significant activation energy estimate (\pm SE) overlapped with the theoretical range of 0.6 – 0.7 eV (Allen & Gillooly 2007) for metabolic and ingestion rate but not for interaction strength UTD models. Although body mass explained much more of the variation in the data than temperature, temperature was a significant factor for all the UTD models of metabolic rate and 4 out of 7 UTD models for ingestion rate and interaction strength (Table 3.2, Figs. 3.1-3.3). The robust regression analysis yielded similar results with slightly different estimates for the model coefficients (Appendix A).

Convex curvature occurred most often in models involving the whelks (Table 3.3). A squared temperature term produced a better fit to the metabolic rate data over the UTD model for *N. canaliculata* and a marginally better fit for *N. ostrina*. By restricting the range of temperatures to the increasing, linear portion of *N. canaliculata*'s metabolic response (water temperatures < 14 °C), the squared term becomes insignificant, and the estimate of the activation energy is much higher ($E_I = 1.40$ (0.23), $p < 0.001$). Adding a squared body mass term improved the fit of the ingestion rate data for *N. canaliculata* when feeding on *B. glandula* and was suggestive of a curved relationship for the *N. ostrina* – *B. glandula* interaction. For the species interaction strength models, a squared

body mass term was a better fit for the interactions of *N. ostrina* with *B. glandula* and *M. trossulus*, and was suggestive for the *N. canaliculata* – *B. glandula* interaction. Finally, an interaction term between body size and temperature improved the fit of the species interaction strength model for *N. canaliculata* – *M. trossulus*.

In both the least-squares and robust regression analyses, consumer metabolic rates tended to be more sensitive to temperature than ingestion rates (*i.e.* a negative CTI), with the exception of the *N. canaliculata* – *M. trossulus* interaction. However, when using the metabolic rate activation energy estimate for the linear portion of the temperature range the CTI for the *N. canaliculata* – *M. trossulus* interaction is negative (Table 3.4).

Although there is clearly variability in species responses, the paired sample t-test indicated that CTI values are marginally more likely to be negative ($t(5) = -2.48, p = 0.056$) with an average CTI of -0.26 (95% CI ± 0.28). When using the metabolic rate activation energy estimate for *N. canaliculata* over the range of temperature where the relationship is linear, the paired sample t-test indicates that CTI values are much more likely to be negative ($t(5) = -7.34, p < 0.001$), with an average CTI of -0.40 (95% CI ± 0.14).

3.4 DISCUSSION

Metabolic rates tended to be more sensitive to temperature than ingestion rates (*i.e.* a negative CTI) for individual species of rocky intertidal invertebrate consumers. This result is consistent with temperature scaling measurements for beetle and spider taxa from forest communities (Rall *et al.* 2010; Vucic-Pestic *et al.* 2011). Furthermore, in a meta-analysis of the thermal responses of a variety of traits from many species across habitats, “autonomic” traits like basal metabolic rate tended to be more sensitive to temperature than “positive motivation” traits such as ingestion rate (Dell *et al.* 2011). This difference was not statistically significant, but a paired sample analysis would be necessary given the large degree of variability between species. Unfortunately, few studies measure both types of traits on the same species. The one exception to the trend toward negative CTIs was the *N. canaliculata* – *M. trossulus* interaction, which had a

positive CTI. However, *N. canaliculata* exhibited convex curvature in the scaling of metabolic rate with temperature, which means the UTD model is inappropriate as it violates a basic assumption of regression analyses. Reducing the temperature range to where the relationship is linear, however, results in a much higher estimate of the activation energy for metabolic rate and a negative CTI.

This difference in temperature scaling between metabolic and ingestion rates may reflect evolutionary pressures to optimize energetic efficiencies of different kinds of physiological performances under variable thermal conditions. In a quantitative model of the evolution of thermal physiology, a wider performance breadth was favored under variable environmental temperatures (Huey & Kingsolver 1993). In Oregon, intertidal invertebrate consumers experience fluctuating water temperatures from ~8-16 °C when foraging underwater at high tide. However, *in situ* evidence indicates that cold water during upwelling limits the predation rate of the keystone predator *P. ochraceus* (Sanford 1999) and lab experiments simulating upwelling indicated a similar trend for *N. canaliculata* (Sanford 2002a). Thus, selection pressure may favor increased foraging performance at low temperatures. This would reduce the slope of the temperature response and cause a reduction in the activation energy for ingestion rate, which could explain the lower sensitivity of ingestion rates to temperature in the results.

Rocky intertidal consumers in Oregon are also exposed to daily aerial temperatures that range from ~5-35 °C, depending on the season and the timing of low tide during the day or night. Most intertidal invertebrates avoid or are unable to forage during low tide. However, they may take advantage of warmer body temperatures to speed up digestion before the next high tide when they can again forage. Many species behaviorally regulate to a higher body temperature when digesting a meal (e.g. snakes, Dorcas *et al.* 1997; and locusts, Coggan *et al.* 2011). Although usually attributed to avoiding chronic exposure to high temperatures (Pincebourde *et al.* 2009), thermoregulatory behavior in intertidal invertebrates may be co-adapted to optimize digestion rates. *P. ochraceus* has the capacity to store energy from periods of intensive feeding as lipids, proteins and glycogen reserves in their pyloric caeca (Lawrence & Lane

1982). When water temperatures are very cold, foraging may be so inefficient that *P. ochraceus* choose to remain inactive in low-zone surge channels and take advantage of depressed metabolic rates to efficiently convert this stored energy into gonadal or somatic growth (Sanford 2002a). Thus, having a metabolic scope that is highly sensitive to temperature may be advantageous to a consumer capable of thermoregulation under extremely variable environmental conditions.

Understanding the community-level effects of environmental temperature is of great concern in a changing climate. Along the west coast of the US, climate-induced trends indicate that upwelling is becoming stronger and more persistent (Bakun 1990; Bakun *et al.* 2010; Iles *et al.* 2012), which would likely cause longer periods of cold upwelled water. With negative CTI's, consumer energetic efficiencies would increase under such conditions, leading to unstable population dynamics (Vasseur & McCann 2005). In regions where the environment is predicted to become warmer, the opposite response would occur: consumer energetic efficiencies would decline, leading to a lower per unit biomass impact on resource species. In the long-term, this would increase resource population stability, with fewer fluctuations in population densities over time, but also increases the risk of starvation and extinction of top trophic level species (Vasseur & McCann 2005; Rall *et al.* 2010). Indeed, in a study that slowly warmed freshwater microcosm communities, both consumer extinction rates and producer biomass increased (Petchey *et al.* 1999). These microcosm results are consistent with model predictions only when consumer metabolic rates are more sensitive to temperature than ingestion rates, as my results indicate is true for these dominant rocky intertidal invertebrates.

My controlled laboratory measurements did not examine the effects of extreme aerial temperatures on metabolic or ingestion rates. Yamane & Gilman (2009) found that although there was no change in the ingestion rates of *N. ostrina* after experiencing aerial body temperatures of 12 to 20 °C, exposure to extremely high aerial temperatures (>28 °C) caused decreased consumption rates during the subsequent high tide. In lab experiments with *P. ochraceus*, acute exposure to high aerial temperatures positively

affected feeding rates, whereas chronic exposure caused reductions in feeding (Pincebourde *et al.* 2008a). Although aerial heat stress at low tide can affect intertidal predation rates, such high temperatures only occur occasionally (Sanford 2002b) and field surveys indicate that *P. ochraceus* seek refuge from chronic exposure (Pincebourde *et al.* 2008a). Sedentary organisms, such as mussels and barnacles that cannot take refuge from chronic exposure, often reach much higher body temperatures than their mobile predators (Broitman *et al.* 2009) and their upper distribution limits are often thermally constrained at warm sites (Harley & Helmuth 2003). Thus, the long term, relative impact of exposure to stressful temperatures compared to physiological rate effects near the center of a species thermal range is likely to be less important for the ingestion rates of mobile species and more important for sedentary ones.

3.4.1 Conclusions

At the organismal level, water temperature is arguably the most important environmental factor dictating rates of biochemical processes in marine poikilotherms (Somero 2002). At the population level, water temperature is the main abiotic factor affecting the distribution of marine, water-breathing animals (Somero 2002; Pörtner & Peck 2010). At the community level, however, we are just beginning to understand the effects of water temperature. In conjunction with previous measurements on terrestrial invertebrates, this study of marine invertebrates advances our understanding by providing compelling evidence for a systematic difference in the temperature scaling of basal metabolic and ingestion rates. Incorporating this general systematic difference into a framework linking variation in environmental temperature to ecological processes embedded in networks of species interactions will enable us to test hypotheses on how climate change will affect community structure and dynamics. However, ecological communities are inherently complex and in order to predict temperature effects on community structure and dynamics, much more work must be done to establish such generalities and to identify where exceptions are likely to occur.

ACKNOWLEDGEMENTS

I thank B. Menge for advice, funding, and the use of the caloric data from his PhD research. I also thank E. Berlow, U. Brose, S. Hacker, D. Lytle, and J. Miller for advice during research planning; facilities management at the Hatfield Marine Science Center (HMSC) for construction support; T. Gouhier for statistics mentoring; and A. Barner, D. Callander, S. Close, J. Feldmann, T. Gouhier, B. Menge and J. Reimer for reviewing drafts of this manuscript. Funding was provided by a National Science and Engineering Research Council of Canada pre-doctoral fellowship, a HMSC Mamie Markham Award to ACI, and from PISCO, a long-term ecological consortium which is partially funded by the David and Lucile Packard Foundation and the Gordon and Betty Moore Foundation.

Table 3.1 Details of the rocky intertidal consumer ingestion rate experimental trials including the resource used for the trial, the amount of resource made available to consumers at the beginning of the trial, and the duration of the trial (days).

Consumer	Resource	Resource amount (STD)	# days
<i>N. canaliculata</i>	<i>M. trossulus</i>	30 indv.	10
<i>N. canaliculata</i>	<i>B. glandula</i>	34.7 (3.2) indv.	8
<i>K. tunicata</i>	<i>S. sessilis</i>	23.1 (0.7) g	7
<i>N. ostrina</i>	<i>M. trossulus</i>	20 indv.	15
<i>N. ostrina</i>	<i>B. glandula</i>	46.5 (21.5) indv.	8
<i>P. ochraceus</i>	<i>M. californianus</i>	30 indv.	9
<i>S. purpuratus</i>	<i>S. sessilis</i>	23.0 (0.7) g	6

Table 3.2 Linear least-squares regression coefficients and statistics for the UTD models of the effect of body mass and water temperature on metabolic rates, ingestion rates, and interaction strengths in rocky intertidal invertebrate species. All the models are of the form $y = b \ln(M) - E \left(\frac{1}{kT} \right) + \ln(c)$, where M is body mass (g), T is water temperature (K), and k is Boltzmann's constant (8.62×10^{-5} eVK $^{-1}$). The coefficients with standard errors in parentheses include b , the allometric exponent; E , the activation energy (eV), and c , the normalization constant.

Species / Interaction	<i>b</i>	<i>E</i> (eV)	<i>ln(c)</i>	<i>R</i> ²	<i>p-val</i>	<i>n</i>
<i>Log metabolic rate</i>						
<i>M. californianus</i>	0.61 (0.04)***	0.76 (0.21)**	22.11 (8.38)*	0.90	8.12E-13	27
<i>N. canaliculata</i>	0.55 (0.09) ***	0.59 (0.16)**	14.93 (6.56)*	0.71	1.09E-06	25
<i>K. tunicata</i>	0.82 (0.06) ***	0.66 (0.16) ***	17.83 (6.36)**	0.89	2.22E-13	29
<i>N. ostrina</i>	0.56 (0.11) ***	1.02 (0.21) ***	32.60 (8.52)***	0.69	2.45E-06	25
<i>P. ochraceus</i>	0.42 (0.08) ***	0.77 (0.25)**	23.22 (10.30)*	0.60	1.17E-05	28
<i>M. trossulus</i>	0.47 (0.05) ***	0.77 (0.13) ***	22.29 (5.19)***	0.86	2.84E-10	25
<i>S. purpuratus</i>	0.43 (0.10) ***	0.63 (0.27) *	17.27 (10.98)	0.46	2.69E-04	30
<i>Log ingestion rate</i>						
<i>N. canaliculata</i> - <i>B. glandula</i>	-0.28 (0.10) **	0.09 (0.24)	-8.31 (9.92)	0.17	0.02	44
<i>N. canaliculata</i> - <i>M. trossulus</i>	0.35 (0.08) ***	0.82 (0.12) ***	27.42 (5.01) ***	0.54	2.38E-09	54
<i>K. tunicata</i> - <i>S. sessilis</i>	0.16 (0.27)	1.04 (0.58) —	36.76 (23.32)	0.17	0.22	19
<i>N. ostrina</i> - <i>B. glandula</i>	0.13 (0.10)	0.54 (0.14) ***	11.26 (5.70) —	0.26	9.62E-04	49
<i>N. ostrina</i> - <i>M. trossulus</i>	0.55 (0.07) ***	0.80 (0.10) ***	26.61 (4.25) ***	0.69	9.00E-13	51
<i>P. ochraceus</i> - <i>M. californianus</i>	0.62 (0.13) ***	0.50 (0.21) *	15.99 (8.57) —	0.50	9.05E-05	30
<i>S. purpuratus</i> - <i>S. sessilis</i>	0.52 (0.33)	0.74 (0.67)	24.59 (27.35)	0.19	0.23	17

Significance codes: 0 < ‘***’ < 0.001 < ‘**’ < 0.01 < ‘*’ < 0.05 < ‘—’ < 0.1; R^2 , coefficient of determination; n , sample size.

Table 3.2 (Continued)

Species / Interaction	b	E (eV)	ln(c)	R²	p-val	n
<i>Species interaction strength</i>						
<i>N. canaliculata</i> - <i>B. glandula</i>	0.38(0.39)	-0.01(0.004)*	-0.008(0.01)	0.16	0.031	44
<i>N. canaliculata</i> - <i>M. trossulus</i>	1.09(0.16)***	0.013(0.002)***	0.026(0.004)***	0.58	1.82E-10	54
<i>K. tunicata</i> - <i>S. sessilis</i>	0.37(0.24)	0.005(0.003)-	-0.009(0.006)	0.24	0.11	19
<i>N. ostrina</i> - <i>B. glandula</i>	2.41(1)*	-0.021(0.018)	-0.057(0.025)*	0.13	0.037	49
<i>N. ostrina</i> - <i>M. trossulus</i>	2.62(0.73)***	0.026(0.013)*	-0.062(0.018)**	0.24	0.0014	51
<i>P. ochraceus</i> - <i>M. californianus</i>	0.85(0.93)	0.046(0.014)**	-0.025(0.023)	0.3	0.0083	30
<i>S. purpuratus</i> - <i>S. sessilis</i>	0.61(1)	0.02(0.012)	-0.016(0.025)	0.18	0.26	17

Significance codes: 0 < ‘***’ < 0.001 < ‘**’ < 0.01 < ‘*’ < 0.05 < ‘-’ < 0.1; R^2 , coefficient of determination; n , sample size.

Table 3.3 Coefficients for the optimal models of the effect of body size and temperature on metabolic rate, ingestion rate and species interaction strengths. AICc values indicated a better fit over the UTD models. The models are of the form: $y = \beta_0 + \beta_1(\ln M) + \beta_2(\ln M^2) + \beta_3 \frac{1}{kT} + \beta_4 \frac{1}{kT^2} + \beta_5 \frac{\ln M}{kT}$, where M is body mass (g), T is water temperature (K), and k is Boltzmann's constant (8.62×10^{-5} eVK $^{-1}$). Note that not all terms are present in each model. All models were statistically significant ($p < 0.05$).

Log metabolic rate	β_0	β_1	β_3	β_4	R^2
<i>N. canaliculata</i>	-2419 (613.2)***	0.55 (0.07)***	119 (30.13)***	-17040 (4294)***	0.84
<i>N. ostrina</i>	-2153 (1000)*	0.57 (0.10)***	106.3 (49.1)*	-15280 (6992)*	0.75
Log ingestion rate	β_0	β_1	β_2	β_3	
<i>N. canaliculata - B. glandula</i>	-5.39 (9.57)	-0.52 (0.14)***	-0.19 (0.09)*	-0.15 (0.23)	0.26
<i>N. ostrina - B. glandula</i>	12.77 (4.87)*	-0.45 (0.16)**	-0.51 (0.12)***	-0.58 (0.12)***	0.47
Species interaction strength	β_0	β_1	β_2	β_5	
<i>N. canaliculata - M. trossulus</i>	1.07 (0.15)***	0.41 (0.17)*	-0.03 (0.004)***	-0.01 (0.004)*	0.63
	β_0	β_1	β_2	β_3	
<i>N. canaliculata - B. glandula</i>	0.49 (0.38)	-0.019 (0.0056)**	-0.0074 (0.0034)*	-0.012 (0.0092)	0.24
<i>N. ostrina - B. glandula</i>	2.6 (0.95)**	-0.09 (0.03)**	-0.06 (0.02)**	-0.06 (0.02)*	0.25
<i>N. ostrina - M. Trossulus</i>	2.49 (0.7)***	0.07 (0.02)**	0.03 (0.013)*	-0.06 (0.017)**	0.33

Significance codes: 0 < *** < 0.001 < ** < 0.01 < * < 0.05 < - < 0.1; R^2 , coefficient of determination

Table 3.4 Consumer thermal impact estimates ($CTI = E_J - E_I$) using only significant ($p < 0.05$) estimates of activation energies from measurements of the temperature dependence of ingestion rate E_J and metabolic rate E_I in the present study and from the literature.

Consumer	Resource	E_J	E_I	CTI
<i>M. californianus</i>	<i>Rhodomonas spp.</i>	0.33*	0.76	-0.43
<i>M. trossulus</i>	<i>Rhodomonas spp.</i>	0.33*	0.77	-0.44
<i>N. canaliculata</i>	<i>M. trossulus</i>	0.82	0.59 / 1.40†	0.23 / -0.58†
<i>N. ostrina</i>	<i>B. glandula</i>	0.53	1.02	-0.49
<i>N. ostrina</i>	<i>M. trossulus</i>	0.80	1.02	-0.22
<i>P. ochraceus</i>	<i>M. californianus</i>	0.50	0.77	-0.27

*This value comes from a weighted average of estimates from the literature (Jorgensen *et al.* 1990; Kittner & Riisgard 2005)

†These estimates are over the range of temperatures where the relationship is linear.

Figure 3.1 Metabolic rates as a function of water temperature (a-g) and body mass (h-n) for seven species of rocky intertidal invertebrates: *M. californianus* (a, h), *N. canaliculata* (b, i), *K. tunicata* (c, j), *N. ostrina* (d, k), *P. ochraceus* (e, l), *M. trossulus* (f, m), and *S. purpuratus* (g, n). Variables were log transformed and metabolic rates were normalized by body mass (a-g) or temperature (h-n). Statistically significant UTD regression models ($\alpha \leq 0.05$) are plotted in black. The grey regression line in subplot b represents a regression on the increasing linear subset of data (temperatures $\leq 14^{\circ}\text{C}$). The temperature axes scale inversely as $1/kT$ (1/eV), where T is temperature (K) and k is Boltzmann's constant (8.62×10^{-5} eVK $^{-1}$). A transformed temperature scale in $^{\circ}\text{C}$ is on the top axis (a-g).

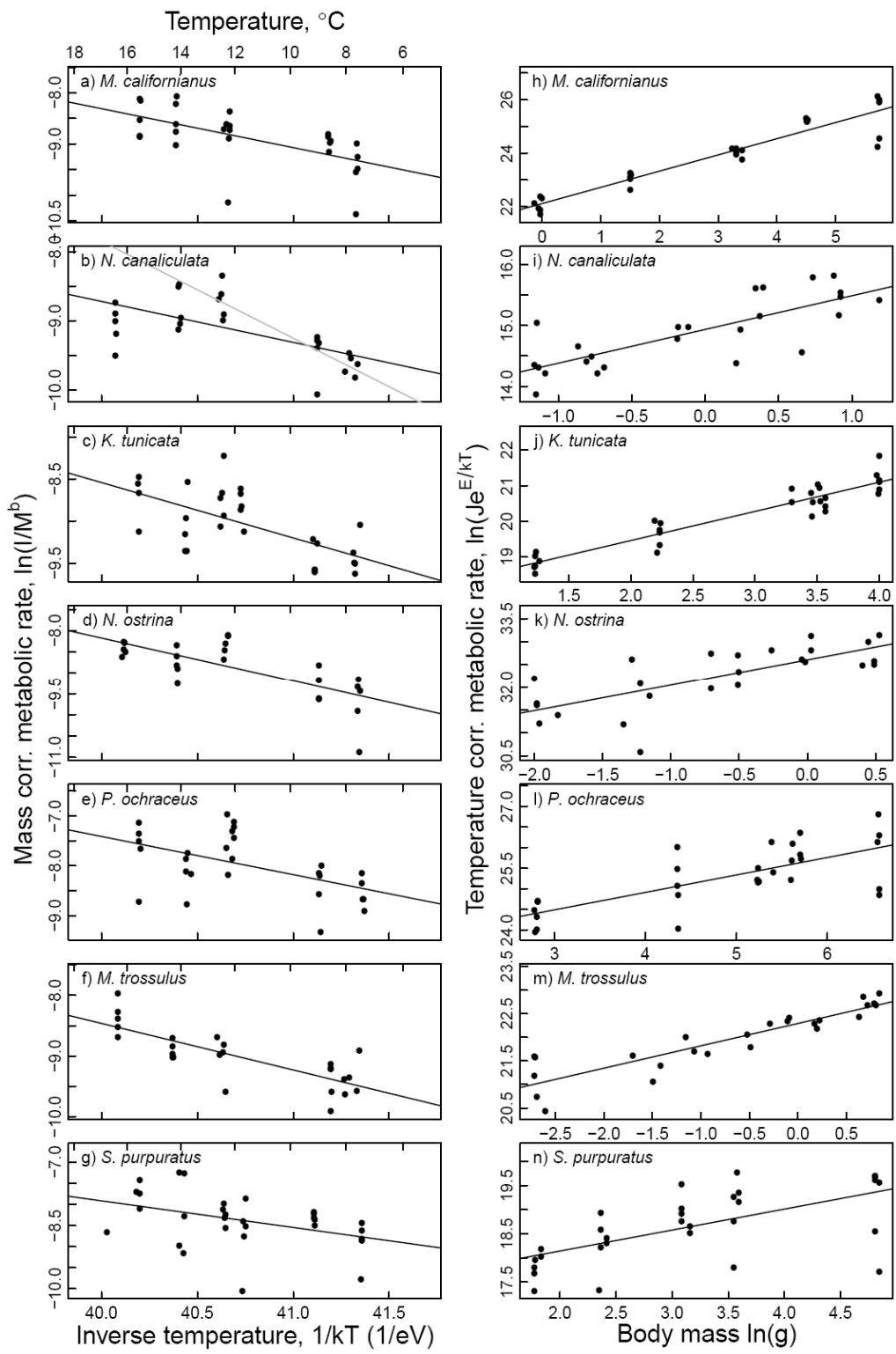
**Figure 3.1**

Figure 3.2 Ingestion rates as a function of water temperature (a-g) and body mass (h-n) for seven rocky intertidal species interactions: *N. canaliculata* - *B. glandula* (a, h), *N. canaliculata* - *M. trossulus* (b, i), *K. tunicata* - *S. sessilis* (c, j), *N. ostrina* - *B. glandula* (d, k), *N. ostrina* - *M. trossulus* (e, l), *P. ochraceus* - *M. californianus* (f, m), and *S. purpuratus* - *S. sessilis* (g, n). Variables were log transformed and ingestion rates were normalized by body mass (a-g) or temperature (h-n). Statistically significant UTD regression models ($\alpha \leq 0.05$) are plotted in black. The temperature axes scale inversely as $1/kT(1/\text{eV})$, where T is temperature (K) and k is Boltzmann's constant ($8.62 \times 10^{-5} \text{ eVK}^{-1}$). A transformed temperature scale in $^{\circ}\text{C}$ is on the top axis (a-g).

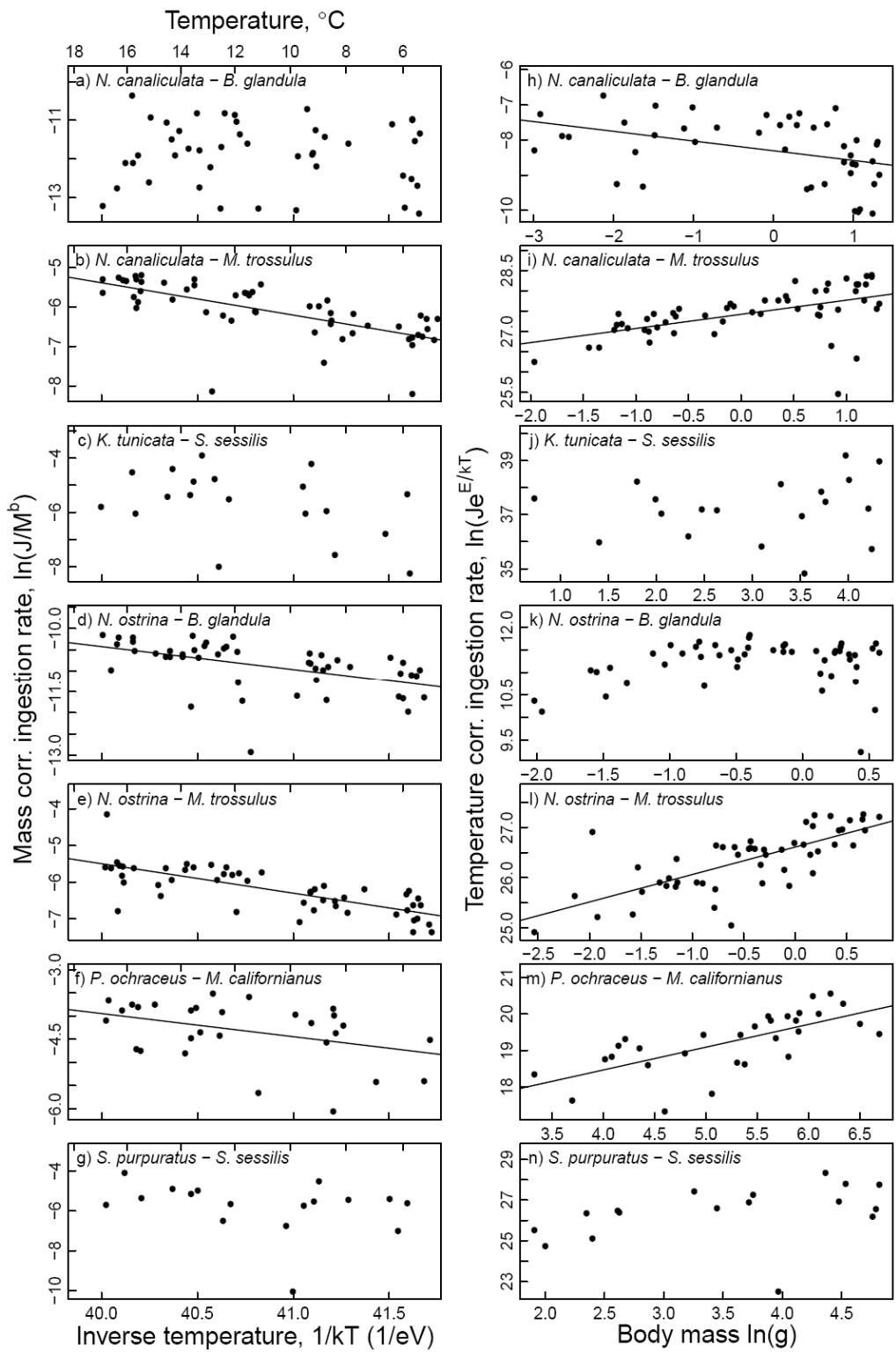
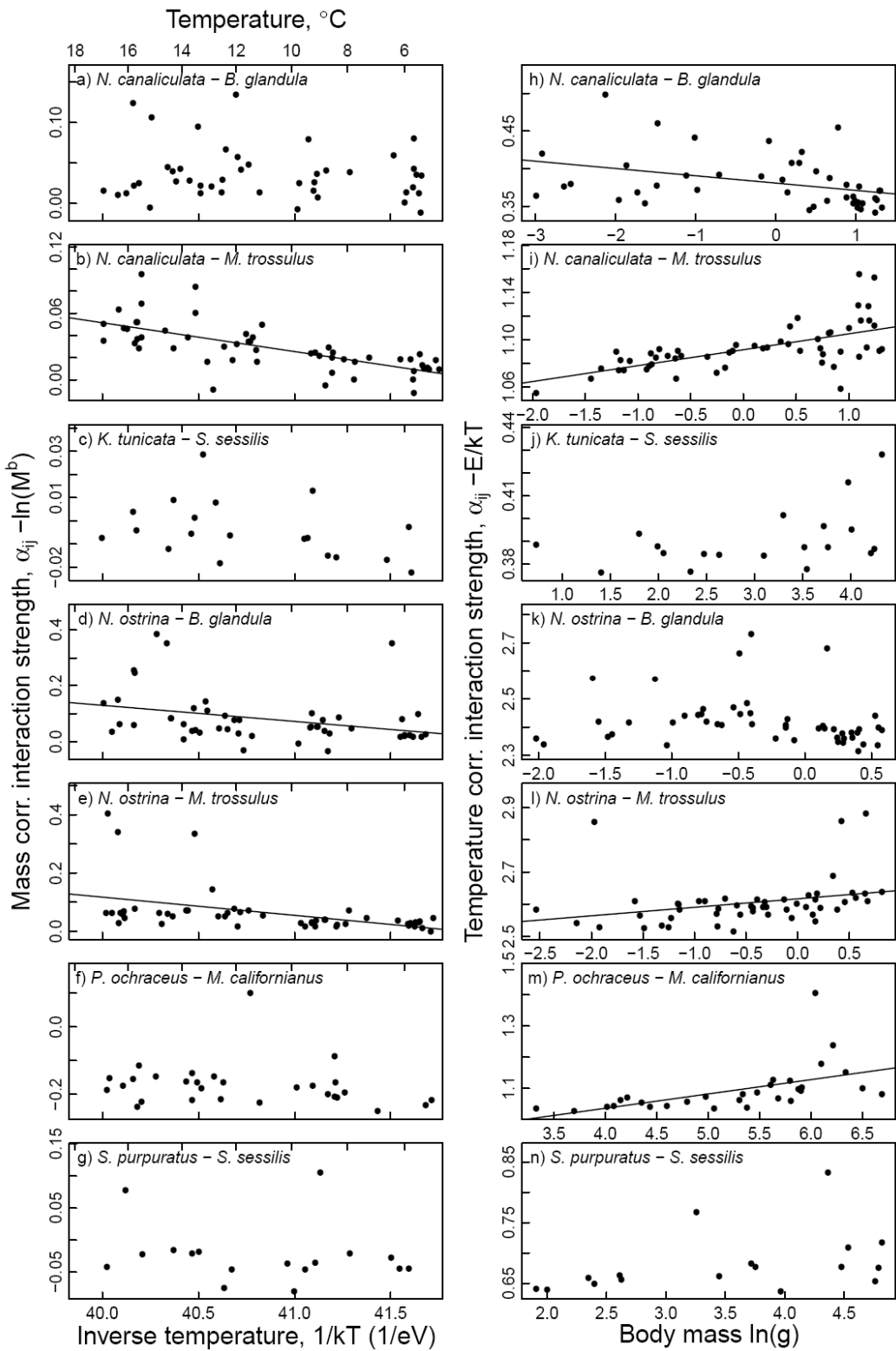
**Figure 3.2**

Figure 3.3 Log ratio interaction strength as a function of water temperature (a-g) and body mass (h-n) for seven rocky intertidal species interactions: *N. canaliculata* - *B. glandula* (a, h), *N. canaliculata* - *M. trossulus* (b, i), *K. tunicata* - *S. sessilis* (c, j), *N. ostrina* - *B. glandula* (d, k), *N. ostrina* - *M. trossulus* (e, l), *P. ochraceus* - *M. californianus* (f, m), and *S. purpuratus* - *S. sessilis* (g, n). Variables were log transformed and interaction strengths were normalized by body mass (a-g) or temperature (h-n). Statistically significant UTD regression models ($\alpha \leq 0.05$) are plotted in black. The temperature axes scale inversely as $1/kT$ (1/eV), where T is temperature (K) and k is Boltzmann's constant (8.62×10^{-5} eVK $^{-1}$). A transformed temperature scale in °C is on the top axis (a-g).

**Figure 3.3**

CHAPTER 4: A Field Test of the Mechanistic Effect of Body Temperature on Species Interaction Strength

ABSTRACT

The metabolic theory of ecology provides a basis from which to scale up the mechanistic effects of temperature (due to the kinetics of biochemical reaction rates) from the organismal level to the level of species interactions. However, this clean, mechanistic effect of temperature is usually quantified under lab conditions. In the field, this temperature effect is complicated by the idiosyncrasies of species behavior that can compensate for such bioenergetic constraints through acclimation and the evolution of coping behaviors, such as seeking refuge from stressful temperatures. We used long term predation rate data to test if the effect of temperature on ingestion rates and the strength of species interactions is apparent under field conditions. We related temperature to a series of field measurements of *per capita* mussel predation rates by the ochre sea star, *Pisaster ochraceus*, which is a keystone predator in rocky intertidal communities and compared results to lab estimates. We used two different temperature measures: mean daily water temperature and a bio-mimetic estimate of *P. ochraceus* body temperature. Whereas mean daily water temperatures is only an accurate estimate of *P. ochraceus* body temperatures at high tide, the bio-mimetic approximates both high and low tide body temperatures. The data showed a strong signal of temperature on *per capita* ingestion rates and species interaction strengths. Bio-mimetic temperature was a better predictor than water temperature, despite nearly half the sample size, providing further evidence for the influence of the mechanistic effect of body temperature on ingestion rates and species interaction strengths of this keystone predator. However, seasonal winter torpor and the effects of the unique method in which *P. ochraceus* avoids high body temperatures were also apparent in the data, leaving room for the wonderful diversity of nature to compensate for this mechanistic constraint.

4.1 INTRODUCTION

The metabolic theory of ecology (MTE) predicts how the temperature and body size dependency of metabolic rate governs energetic requirements and the pace of ecological processes from the organismal level to the community level (Brown *et al.* 2004). Indeed, body temperature and body size affect a wide range of organismal biological rates, particularly for ectotherms. These effects include metabolic rate (Gillooly *et al.* 2001), larval developmental rate (O'Connor *et al.* 2007), autotroph production rates (Lopez-Urrutia *et al.* 2006), and many others (see reviews by Dell *et al.* 2011; Somero 2011). Effects at the level of species interactions, including ingestion rates and the *per capita* strength of species interactions, are the end result of a series of physiological processes occurring at the organismal level (Woodward *et al.* 2010). These include foraging activity, prey handling times and digestion rates, all of which are influenced by temperature and body size (Sanford 1999, 2002a, b; Yee & Murray 2004; Pincebourde *et al.* 2008a, b; Yamane & Gilman 2009; Rall *et al.* 2010; Englund *et al.* 2011; Vucic-Pestic *et al.* 2011). Since warming is the most evident consequence of climate change, the MTE may be a useful theoretical framework for understanding climate change effects on ecological communities (Woodward *et al.* 2010).

That such a fundamental effect of temperature on the kinetics of biochemical reactions can manifest itself in such diverse ways is remarkable. Equally remarkable, are the diverse strategies in which organisms evolve to compensate for these bioenergetic constraints or to take advantage of fluctuating environmental conditions. Many ectothermic species behaviorally optimize their body temperatures, such as lying in the sun to speed up the digestion of a meal (e.g. snakes, Dorcas *et al.* 1997; and locusts, Coggan *et al.* 2011). In rocky intertidal ecosystems along the Oregon coast, many species exhibit behavioral regulation of body temperature and adaptation to wide temperature fluctuations. At high tide, water temperatures vary from ~8 to 17°C; however, at low tide, over the course of only a few hours, temperatures may drop below freezing or approach 30 °C due to fluctuations in air temperature. Most mobile organisms avoid the

extremes of these temperature fluctuations by foraging at high tide and taking refuge at low tide in the subtidal zone or in cracks and crevices. Sedentary organisms are dependent on energetically expensive coping mechanisms, such as the production of heat shock proteins. Some species may also enter a low energy use state known as torpor or diapause to conserve energy during periods of unfavorable conditions. For example, the sea star *Pisaster ochraceus* (Brant), keystone predators in the rocky intertidal, stockpile nutrients from periods of intensive feeding in their digestive glands (Mauzey 1966; Lawrence & Lane 1982). When temperatures are cold and foraging is inefficient, *P. ochraceus* remain inactive in low-zone surge channels and slowly, but efficiently, convert this stored energy into growth (Sanford 2002a).

Because most measurements quantifying the effect of temperature on ingestion rates and species interaction strengths are made under lab conditions, a key question that remains unanswered is: What is the capacity of species to adjust their behavior, adapt or acclimate to the energetic constraint imposed by temperature? The answer will help determine the usefulness of the MTE for generalizing the effect of body temperature and body size on the strength of species interactions.

Our objective was to analyze the effect of temperature in field measurements of ingestion rates and *per capita* species interaction strengths, and compare the results to measurements taken under controlled lab conditions. Quantifying the ability of species to compensate for temperature effects is particularly important in systems with highly fluctuating temperatures, such as the rocky intertidal, which provide many opportunities for species to optimize their energy use. We used arguably the most pivotal species interaction in the rocky intertidal community, the strength of predation by the keystone predator *P. ochraceus* on its preferred prey and dominant space occupier, the mussel *Mytilus californianus*. We hypothesized that field measurements of ingestion rates and *per capita* species interaction strengths of *P. ochraceus* on *M. californianus* would: 1) increase with water temperature due to faster rates of

metabolism, and 2) increase with body size, since larger organisms can move faster and eat faster.

4.2 METHODS

In Chapter 3, I parameterized the ‘universal temperature dependence’ (UTD) model, a theoretical model derived from first principles of biochemical kinetics and allometry (Gillooly et al. 2001; Brown et al. 2004), for *P. ochraceus* by measuring predation rates on *M. californianus* under lab conditions at various water temperatures and body sizes. Under the UTD, ingestion rates, J_{ij} (J·s-1), and *per capita* species interaction strength, α , of ectothermic organisms depend jointly on body mass, M (g) and environmental temperature, T (K) as:

$$J = j_0 M_j^{b_J} e^{\frac{-E_J}{kT}} \quad (1a)$$

$$e^\alpha = \alpha_0 M_j^{b_\alpha} e^{\frac{-E_\alpha}{kT}} \quad (1b)$$

where b is an allometric exponent, E (eV) is the activation energy, k is the Boltzmann’s constant (8.62×10^{-5} eV·K-1) and j_0 and α_0 are normalization constants. The exponential function is used for species interaction strength because the metric for interaction strength is calculated as the natural logarithm (see the calculations for the log-response ratio below). Taking the natural logarithm of both sides of equations 1a-b linearizes the UTD model and makes it easier to visualize the scaling coefficients for the effects of body size and temperature as b and E , respectively:

$$\ln(J) = b_J \ln(M_j) - E_J \left(\frac{1}{kT} \right) + \ln(j_0) \quad (2a)$$

$$\alpha = b_\alpha \ln(M_j) - E_\alpha \left(\frac{1}{kT} \right) + \ln(\alpha_0) \quad (2b)$$

4.2.1 Field data

All data were collected by the Partnership for the Interdisciplinary Study of Coastal Oceans (PISCO) from 2007 through 2012 at five rocky intertidal sites along the Oregon, USA coastline: Fogarty Creek (FC; $44^\circ 50' 24''$ N, $124^\circ 3' 36''$ W), Boiler Bay

(BB; 44° 49' 48" N, 124° 3' 36" W), Yachats Beach (YB; 44° 19' 12" N, 124° 7' 12" W), Strawberry Hill (SH; 44° 15' N, 124° 7' 12" W), and Cape Blanco (CB; 42° 50' 24" N, 124° 34' 12" W).

Ingestion rates and species interaction strengths of *P. ochraceus* on *M. californianus* were determined by the speed at which *P. ochraceus* consumed transplanted *M. californianus*. In May of each year, *M. californianus* (~ 5 cm in length) were translocated to all the study sites from one collection site, Bob Creek (44° 14' 40" N, 124° 6' 49" W). Five replicate plots of 50 mussels each were placed on cleared rock just below the existing mussel bed at each site. The mussels were held byssal thread side down in cages of black plastic mesh, which allowed the mussels to reattach to the rock. The mesh was removed in July of each year, and the number of live *M. californianus* in each plot was counted at ~2-4 week intervals until the end of each year.

The density and body size structure of the *P. ochraceus* populations at each site were quantified in July of each year for all sites except YB, for which only data for 2012 were available. Average density was determined from counts within 5, 10 m x 1 m belt transects in the low zone of each site. The first 200 individuals encountered within the belt transects were weighed to determine the body size distribution.

The analyses were repeated using two different temperature data sets. The first data set was mean daily water temperatures from temperature loggers (StowAway Tidbit Temperature Loggers, Onset Computer Corporation, TBI32-05+37) bolted to low zone rocks within wire mesh cages at each site. The loggers measured ambient temperature at 1 hour intervals. Tide tables were used to remove low tide air temperature measurements and the remaining water temperature measurements were averaged for each day. The second, bio-mimetic temperature data set more closely estimated the body temperature of *P. ochraceus* (Pincebourde *et al.* 2008a), which are typically exposed to aerial temperatures at low tide but have the capacity to buffer their body temperatures against air temperature by retaining water (Pincebourde *et al.* 2009). We used a bio-mimetic data logger based on the design developed by Lauren Szathmary (University of South Carolina, Columbia) and described in Pincebourde *et al.* (2008a). We modified the design

for use on the U.S. West coast where wave forces are considerably higher. After placing the TidbiT temperature logger inside a commercially available cleaning sponge, we inserted the sponge into the center of a double-walled mesh tube created by unfolding two S.O.S Tuffy® mesh pads and inserting one into the other. The ends of the mesh tubes were folded under and secured at each end with two 2 ¼" stainless steel lag screws with wide, 1 ½" washers. We left enough room in the mesh so that when attached to the rock the mesh was snug but did not compress the water out of the sponge. Two bio-mimetic loggers were bolted to rock just below the mussel bed at each site. In addition to the four lag screws, the central sponge part of the logger was secured to the rock using epoxy putty (Z-spar splash zone compound A-788, Kop-Coat), which creates good thermal contact with the rock and helps prevent wave action from tearing the mesh away from the lag screws. Due to deterioration of the sponge over time, loggers were replaced twice per year. Daily averages of the bio-mimetic temperature data were used without removing low-tide temperatures. Bio-mimetic temperature data were only available for 2009 through September of 2011.

4.2.2 Calculations

We calculated *P. ochraceus* – *M. californianus* ingestion rates and species interaction strengths over each 2-4 week sampling interval for each plot. If all the mussels were eaten in a plot, that sampling interval (and all remaining intervals for that replicate plot) was removed from the analysis since we could not calculate how quickly they were eaten.

To more easily compare statistical models developed from the field data to the theoretical models parameterized with lab experiments, we used the same units for the response and predictor variables. Ingestion rate, J ($\text{J}\cdot\text{s}^{-1}$), was estimated as:

$$J = (N_e M \varepsilon) / t \quad (3)$$

where N_e is the number of mussels eaten, M is the estimated average mussel shell-free wet mass (7.95 g) based on a length-mass relationships (ACI, unpublished data), t is time in seconds, and energy content of *M. californianus*, ε , was set to 6173 $\text{J}\cdot\text{g}^{-1}$

¹ of ash free wet mass (BAM, unpublished data). We chose the most widely used metric of species interaction strength, α , the log ratio of prey abundance at the end and the start of each sampling interval divided by the number of days in the interval (Berlow *et al.* 1999; Rall *et al.* 2010):

$$\alpha = \left| \frac{\ln \left(\frac{N_i - N_e}{N_i} \right)}{t} \right| \quad (4)$$

where t the number of days, N_i is the mussel abundance at the beginning of the sampling interval and N_e is the number of prey eaten over the sampling interval. These population measures of ingestion rate and species interaction strength were converted to *per capita* measures by dividing by the annual density of *P. ochraceus* (m^{-2}) measured at each site. It was necessary to use the log-transformation of these response variables to meet the assumption of Gaussian distribution in the regression analyses. So that the zeros in the analysis could also be logged, I added 0.5 to all the counts of number of mussels eaten, N_e . For the predictor variables, body mass was logged, and the temperature data was converted to the units used in the UTD model (inverse temperature in Kelvin multiplied by the Boltzmann's constant).

4.2.3 Statistical analyses

Our *a priori* objective was to assess *P. ochraceus* – *M. californianus* *per capita* ingestion rates and species interaction strengths as a function of temperature and body size as predicted by the UTD model. However, we also assessed alternative, optimal statistical models using day-of-the-year for each sampling event as potential covariate. Because repeated measures were made successively on each replicate plot and plots were nested spatially within each site and within each year, we could not assume these measurements were independent of each other. We used linear mixed effects regression analysis to assess the value of incorporating the nested structure as well as an auto-correlation structure as random effects in the model. Using sample size corrected Akaike's Information Criterion (AICc) comparisons, the optimal random effects included random intercepts for the nested spatial structure of the plots. An auto-regressive model

of order 1 was the optimal auto-correlation structure, although this was not a statistically significant improvement in fit.

We initially fit the field data to the theoretical UTD model, but then used AICc-based model selection techniques to determine the optimal fixed structure of the models predicting *per capita* ingestion rates and species interaction strengths based on inverse temperature (both water and bio-mimetic), log body size and day of the year.

4.3 RESULTS

As expected from the laboratory measurements, *per capita* species interaction strength increased with both water temperatures and bio-mimetic temperatures (or decreased with respect to inverse temperature), in the fit to the theoretical UTD model, although the slopes were not as steep as for the laboratory measurements (Table 4.1). Unlike the laboratory measurements, the effect of temperature on *per capita* ingestion rates was not statistically significant in the UTD model and there was little effect of body mass (Table 4.1).

All four optimal models fit the data better over the UTD models, based on AICc comparisons (Table 4.2). The optimal structure of the fixed effects differed between the two temperature data sets, but was the same for each of the response variables, *per capita* interaction strength and ingestion rate. The bio-mimetic temperature data produced a better fit to the both the SIS and ingestion rate data sets than the water temperature data, despite only half the sample size. For the analyses with mean daily water temperature there was a significant interaction between log body mass and inverse water temperature. A one unit increase in the log body mass of *P. ochraceus* caused the effect of inverse temperature to be more negative and closer to the slopes calculated in the analyses with the bio-mimetic data.

Body size did not have a statistically significant main effect on either ingestion rates or species interaction strength, however body size did modify the effects of temperature or day-of-the-year on ingestion rates and species interaction strength. There

was a limited range of mean body masses among the five *P. ochraceus* populations (Fig. 4.1).

Day-of-the-year had a significant, negative effect on both species interaction strength and ingestion rates with both temperature data sets. There was a relatively high negative correlation between day-of-the-year and mean daily water temperatures ($r = -0.41$), however this correlation was reduced with the mean daily bio-mimetic temperature data ($r = -0.27$). An interaction term with body size in the analyses with the bio-mimetic temperature data, suggests that large-bodied sea stars do not exhibit reduced ingestion rates as winter approaches.

4.4 DISCUSSION

Our first hypothesis that increased water temperatures would increase consumer *per capita* ingestion rates and interaction strengths with their prey was supported by the field data. These data did not support the second hypothesis that body size would increase *per capita* ingestion rates and interaction strengths. We argue below that this data set was an insufficient test of the body size hypothesis. The theoretical UTD models were partially supported with respect to temperature; however, the optimal statistical models also included interaction terms with body size and temperature or day-of-the-year and a seasonal effect of day-of-the-year.

Bio-mimetic temperature was a better predictor than mean daily water temperatures for both species interaction strength and ingestion rate analyses. Although water temperature is a good proxy for body temperatures at high tide, bio-mimetic temperatures are also able to characterize body temperatures at low tide. Although *P. ochraceus* do not actively forage at low tide, they do continue to digest previously consumed prey items, thus higher body temperatures would speed up digestion rates (Dorcas *et al.* 1997; Coggan *et al.* 2011) and bio-mimetic temperatures would be a better representation of the kinetic effect of body temperature on ingestion rates. The improvement in model fit provided by the bio-mimetic temperature data is further evidence that the effect of temperature is due to kinetic effects on physiology.

The interaction term between water temperature and body size did not appear in the analysis with the bio-mimetic temperature data. This may be because of the unique strategy that *P. ochraceus* has for regulating body temperatures at low tide (Pincebourde et al. 2009). Exposure to high air temperatures at low tide causes *P. ochraceus* to absorb more sea water and increase the volume of its coelomic fluid system during the following high-tide. This added body mass results in greater thermal inertia during the next low-tide and buffers *P. ochraceus* body temperatures against high air temperatures (Pincebourde et al. 2009). Because a larger sea star would have a greater capacity to regulate body temperatures in such a manner, mean daily water temperatures would be a better approximation for the body temperatures of larger sea stars than smaller ones, resulting in a significant interaction term between body size and temperature.

The negative effect of day-of-the-year on ingestion rates and species interaction strength supports previous observations of a reduction in feeding activity of *P. ochraceus* from 60% feeding during the summer to about 10% during the winter (Mauzey 1966); however there was also a correlation between day-of-the-year and water temperature, which reflects the increase in water temperatures after the fall transition from summer upwelling of cold, nutrient rich water bottom waters to warm, nutrient depleted surface waters. If the effect of day-of-the-year was due to temperature, then day-of-the-year would have had a positive effect on predation rates. This correlation was not as strong for the bio-mimetic temperature data, likely because the bio-mimetic data also reflect lower air temperatures later in the year. The positive interaction between day-of-the-year and body size indicates that this seasonal effect is reduced for populations of larger-bodied *P. ochraceus*. This may also be a result of the greater thermal inertia of larger-bodied sea stars (Pincebourde et al. 2009). In winter, the water is relatively warmer compared to the cold, aerial temperatures and large-bodied sea stars would be better equipped to maintain higher body temperatures at low tide.

The lack of a direct effect of body mass did not support our second hypothesis. However, this may be because we were unable to measure the body sizes of the individual *P. ochraceus* that actually consumed the mussels and were forced to use

population means. Since there was little variation between population means at most sites, this data set may not be able to adequately test this hypothesis. Furthermore, only one body size of mussel prey was provided, which may have attracted only a particular size class of *P. ochraceus*. Small *P. ochraceus* are less likely to forage for prey that are too large for them to handle efficiently and it may be more energetically efficient for larger *P. ochraceus* to go after larger prey. Thus, there may have been an even smaller variation in body size between sites for the sea stars that actually consumed the mussels.

We chose to calculate and analyze two metrics of the predation data: *per capita* ingestion rates and species interaction strength. Although this was useful for the comparison to prior lab measurements and readers may find having the two metrics useful for comparisons to other species interactions, in this case the two metrics are essentially measuring the same thing. There is little evidence of any strong indirect, or non-trophic, effects of *P. ochraceus* on *M. californianus*.

Our study demonstrates that ingestion rates and species interaction strengths of the keystone predator *P. ochraceus* show a clear influence of the mechanistic, kinetic effect of temperature in both laboratory and field studies. This result supports the use of simple energetic constraints when scaling up temperature effects from the organismal level to the community level. However, our analysis also reveals the influence of seasonal torpor and behavioral regulation of body temperatures. Thus allometric and temperature scaling of biological rates in community models would likely make a useful baseline model, but must be built upon with the complexities of unique species adaptations, particularly. This is especially important for keystone species with are highly influential on many other species in their communities.

ACKNOWLEDGEMENTS

Many thanks go to all the lab technicians that routinely deploy and monitor the predation rate experiments and manage the data. Funding was provided by a National Science and Engineering Research Council of Canada pre-doctoral fellowship to ACI and

from PISCO, a long-term ecological consortium which is partially funded by the David and Lucile Packard Foundation and the Gordon and Betty Moore Foundation.

Table 4.1 Regression coefficients and statistics for the UTD models of the effect of body mass and water temperature on *per capita* ingestion rates and interaction strengths of *P. ochraceus* feeding on *M. californianus*. The coefficients with standard errors in parentheses include b , the allometric exponent for the effect of body size; E , the activation energy (eV) for the effect of temperature, and $\ln(c)$, the normalization constant. Parameter estimates are provided based on lab measurements from Chapter 3 and field measurements using either mean daily water temperatures or mean daily bio-mimetic temperatures.

UTD Model for:	b	E (eV)	$\ln(c)$	R^2	p-val	n
Log per capita ingestion rate						
Lab measurements	0.62 (0.13) ***	0.50 (0.21) *	15.99 (8.57) $^-$	0.50	9.05E-05	30
Field (water temperatures)	-0.97 (0.61)	-0.05 (0.41)	-0.48 (17.27)			305
Field (bio-mimetic temperatures)	-1.16 (1.14)	1.39 (0.83)	59.29 (34.52)			146
Log per capita species interaction strength						
Lab measurements	0.85 (0.93)	0.046 (0.014)**	-0.025 (0.023)	0.3	0.0083	30
Field (water temperatures)	-0.01(0.005) $^-$	0.006 (0.003)*	0.32 (0.13)*			305
Field (bio-mimetic temperatures)	-0.01 (0.01)	0.02 (0.005)***	0.88 (0.20)			146

Table 4.2 The optimal fixed structure for the models predicting field measurements of log *per capita* species interaction strength and log *per capita* ingestion rate based on inverse temperature (Temp), log body mass (Mass) and day-of-the-year (Day). Each analysis was performed separately for the two temperature data sets: mean daily water temperatures and mean daily bio-mimetic temperature data. ΔAICc values are in comparison to the UTD models presented in Table 4.1.

	Coefficient (SE)	df	t-value	p-value
Water temperature data:				
Log ingestion rate, ΔAICc to UTD model: -28.07				
(Intercept)	-3.614 (0.327)	194	-11.07	0.000
Temp	-0.739 (0.424)	194	-1.74	0.083
Mass	-0.751 (0.574)	17	-1.31	0.208
Day	-0.013 (0.002)	194	-5.94	0.000
Temp:Mass	-2.440 (0.929)	194	-2.63	0.009
Log <i>per capita</i> SIS, ΔAICc to UTD model: -12.17				
(Intercept)	-6.287 (0.305)	194	-20.61	0.000
Temp	-1.170 (0.455)	194	-2.57	0.011
Mass	-1.281 (0.690)	17	-1.86	0.081
Day	-0.007 (0.002)	194	-2.80	0.006
Temp:Mass	-2.960 (1.002)	194	-2.96	0.004
Bio-mimetic temperature data:				
Log ingestion rate, ΔAICc to UTD model: -25.46				
(Intercept)	-3.677 (0.800)	93	-4.60	0.000
Day	-0.014 (0.003)	93	-5.10	0.000
Mass	-0.334 (1.084)	7	-0.31	0.767
Temp	-2.151 (0.799)	93	-2.70	0.008
Day:Mass	0.027 (0.009)	93	2.99	0.004
Log <i>per capita</i> SIS, ΔAICc to UTD model: -12.34				
(Intercept)	-6.457 (0.827)	93	-7.80	0.000
Day	-0.008 (0.003)	93	-2.53	0.013
Mass	-0.254 (1.121)	7	-0.23	0.827
Temp	-3.227 (0.838)	93	-3.85	0.000
Day:Mass	0.033 (0.010)	93	3.45	0.001

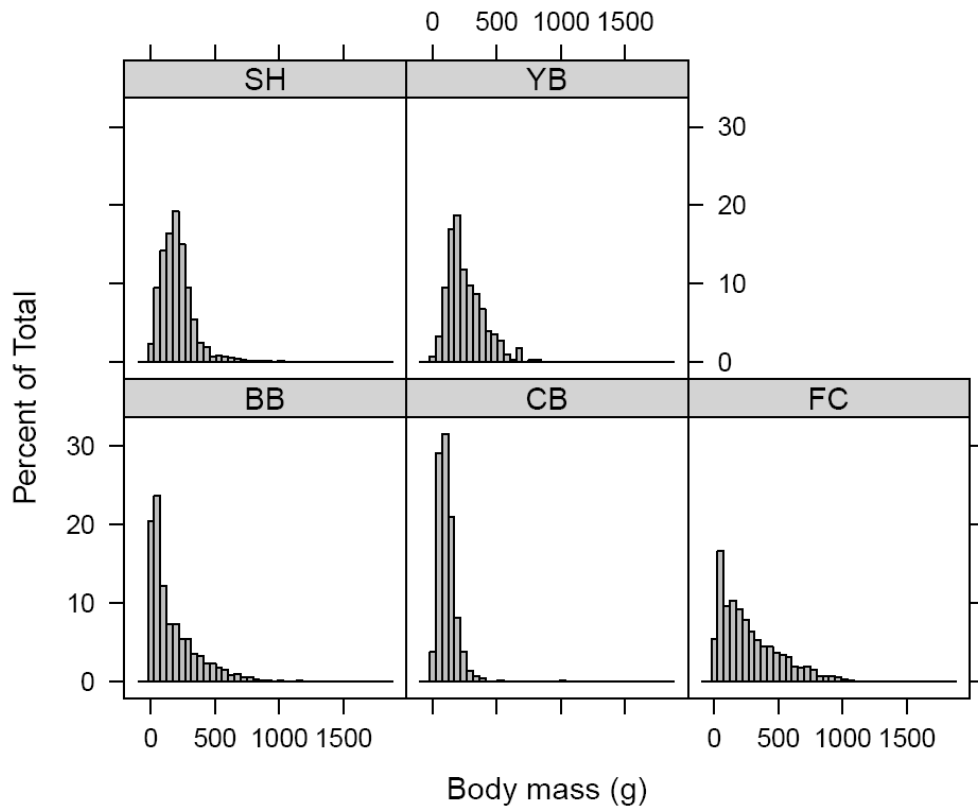


Figure 4.1 Histograms of *P. ochraceus* body mass distributions for each of the field sites from 2007 to 2012. Data for YB are only from 2012.

**CHAPTER 5: Climate-Driven Trends and Ecological Implications of Event-Scale
Upwelling in the California Current System**

Alison C. Iles, Tarik C. Gouhier, Bruce A. Menge, Julia S. Stewart, Alison J. Haupt, and
Margaret C. Lynch

Global Change Biology
Volume 18(2): 783-796
doi: 10.1111/j.1365-2486.2011.02567

ABSTRACT

Eastern boundary current systems are among the most productive and lucrative ecosystems on Earth because they benefit from upwelling currents. Upwelling currents subsidize the base of the coastal food web by bringing deep, cold and nutrient-rich water to the surface. As upwelling is driven by large-scale atmospheric patterns, global climate change has the potential to affect a wide range of significant ecological processes through changes in water chemistry, water temperature, and the transport processes that influence species dispersal and recruitment. We examined long-term trends in the frequency, duration, and strength of continuous upwelling events for the Oregon and California regions of the California Current System in the eastern Pacific Ocean. We then associated event-scale upwelling with up to 21 years of barnacle and mussel recruitment, and water temperature data measured at rocky intertidal field sites along the Oregon coast. Our analyses suggest that upwelling events are changing in ways that are consistent with climate change predictions: upwelling events are becoming less frequent, stronger, and longer in duration. Additionally, upwelling events have a quasi-instantaneous and cumulative effect on rocky intertidal water temperatures, with longer events leading to colder temperatures. Longer, more persistent upwelling events were negatively associated with barnacle recruitment but positively associated with mussel recruitment. However, since barnacles facilitate mussel recruitment by providing attachment sites, increased upwelling persistence could have indirect negative impacts on mussel populations. Overall, our results indicate that changes in coastal upwelling that are consistent with climate change predictions are altering the tempo and the mode of environmental forcing in nearshore ecosystems, with potentially severe and discontinuous ramifications for ecosystem structure and functioning.

5.1 INTRODUCTION

Eastern boundary current systems, such as the California Current System (CCS) in the eastern Pacific Ocean, are among the most productive ecosystems on Earth. Although such regions account for less than 1% of the ocean surface, they support 20%

of global commercial fishery yields (Pauly & Christensen 1995). The high productivity of these systems is largely dependent upon coastal upwelling, a wind-driven process that promotes the growth of phytoplankton, the base of the coastal food web, by bringing large pulses of deep, nutrient-rich water to the sunlit surface. As the upwelling process is driven by large-scale atmospheric patterns, it is expected to respond to global climate change. In 1990, Andrew Bakun hypothesized that increased concentrations of greenhouse gases would drive stronger and more persistent upwelling (Bakun 1990), a prediction recently confirmed along the coast of California (Garcia-Reyes & Largier 2010). Coastal ecosystems—and the services they provide—will likely demonstrate a diverse range of significant, complex, and potentially discontinuous responses to changes in the upwelling process (Harley *et al.* 2006). Our understanding of these responses is critical for successful ecosystem-based management of these important systems.

Coastal upwelling occurs when equatorward wind stress along the coast drives surface waters offshore, a phenomenon known as Ekman transport. Surface waters are replaced by subsurface waters that are drawn up from depth along the coast (Huyer 1983). Periodic reversals of upwelling favorable winds, termed ‘wind relaxations’, break the upwelling process into a series of upwelling events (Huyer 1983; Papastefanou *et al.* 2006; Melton *et al.* 2009). Upwelling events are particularly characteristic off the coast of Oregon, with periods of days to weeks, whereas upwelling further south tends to be more persistent with fewer wind relaxations (Huyer 1983). However, there is increasing evidence to suggest that climate change is causing stronger and more persistent upwelling in Eastern boundary current systems around the world (Bakun 1990; Mendelsohn & Schwing 2002; McGregor *et al.* 2007; Garcia-Reyes & Largier 2010). Increased greenhouse gas concentrations cause continents to warm faster than oceans, and thus lead to a more intense pressure gradient in coastal regions as hot air rises over land and cooler air sinks over water (Bakun 1990; Snyder *et al.* 2003). In eastern boundary systems, this increased pressure gradient would favor fewer, longer upwelling events over the course of the upwelling season.

Most prior studies of the long-term effects of global climate change on upwelling systems have focused on the atmospheric and oceanographic conditions that change with the coastal upwelling process, typically at an annual or seasonal temporal scale, such as changes in the seasonal onset of upwelling (Garcia-Reyes & Largier 2010). The scale and focus of this study is on the changing frequency and duration of upwelling events in the CCS and the potential ecological ramifications for a model ecosystem, the rocky intertidal. The Oregon rocky intertidal has long been a hotbed of experimental ecology, which makes it an ideal model system to begin to understand the ecological ramifications of long-term changes to the upwelling regime. Much is understood about how environmental forcing drives community structure in the rocky intertidal, particularly through the recruitment dynamics of two major space occupiers, mussels and barnacles (e.g. Menge *et al.* 1997a; Menge *et al.* 1997b; Menge *et al.* 2003; Menge *et al.* 2009).

Increases in the strength and persistence of upwelling due to climate change has the potential to affect a wide range of significant ecological processes through changes in water chemistry, water temperature, and the transport processes that influence species dispersal and recruitment. The most important and widely recognized ecological consequence of upwelling is the delivery of nutrient-rich waters to the surface, causing blooms of phytoplankton that drive the high productivity of these coastal ecosystems. However, upwelled waters are also low in dissolved oxygen and any phytoplankton production that enters the detrital pool can further deplete oxygen concentrations at depth, due to bacterial respiration of sinking detritus (Bakun *et al.* 2010). Additional phytoplankton production resulting from more persistent upwelling would likely exacerbate the current hypoxic, and sometimes anoxic, summertime conditions at depth on the continental shelf (Grantham *et al.* 2004; Chan *et al.* 2008).

Changes in the frequency and duration of upwelling events would also have consequences for how local oceanographic circulation patterns affect larval dispersal and recruitment. For the majority of intertidal and subtidal invertebrates and fishes, reproductive success depends on the dispersal of tiny pelagic larvae and their return to shore (Scheltema 1986). Larvae have been observed to recruit to the adult, rocky

intertidal habitat in episodic pulses linked to the periodic relaxation of upwelling-favorable winds and the subsequent onshore flow of surface waters (Farrell *et al.* 1991; Roughgarden *et al.* 1991; Dudas *et al.* 2009). Not all species exhibit this response however, due to behavioral differences in their position in the water column (Shanks & Brink 2005; Broitman *et al.* 2008; Rilov *et al.* 2008; Shanks & Shearman 2009). Changes in the upwelling regime may also result in species range expansion/contraction. For example, Lima *et al.* (2006) documented the northern expansion of the limpet *Patella rustica* that coincided with a period of weak upwelling, strong inshore poleward circulation, and warmer sea surface temperatures.

The relationship between larval recruitment and wind relaxations also depends on the strength of offshore advection and the effects of coastline and bathymetry on circulation patterns. For example, during upwelling conditions in northern Oregon (north of ~44.5°N), the upwelling current flows roughly parallel and relatively close (<30 km) to the coastline, causing classic Ekman circulation nearshore and setting up a barrier to extreme offshore transport (Castelao & Barth 2005). In central Oregon, from ~44.5 to 43°N, the large shallow submarine Heceta Bank extends >100 km out to sea, causing the upwelling current to flow around its margin. Between the current and the coastline is a large retentive area of re-circulating upwelled water (Barth *et al.* 2005; Kirincich *et al.* 2005). Here, advection is low and plankton biomass is considerably higher than in other areas along the coast (Keister *et al.* 2009). Farther south at 42.8°N, the current encounters Cape Blanco, where the angle of the coastline deviates and the upwelling current separates from the coast and flows strongly offshore. This results in large advective losses far offshore for the plankton community, but the flow is generally weak and not strongly directional in areas close to shore, where surface waters still flow shoreward during wind relaxations (Keister *et al.* 2009). Upwelling in southern Oregon is generally much stronger than further north, with offshore Ekman transport about 3-4 times larger (Samelson *et al.* 2002), making successful larval recruitment potentially more reliant on wind relaxations.

The different response of local currents to upwelling favorable winds has been shown to affect community structure, particularly in rocky intertidal ecosystems (Menge *et al.* 1997a; Kirincich *et al.* 2005). For instance, sites within the retentive Heceta Bank region have higher phytoplankton productivity, higher recruitment and growth rates of filter feeding mussels and barnacles, and stronger rates of predation and grazing than sites further north or south (Menge *et al.* 1997b; Menge *et al.* 2011a). Hence, at sites located within the Heceta Bank region, competitively-superior filter feeding mussels are abundant in the low intertidal zone. Whereas outside of the Heceta Bank region, competitively-inferior macrophytes dominate the low zone (Menge *et al.* 1997b).

In addition to altering recruitment patterns, upwelling can have a profound impact on coastal communities by reducing nearshore water temperatures. The effects of temperature at the organismal level (i.e. biochemical kinetics) are well known, and we are beginning to understand the effects at the population and community levels (Gillooly *et al.* 2001; Brown *et al.* 2004). For instance, cooler water temperatures suppress larval developmental rates and increase the duration of the larval period, which alters dispersal distances and survival (O'Conner 2009). Cooler water decreases the growth rates of the dominate space occupier in the rocky intertidal, the mussel *Mytilus californianus* (Menge *et al.* 2008), but also decreases the feeding rate of its main predator, the sea star *Pisaster ochraceus* (Pincebourde *et al.* 2008a, b). Thus, by altering demographic rates and species interactions in sometimes countervailing ways, temperature can have complex and critical effects on the structure and dynamics of ecological communities.

To detect changes in event-scale upwelling and assess their ecological consequences, we quantified long-term temporal trends in upwelling event frequency, duration and strength over 43 years in Oregon and California. We then related event-scale upwelling to water temperature measurements and recruitment patterns of mussels and barnacles at three rocky intertidal sites over the last 10-21 years. We hypothesized that there would be long-term increasing trends in the persistence and strength of upwelling events, consistent with climate change predictions (Bakun 1990; Bakun *et al.* 2010). We also hypothesized that increased duration of upwelling events would be related to lower

water temperatures and reduced recruitment. Our analyses of long-term upwelling, water temperature and recruitment along the CCS provide us with a unique opportunity to (1) test existing predictions about how climate change will affect the frequency, duration and magnitude of upwelling events along Eastern boundary currents, and (2) determine the likely impacts on the structure and functioning of coastal ecosystems.

5.2 METHODS

5.2.1 Regional upwelling index dataset

We used the Pacific Fisheries Environmental Laboratory (PFEL) 43-year time series (1967 – 2010) of 6-hourly upwelling indices for 5 latitudes along the CCS: 45°N, 42°N, 39°N, 36°N, and 33°N (www.pfeg.noaa.gov; Fig. 1). PFEL calculates coastal upwelling indices from 1°-resolution sea level pressure fields obtained from the U.S. Navy Fleet Numerical Meteorology and Oceanography Center. The index is based on estimates of Ekman mass transport of surface water due to wind stress and the Coriolis force (Bakun et al. 1974). Positive values, the result of equatorward wind stress, are an estimate of the amount of water upwelled from the base of the Ekman layer ($m^3 \cdot \text{second}^{-1} \cdot 100m^{-1}$ of coastline). Negative values imply downwelling, accompanied by the onshore advection of surface waters. We performed all analyses on the offshore component of the upwelling index and replaced missing values using linear interpolation.

5.2.2 Trends in the annual number, duration and magnitude of upwelling events

We calculated annual summary statistics to characterize the frequency, duration, mean and total magnitude of upwelling events, and then related the summary statistics to time using simple linear regression. We considered ‘upwelling events’ as periods of time when the upwelling index is positive. The end of an upwelling event is termed a ‘wind relaxation’ and marks the transition from upwelling to downwelling. For each upwelling event, we recorded the end date (the date of the wind relaxation), the event duration, and the mean and total magnitude of upwelled water over the course of the event. Because there is a lag period between when the winds build and when upwelled water actually

reaches the surface, others have classified only those upwelling events that last for at least 3 days as ‘ecologically significant’ (Garcia-Reyes & Largier 2010). We did not impose an arbitrary minimum duration for upwelling events to qualify as ‘ecologically significant’; instead we determined the robustness of the results using sensitivity analyses. Sensitivity analyses involved sequentially changing the definition of an upwelling event from 0–14 days and rerunning all regressions.

We limited our analyses to the upwelling season, which we defined using the mean daily cumulative upwelling index following Schwing et al. (2006). Specifically, for each latitude, the start (end) of the upwelling season is defined as the date when the climatological mean daily cumulative upwelling index first becomes positive (starts to decline). The upwelling season spanned the spring and the summer in Oregon, the spring through the fall in northern California, and extended to almost the entire year in southern California.

Because the distributions of upwelling event duration, mean magnitude and total magnitude were heavily right-skewed, we applied log-transformations ($\log_{10}+1$) prior to conducting simple linear regression in order to limit the effects of outliers and attain quasi-normality. The p-values of the regressions were calculated by performing 1,000 permutations of the data and determining the proportion of permutations that yielded a coefficient of determination that was greater than or equal to the one obtained with the original data (Legendre and Legendre 1998).

5.2.3 Trends in the intra-annual distribution of event duration and magnitude

Summary statistics such as the annual mean can often conceal more complex intra-annual temporal trends. The sensitivity of the annual trends to the minimum duration defining an upwelling event indicated the need to document these trends. To accomplish this, we determined how the entire intra-annual distribution of upwelling event duration and magnitude shifted over time by calculating quantiles of upwelling event duration, mean magnitude and total magnitude for each year and regressing them against time. This approach is similar to regressing the annual minimum or maximum

against time, but by dividing the data into many different quantiles, we were able to quantify the temporal trends across the entire distribution. Specifically, for data X consisting of N values sorted from lowest to highest, the k^{th} q-quantile $Q_k(X)$ was

obtained by selecting the value of X at index $N\frac{k}{q}$. For each year, we used this method

to calculate 25 quantiles of the data, from very low (0.03) to very high (0.99).

5.2.4 Determining the temporal trends in the raw upwelling time series

To confirm the temporal trends observed in the annual summary statistics, we used wavelet analysis to document how the variability of the raw upwelling time series changed from 1967 to 2010. Wavelet analysis decomposes a time series into its component periodicities and reveals the relative contribution of the variability at each period to the total variability over time (Cazelles et al. 2008; Torrence & Compo 1998). Because wavelet analysis is well-resolved in both the time and frequency domains, it can reveal trends that would go unnoticed with simpler methods that are either unresolved or poorly resolved in time/frequency such as annual means. A complete description of wavelet analysis is provided in appendix C.

5.2.5 Intertidal water conditions in response to upwelling events

The upwelling index is generated from large-scale, regional atmospheric forcing far offshore in the CCS, yet the index is an estimate of how much cold, nutrient-rich upwelled water is being brought to the surface in the near-shore environment. To test the influence of temporal trends in upwelling event variability on intertidal water conditions, we related the index to long-term measurements of mean daily water temperatures at three intertidal sites collected by the Partnership for Interdisciplinary Studies of Coastal Oceans (PISCO). Boiler Bay (BB; $44^{\circ} 49' 48''$ N, $124^{\circ} 3' 36''$ W) is located at the southern edge of the region where the upwelling current runs close and parallel to shore and classic Ekman circulation dominates (Fig. 1). Strawberry Hill (SH; $44^{\circ} 15'$ N, $124^{\circ} 7' 12''$ W) is located within the Heceta Bank region, where a large, sluggish, re-

circulation zone retains plankton and upwelling drives high productivity (Fig. 1). Cape Blanco (CB; $42^{\circ} 50' 24''$ N, $124^{\circ} 34' 12''$ W) is located on Cape Blanco in southern Oregon where the upwelling current separates from the coastline and flows offshore (Fig. 1). Of the many PISCO sites, Boiler Bay and Strawberry Hill have the longest time-series of daily water temperature measurements (1993 to 2009) and are within 1° latitude of the 45° N upwelling index. Although we only had 11 years of data for Cape Blanco (1999 to 2009), including this site allowed us to assess the relationship between temperature and a different upwelling time series, the index for 42° N, where upwelling tends to be 3-4 times stronger.

The temperature data are point source from temperature loggers (StowAway TidbiT Temperature Loggers, Onset Computer Corporation, TBI32-05+37) that were bolted to rocks inside wire cages in the low zone at each site with three replicates per site. Although temperature was recorded at 1 hour intervals, we used tide tables to remove low tide air temperature measurements and averaged the remaining water temperature measurements for each day.

We computed the cross-correlation between daily temperature and upwelling index at each of the three Oregon locations during the upwelling season to determine the temporal lag between changes in regional upwelling conditions and local intertidal temperature. We also tested whether longer upwelling events resulted in colder water temperatures. Using simple linear regression, we related the duration of upwelling events to the change in water temperature, calculated as the difference between the average water temperature during an event and the water temperature on the day before the event started.

Additionally, we used wavelet coherence (Torrence & Compo 1998; Grinsted *et al.* 2004; Cazelles *et al.* 2008), a bivariate extension of wavelet analysis that describes patterns of correlation between pairs of time series in the time-frequency domain to assess the temporal variability in the relationship between daily upwelling and intertidal temperature from 1999 to 2009 at all three Oregon locations (see appendix C for a full description of wavelet coherence). Although we used wavelet coherence to document

how the correlation in the fluctuations of upwelling and temperature varies over time at periods ranging from 2 to 1024 days, we focused on event-scale (<40 days), sub-annual (41-255 days) and annual (256-512 days) period blocks. These divisions were motivated by strong differences in the temporal patterns of variability across these period blocks, with upwelling and temperature exhibiting (1) seasonal and high variability at event-scale periods, (2) seasonal and weak variability at sub-annual periods, and (3) persistently high variability at annual periods (Appendix D Fig. C2-1, D3). The different temporal patterns of variability summarized above are presented in greater detail in appendix D.

5.2.6 Response of intertidal ecosystem productivity to upwelling

In addition to the temperature analyses, we determined if local ecosystem productivity at our field sites was also responding to upwelling conditions. We examined PISCO's long term nitrate, phosphate and chlorophyll-a data from Boiler Bay (1993-2010), Strawberry Hill (1993-2010) and Cape Blanco (1995-2010). Each month during the upwelling season, replicated ($n = 3$) samples were collected at low tide in flowing water at a depth of ~30 cm using opaque plastic (HDPE) bottles. For chlorophyll-a, a 100 mL subsample was filtered through a 25 mm combusted Whatman glass fiber filter (pore size 0.7 μm) and stored on ice. The filter was extracted in 90% HPLC acetone for 12 h in the dark at -20°C, and the concentration of chlorophyll-a was determined using a Turner Designs Model 10 fluorometer calibrated with a pure chlorophyll-a standard (Sigma Chemical). Nitrate and phosphate were quantified from 20 ml subsamples of the filtrate by standard auto-analyzer techniques (Atlas et al. 1971). We used Spearman's rank correlations to analyze the association between nutrient and chlorophyll-a concentrations and (1) the number of wind relaxations, (2) the mean duration of upwelling events, and (3) the mean upwelling index over the days prior to each water sample. For nutrients we examined upwelling event conditions from 1 to 10 days prior to the sample and from 5 to 50 days for chlorophyll-a.

5.2.7 Effects of upwelling events on recruitment to the intertidal

We investigated whether the number of wind relaxations that mark the end of upwelling events and upwelling event duration were associated with the recruitment of barnacles and mussels. We obtained long-term recruitment data from PISCO for the same three sites as the temperature analyses. We used 21 years of barnacle and mussel recruitment data for Boiler Bay and Strawberry Hill, 1989 to 2009, and 10 years of recruitment data for Cape Blanco, 1999 to 2009.

As described elsewhere (Menge *et al.* 2009; Menge *et al.* 2011b), recruitment of barnacles and mussels was measured using artificial substrates on which larvae readily settle when deployed in the rocky intertidal. Briefly, Safetywalk® anti-slip tape on PVC plate (“plates”) and S.O.S Tuffy® mesh pads (“tuffies”) were used as substrates (“collectors”) for barnacle and mussel recruitment respectively. Collectors were bolted to rocks in the rocky intertidal at two wave exposures (exposed and protected) and two tidal heights (mid and low zones of the intertidal), except at CB where they were deployed in the mid exposed intertidal only. Plates and tuffies were deployed for 2 to 4 weeks, with 5 to 8 replicates of each. The collectors were then brought to the laboratory where barnacle cyprids and metamorphs and whole mussels were identified and counted using dissecting microscopes. Because post-settlement mortality can increasingly influence recruitment measurements as deployment time increases (Shanks 2009a), we did not use recruitment data for plates or tuffies deployed longer than 35 days.

For each deployment interval, we calculated the mean daily barnacle and mussel recruitment rates. Replicate measurements were averaged together before averaging over wave exposures and tidal heights. This reduced the data to one measure of mean daily recruitment for the barnacles *Balanus glandula* and *Chthamalus dalli*, and for the mussels *Mytilus* spp. for each deployment interval at each site. Because the data contain zeros and are not normally distributed, we used Spearman's rank correlations to analyze the association between recruitment and (1) the number of wind relaxations that occur during the deployment interval, (2) the mean duration of the upwelling events prior to those wind relaxations, and (3) the mean duration of the downwelling events that occur after those wind relaxations. Since both recruitment and the upwelling index exhibit annual-

scale variability (both are low during winter and high during summer), and we were interested in event-scale associations, we confined the data to Oregon's upwelling season, April through September. To assess the sensitivity of the results to the minimum duration defining an upwelling event, we repeated the analysis for minimum durations from 0 to 12 days. All data processing and analyses were conducted using MATLAB 7.8 (MathWorks, R2009a), and R 2.11.1 (R Development Core Team 2010).

5.3 RESULTS

5.3.1 Trends in the annual number, duration and magnitude of upwelling events

At each of the 5 latitudes along the CCS, the number of upwelling events has declined by 23 – 40% from 1967 to 2010 (Table 5.1a). In addition, the annual mean duration of upwelling events has increased from 26 – 86% (Table 5.1b), and the annual mean and total magnitude of upwelling events are increasing over time (Table 5.1c-d). The sensitivity analyses, which sequentially redefined the minimum duration of an upwelling event, reveal that the increase in the mean annual duration of upwelling is partially due to short events (< 1 day) becoming less frequent and partially due to long events (> 6 days) becoming more frequent (Appendix E Fig. E3-1).

5.3.2 Trends in the intra-annual distribution of event duration and magnitude

Overall, the intra-annual distribution of event durations is shifting towards higher values over time (positive slopes) at all sites (Fig. 2). Similar trends occur in the distributions of upwelling event mean and total magnitude, indicating that events are not only becoming longer, but are also becoming stronger (Appendix E Figs. E5, E6). This analysis also confirms the different trends of short and long upwelling events seen in the sensitivity analysis. Indeed, the frequency of intermediate to long upwelling events durations is increasing at a faster rate than that of short upwelling events (Fig. 2). Specifically, very low quantiles (e.g., < 0.2) and very high quantiles (e.g., > 0.9) of upwelling event duration have smaller positive slopes than intermediate-to-high quantiles at 42°N, 36°N and 33°N (Fig. 2c, d, g, h, i, j). At 45°N and 39°N, the relatively low

quantiles are the ones showing stronger increases (largest slopes) over time (Fig. 2a, b, e, f).

The wavelet analysis of the raw upwelling time series indicates that upwelling is being increasingly dominated over time by variability at event-scale (<40 days), sub-annual (41-255 days) and super-annual (>512 days) periods instead of annual periods (256-512 days) at several latitudes (Appendix D Fig. D2-2). This is consistent with the observed annual trends in upwelling events: by becoming stronger and more persistent, upwelling events are accounting for a greater proportion of the variability in upwelling over time.

5.3.3 Intertidal water conditions in response to upwelling events

The regional upwelling index and local intertidal water temperature are negatively correlated at time lags of 0-9 days at all three Oregon sites during the upwelling season, with the cross-correlation being strongest at time lags of 2-3 days (Fig. 3a, c, e). Furthermore, at all three Oregon sites, the change in water temperature is strongly negatively associated with the duration of upwelling events ($p < 0.0001$; Fig. 3b, d, f). Thus, upwelling events at the regional scale lead to a systematic decrease in local intertidal temperature after a 0-3 day lag period, with longer upwelling events generating colder intertidal temperatures. Overall, these results indicate that changes in daily upwelling have both a quasi-instantaneous and a cumulative effect on local intertidal water temperature.

To determine how the relationship between fluctuations in daily upwelling and temperature at different periodicities varied over time, we conducted wavelet coherence analysis at all three Oregon sites from 1999-2010. Upwelling and temperature show coherent fluctuations (coherence > 0.8) at event-scale (<40 days) and sub-annual periods (41-255 days) at all three sites during the summer months, with a phase difference between the cycles of upwelling and temperature of $-\pi / 2$ (Fig. 4). This phase difference means that there is a time lag between changes in upwelling conditions and water temperature, with peaks in upwelling trailing peaks in temperature by a quarter of

the amount of time a complete cycle takes. This means that through time, temperature drops follow peaks in upwelling. This pattern is consistent with a causal relationship between upwelling and temperature fluctuations at event-scale and sub-annual periods.

Upwelling and temperature undergo coherent fluctuations at annual periods (256–512 days) at Cape Blanco only, with upwelling leading temperature by $\pi/2$ (i.e. a temporal lag of approximately three months; Fig. 4f). These coherent annual fluctuations are unlikely to be causally related but due instead to seasonality in both temperature and upwelling patterns. Upwelling peaks earlier in the year than water temperature because the sun warms the air much faster than water during the spring months, thus generating a thermal gradient between the heated land mass and the cooler coastal ocean (Bakun 1990). The thermal gradient then generates strong alongshore winds that cause coastal upwelling to arise. This leads to a $\pi/2$ phase difference between upwelling and temperature at annual periods, with upwelling peaking in the spring and water temperature peaking in the summer (Fig. 4f, Appendix D Fig. D2-5f).

All water productivity indicators showed similar trends in response to upwelling at all sites. Chlorophyll-a, nitrate and phosphate concentrations were negatively related to the number of wind relaxations and positively related to the mean duration of upwelling events and the mean upwelling index (Appendix F Fig. F1a,b,c).

5.3.4 Effects of upwelling events on recruitment to the intertidal

Overall, barnacle and mussel recruitment varied with the number and mean duration of upwelling events, and these relationships depended on the minimum duration defining an upwelling event (Fig. 5). The trends observed for Boiler Bay and Strawberry Hill were stronger than for Cape Blanco. Recruitment of mussels and barnacles was positively associated with the number of wind relaxations, although this relationship often did not appear unless short upwelling events were excluded from the analysis, which indicates that larvae do not recruit in response to wind relaxations at the end of short events (Fig. 5). However, the minimum duration of upwelling events with which recruitment was most strongly associated differed between sites. The correlation

coefficients of *Balanus* spp. recruitment peaked at a minimum duration of 2 days at Boiler Bay (Fig. 5a), 6 days at Strawberry Hill (Fig. 5d), and 12 days at Cape Blanco (Fig. 5g). The correlation of *C. dalli* recruitment also peaked at 2 days for Boiler Bay (Fig. 5b) and 6 days at Strawberry Hill (Fig. 5e), but the patterns of the correlation coefficients at Strawberry Hill and Cape Blanco for this species were non-significant and close to zero. *Mytilus* spp. recruitment was also positively associated with the number of wind relaxations at a minimum duration of 6 days at Boiler Bay (Fig. 5c), 6 days at Strawberry Hill (Fig. 5f), and a peak in the correlation coefficient at 12 days at Cape Blanco (Fig. 5g), although the latter was not statistically significant. Barnacle recruitment at Boiler Bay was negatively associated with upwelling event duration (Fig. 5a, b). However, for *Mytilus* spp. recruitment at all three sites (Fig. 5c, f, i) and for *Balanus* spp. recruitment at Strawberry Hill (Fig. 5d) and Cape Blanco (Fig. 5g), the association with the mean duration of upwelling event is positive when short events are included in the analysis. This relationship is only significant for mussel recruitment at Boiler Bay and Strawberry Hill and as short events are excluded, these relationships decline and become non-significant (Fig. 5c, f).

The positive association of mussel recruitment with the duration of short upwelling events at Strawberry Hill is complemented by negative associations with the duration of downwelling events (Fig. 5f). Similar relationships are evident for mussels at Boiler Bay (Fig. 5c) and *Balanus* spp. at Cape Blanco (Fig. 5g), but these are not significant. Similarly, the negative association of barnacle recruitment with the duration of upwelling events at Boiler Bay is reflected in positive associations with duration of downwelling events (Fig. 5a, b), although this relationship is only significant for *C. dalli* recruitment.

5.4 DISCUSSION

Upwelling events in the California Current System have become longer in duration, stronger in magnitude and fewer in number, which is consistent with Bakun's hypothesis for how climate change would impact Eastern Boundary Currents (Bakun

1990). The increase in upwelling event duration reflects both the increased persistence of events and the loss of short events (<1 day long), especially in the southern regions of the CCS. The strong, quasi-instantaneous, and cumulative effect of upwelling events on intertidal water temperatures suggests that the increased persistence and strength of upwelling events will result in colder upwelled water shoaling over longer periods in the nearshore environment. Furthermore, our results show that larval recruitment, nutrient availability and phytoplankton concentration in coastal regions are strongly related to larger-scale upwelling events. Overall, our findings suggest that changes in the distribution, persistence and strength of event-scale upwelling are likely to have important consequences for the structure and functioning of nearshore ecosystems.

5.4.1 Temporal trends and climate change hypotheses

The observed increase over time in the duration and magnitude of upwelling events in Oregon is consistent with the recently documented increase in annual upwelling in California (Garcia-Reyes & Largier 2010). The similarity in these trends over 12° of latitude (~1,400 km) along the U.S. west coast suggests that coastal climate forcing at the scale of the entire CCS is shifting. Our results are consistent with Bakun's 1990 upwelling intensification hypothesis, which predicts that increased greenhouse emissions lead to a stronger thermal gradient between the warm land mass and the cooler coastal ocean, thereby driving more persistent upwelling-favorable winds in coastal upwelling systems worldwide (Bakun 1990; Mendelsohn & Schwing 2002; Santos *et al.* 2005; McGregor *et al.* 2007; Bakun *et al.* 2010). Thus, we predict that these trends would likely be found in similar coastal upwelling systems and that they will continue to strengthen with further global climate change (Bakun 1990; Snyder *et al.* 2003).

5.4.2 Intertidal water temperature response to upwelling conditions

On a global scale, climate change is causing higher average sea surface temperatures (Scavia *et al.* 2002). However, this effect is negated or reversed in coastal upwelling regions where climate change is predicted to cause stronger and more

persistent upwelling during the upwelling season. We have shown that upwelling event conditions at the regional scale are strongly associated with the quasi-instantaneous shoaling of cold water in local nearshore environments and that upwelling events have a cumulative effect on nearshore temperatures, with longer upwelling events leading to colder temperatures. Hence, our results suggest that stronger and more persistent upwelling may lead to a reduction in water temperatures in the coastal ocean despite a global trend toward higher temperatures. However, increased solar heating and reduced mixing may enhance stratification and deepen the thermocline to the point at which upwelling would only turnover water above the thermocline and no longer bring cold, nutrient rich deep water to the surface (Harley *et al.* 2006). Although such a deepening of the thermocline can decouple upwelling events from their expected effects on the temperature and productivity of coastal waters (Roemmich & McGowan 1995), our results indicate that upwelling remains strongly related to (1) temperature, (2) nutrients, and (3) chlorophyll-a despite a 26-86% increase in upwelling strength and persistence over the last 43 years.

Colder water temperatures will have consequences for nearshore ecosystems through direct effects of temperature on species performance and indirectly through species interactions. The direct, physiological effect of temperature is the main factor defining the geographic distribution of marine animals (Hutchins 1947; Helmuth *et al.* 2006). Temperature-induced changes to the distribution and population sizes of species affect other species indirectly, as mediated through the network of species interactions (Leonard *et al.* 1999; Moore *et al.* 2007). Furthermore, the strengths of species interactions are also directly dependent on temperature (Rall *et al.* 2010). Colder temperatures typically cause lower consumption rates by reducing the metabolic rates of consumers, thus weakening top-down control in ecosystems (Vasseur & McCann 2005). Enhanced bottom-up effects from the increased provision of nutrient rich water potentially compounds the situation. This unchecked growth of lower trophic levels could further exacerbate hypoxia and anoxia at depth on the continental shelf (Grantham *et al.* 2004; Chan *et al.* 2008).

5.4.3 Effects of upwelling events on recruitment

Regional scale variability in upwelling conditions within the CCS have been linked to recruitment patterns (Menge *et al.* 2011b), however, there is some debate over the physical oceanographic mechanism responsible for delivering larvae to shore. The transport hypothesis suggests that persistent upwelling limits recruitment in the southern CCS by preventing onshore larval transport and advecting larvae offshore, whereas frequent wind relaxations in the northern CCS cause current reversals and result in saturating recruitment pulses (Farrell *et al.* 1991; Connolly *et al.* 2001; Menge *et al.* 2003; Noda 2004; Dudas *et al.* 2009). Our results partly support this hypothesis, as recruitment of both barnacles and mussels was positively associated with the number of wind relaxations. However, offshore larval distributions have not been found to be susceptible to offshore advection during upwelling (Shanks & Brink 2005; Morgan *et al.* 2009; Shanks & Shearman 2009) and recruitment does occur in the absence of major wind relaxations. Thus, other physical oceanographic processes, such as internal waves and tidal currents, and site-specific differences in hydrodynamics may also be responsible for larval delivery (Menge *et al.* 1997a; Shanks 2009b; Shanks *et al.* 2010).

The behavior of different taxa is likely to affect the recruitment response to upwelling conditions. In fact, within-site differences between mussel and barnacle recruitment are apparent in our results. At each site, barnacle recruitment tended to be negatively (or less positively) related to the mean duration of upwelling events than was mussel recruitment. Mussel recruitment was consistently positively associated with event duration and only becomes positively associated with the number of upwelling events once short upwelling events are excluded from the analysis. One reason for this may be that mussel larvae are typically found below the thermocline and thus would not be susceptible to offshore advection during upwelling, whereas barnacles are often found in the surface Ekman layer (Shanks & Brink 2005; Broitman *et al.* 2008; Rilov *et al.* 2008; Shanks & Shearman 2009). If mussel larvae are not susceptible to offshore advection of the top water layer during upwelling, the positive effect of upwelling duration seen in the results may be due to the onshore advection of deeper water or the increased food

availability associated with upwelled waters (Broitman *et al.* 2008; Menge *et al.* 2009). Because mussels respond positively as the duration of upwelling events increases, they will likely be positively affected by climate driven increases in upwelling persistence.

Although barnacle recruitment is generally positively associated with the number of wind relaxations, there are large differences between sites that are likely due to how regional currents respond to upwelling events and wind relaxations. At Boiler Bay where the continental shelf is narrow and the upwelling current runs parallel and relatively close to shore (Castelao & Barth 2005), we expect barnacle larvae to be highly dependent on wind relaxations for recruiting onshore. Conversely, we would not expect barnacle larvae to be as dependent on wind relaxations for recruitment at Strawberry Hill because of the large retentive zone which retains larvae close to shore (Keister *et al.* 2009). Our results support this interpretation, as barnacle recruitment at Boiler Bay was positively associated with both the number of wind relaxations and the duration of the subsequent downwelling events and negatively associated with upwelling event duration whereas the relationships at Strawberry Hill were much weaker. Further south at Cape Blanco, the upwelling current separates from the coast (Springer *et al.* 2009) causing advection of surface waters and their associated planktonic communities far offshore (Keister *et al.* 2009). Although much less is known about nearshore currents in the shadow of the upwelling current, there is evidence to suggest that they are generally weak and not strongly directional, yet still flow shoreward during wind relaxations (Keister *et al.* 2009). Thus, barnacle larvae at Cape Blanco may not be subject to strong advection in the upwelling current and thus not as dependent on wind relaxations for onshore recruitment. This is consistent with our weak results for Cape Blanco, although the small sample size for this site may also be a factor.

Climate-induced changes to recruitment have the potential to affect community structure and dynamics, but only if the abundance of adult populations are ultimately affected (Svensson *et al.* 2005; Poloczanska *et al.* 2008). This is not always the case because of post-recruitment processes. For example, the orders-of-magnitude increases in mussel recruitment observed at many sites within the last decade (Menge *et al.* 2009)

usually were not accompanied by a corresponding increase in adult mussel abundance (Menge *et al.* 2011a). Menge *et al.* (2011a) hypothesized that the lack of response of the adult mussel populations was because recruitment of their main facilitator, barnacles, failed to increase over the same period. Barnacles facilitate mussel recruitment by providing many tiny crevices for mussel recruits to attach to the substratum (Berlow 1997). Thus, in regions where barnacle recruitment responds even to short upwelling events, increasing persistence of upwelling will not only impact barnacle populations, but will indirectly impact mussel populations too. Such context-dependent, non-linear responses of different species to environmental forcing are likely to be the norm.

5.4.4 Broader impacts

In addition to the effects of upwelling on productivity, temperature, and larval distribution, upwelled waters are also high in dissolved carbon dioxide, low in dissolved oxygen and low in pH (Grantham *et al.* 2004; Chan *et al.* 2008; Hauri *et al.* 2009). In 2002, persistent upwelling caused severe inner-shelf (<70 m) hypoxia ($[O_2] \leq 0.5 \text{ ml l}^{-1}$) to develop from 44.00°N to 44.65°N, which resulted in mass die-offs of fish and invertebrates (Grantham *et al.* 2004). In the summer of 2006, extremely high productivity in the same region resulted from a prolonged period of unusually intense upwelling and contributed to widespread and severe hypoxia and the first recorded instance of anoxia in the CCS (Chan *et al.* 2008). Indeed, upwelling was so persistent in 2006 at 45°N that the number of wind relaxations was the lowest of any year on record. Respiration of excess phytoplankton production also adds to dissolved CO₂ levels, which decreases pH and the carbonate saturation state (Hauri *et al.* 2009). Low pH and under-saturated waters have been observed during strong upwelling events (Feely *et al.* 2008), so longer upwelling events will likely mean higher shoaling and longer exposure to acidic waters in the near shore environment.

Climate-driven changes in the phenology of upwelling events are altering the tempo and the mode of environmental forcing in nearshore ecosystems of the California Current System: upwelling events have become longer in duration, stronger in magnitude

and fewer in number. By affecting water temperature, nutrient availability, phytoplankton productivity, larval recruitment and species interaction strength, changes in the duration, frequency and magnitude of upwelling are likely to significantly impact the structure and functioning of coastal ecosystems in Eastern boundary currents around the world.

ACKNOWLEDGEMENTS

We thank Brock Woodson, Olivia Cheriton, Jack Barth, Libe Washburn, Margaret McManus and the rest of the PISCO (Partnership for Interdisciplinary Studies of Coastal Oceans) 2008 Coastal Physical Oceanography class for their guidance, expertise, and hard work during the course. Thanks also to Jerod Sapp and Sally Hacker for their assistance with early analyses. Funding was provided by an NSERC pre-doctoral fellowship (to ACI), and by grants from NSF, the Wayne and Gladys Valley Foundation, the Andrew Mellon Foundation, the David and Lucile Packard Foundation, and the Gordon and Betty Moore Foundation. This is publication number 402 from PISCO, a long-term ecological consortium which is partially funded by the David and Lucile Packard Foundation and the Gordon and Betty Moore Foundation.

Table 5.1 Temporal trends from 1967 to 2010 in the frequency, mean duration, mean magnitude and total magnitude of upwelling events at five latitudes across the California Current System. Only upwelling events occurring during the upwelling season of each latitude are included. Statistics represent simple linear regression models ($y = \beta_0 + \beta_1x$) of the effect of year on the (a) frequency, (b) mean duration ($\log_{10}+1$), (c) mean magnitude ($\log_{10}+1$), and (d) total magnitude ($\log_{10}+1$) of upwelling events. For each analysis we present the p-value (bolded when < 0.05), coefficient of determination (R^2), intercept (β_0), and slope (β_1).

Latitude	p-val	R^2	β_0	β_1
a. Frequency of upwelling events				
45	0.040	0.103	371.332	-0.172
42	0.002	0.253	660.587	-0.317
39	0.010	0.164	475.072	-0.226
36	0.001	0.350	965.509	-0.465
33	0.007	0.175	731.596	-0.344
b. Mean duration of upwelling events				
45	0.077	0.078	-3.147	0.002
42	0.001	0.249	-7.947	0.004
39	0.053	0.093	-4.205	0.002
36	0.001	0.453	-10.520	0.006
33	0.001	0.253	-5.775	0.003
c. Mean magnitude of upwelling events				
45	0.208	0.033	-1.581	0.001
42	0.030	0.112	-6.523	0.004
39	0.436	0.016	-1.187	0.001
36	0.007	0.165	-5.700	0.004
33	0.088	0.067	-1.548	0.001
d. Total magnitude of upwelling events				
45	0.068	0.074	-7.290	0.005
42	0.003	0.201	-19.407	0.011
39	0.149	0.052	-7.231	0.005
36	0.001	0.352	-21.616	0.012
33	0.002	0.205	-10.341	0.006

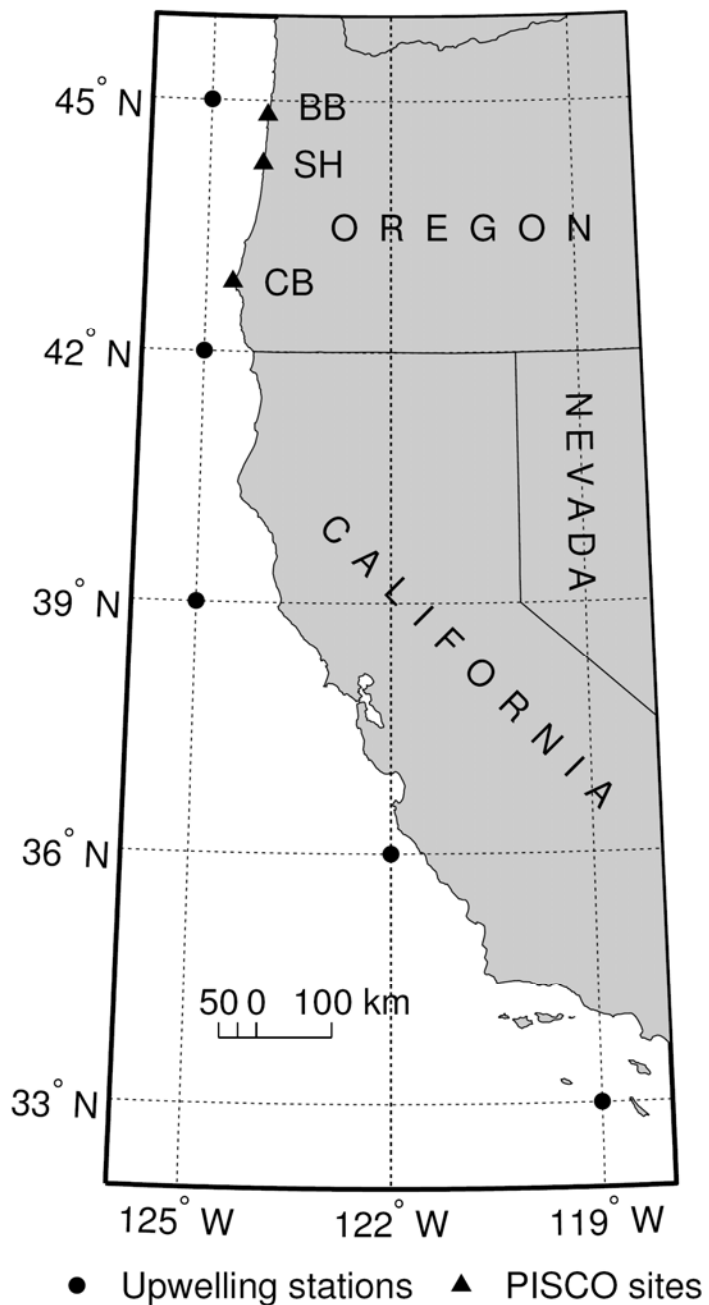


Figure 5.1 Map of the study region. Shown are the locations of the five PFEL upwelling stations in the CCS off the coast of Oregon and California (circles) and the three rocky intertidal field sites along the Oregon coast (triangles): Boiler Bay (BB), Strawberry Hill (SH), and Cape Blanco (CB).

Figure 5.2 Temporal trends in the intra-annual distribution of \log_{10} upwelling event durations from 1967 to 2010. Within each year for each of the five latitudes, we identified the different quantiles of \log_{10} upwelling event duration. The quantiles were related to year via simple linear regression models ($y = \beta_0 + \beta_1 x$), yielding a coefficient of determination (R^2 , left column) and a slope (β_1 , right column). Closed (open) circles indicate regressions with p-values < 0.05 (> 0.05). The p-values were assessed by performing 1,000 permutations of the data and determining the proportion of permutations that yielded a coefficient of determination that was greater than or equal to the one obtained with the original data.

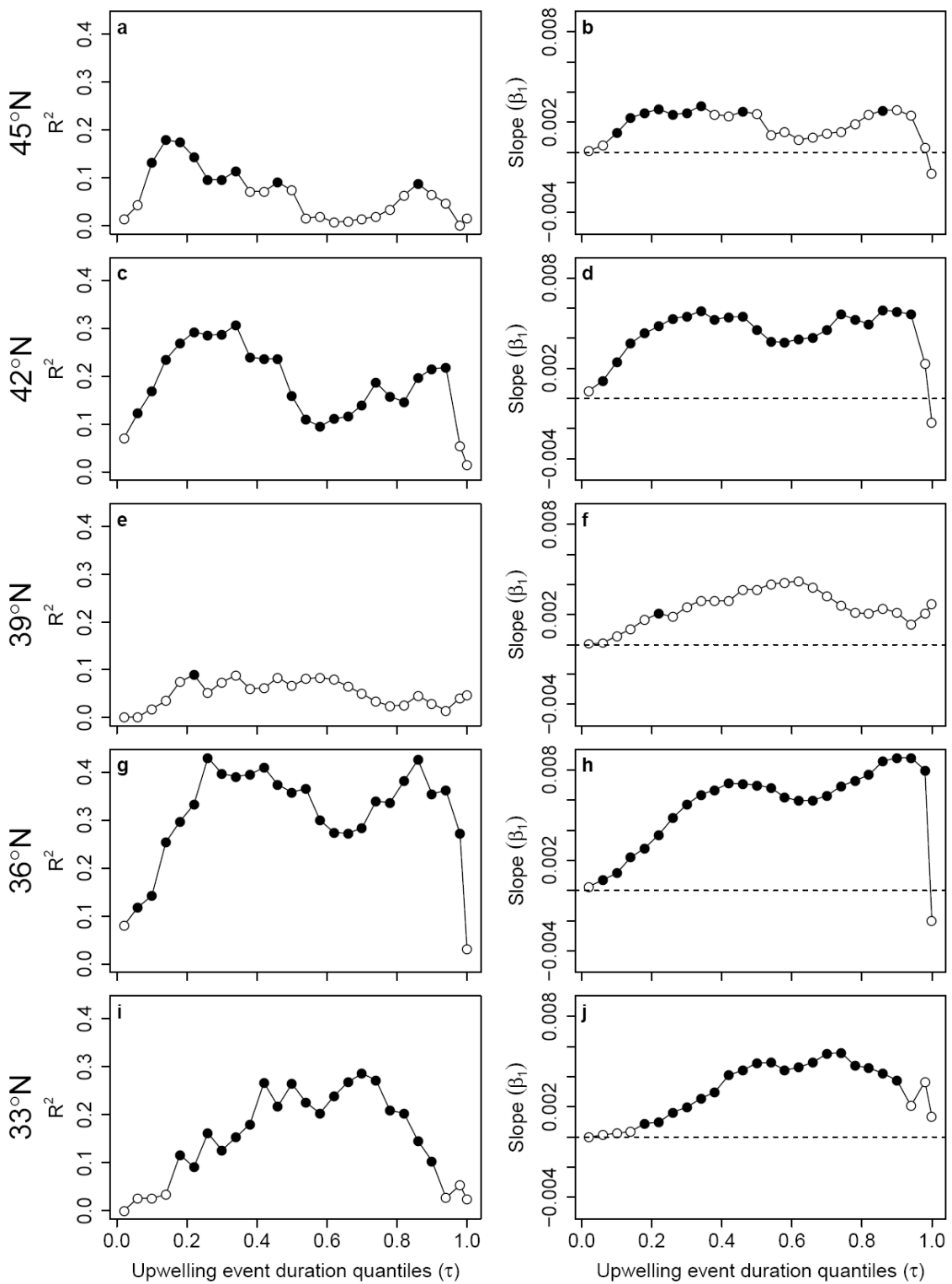


Figure 5.2

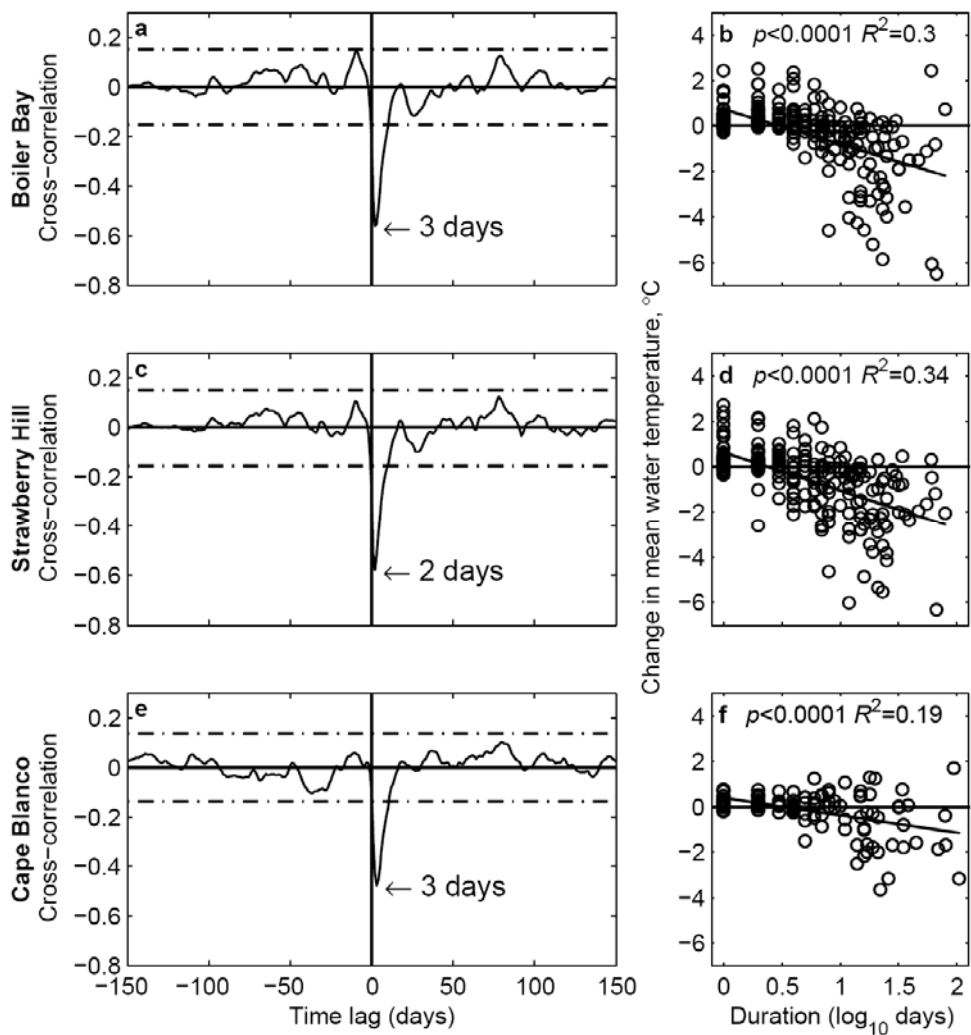


Figure 5.3 The effect of daily upwelling conditions on daily rocky intertidal water temperatures from 1999 to 2010. Subplots represent cross-correlations of mean daily water temperature and mean daily upwelling index at (a) Boiler Bay, (c) Strawberry Hill and (e) Cape Blanco. The dashed lines indicate the 95% confidence interval of cross-correlation values predicted for two uncorrelated time series. Cross-correlations outside of the confidence interval are thus significant at the $\alpha = 0.05$ level. The lag time at which water temperature was most highly correlated to the upwelling index is indicated with an arrow for each plot. Side plots represent simple linear regressions of the effect of upwelling event duration on the change in water temperature at (b) Boiler Bay, (d) Strawberry Hill and (f) Cape Blanco. The change in water temperature is the difference between the water temperature the day before an upwelling event starts and the mean water temperature over the course of the event. The regression statistics are indicated on each plot.

Figure 5.4 Pairwise wavelet coherence analysis of daily upwelling and temperature time series from 1999 to 2010 at (a, b) Boiler Bay, (c, d) Strawberry Hill and (e, f) Cape Blanco. The left column represents wavelet coherence analyses between (a) 45°N upwelling index and temperature at Boiler Bay, (c) 45°N upwelling index and temperature at Strawberry Hill and (e) 42°N upwelling index and temperature at Cape Blanco. Wavelet coherence represents regions of high (low) common fluctuations between the time series in warm (cold) colors. Black arrows indicate the phase angle between the time series. When the time series move in the same direction (i.e., in phase), the arrows point to the right and when they move in opposite directions (i.e., anti-phase), the arrows point to the left. Arrows pointing down indicate a $\pi/2$ phase difference between the time series, with upwelling leading temperature, and arrows pointing up indicate a $-\pi/2$ phase difference between the time series, with temperature leading upwelling. Black contours represent regions of statistically significant common variability at the $\alpha=0.05$ level. Regions within the black dashed lines (the cone of influence) are not affected by edge effects. (b, d, f) The right column shows the distribution of phase differences between upwelling and temperature across all significant wavelet coherence regions for event-scale (<40 days; green), sub-annual (41-255 days; blue) and annual (256-512 days; red) periodicities.

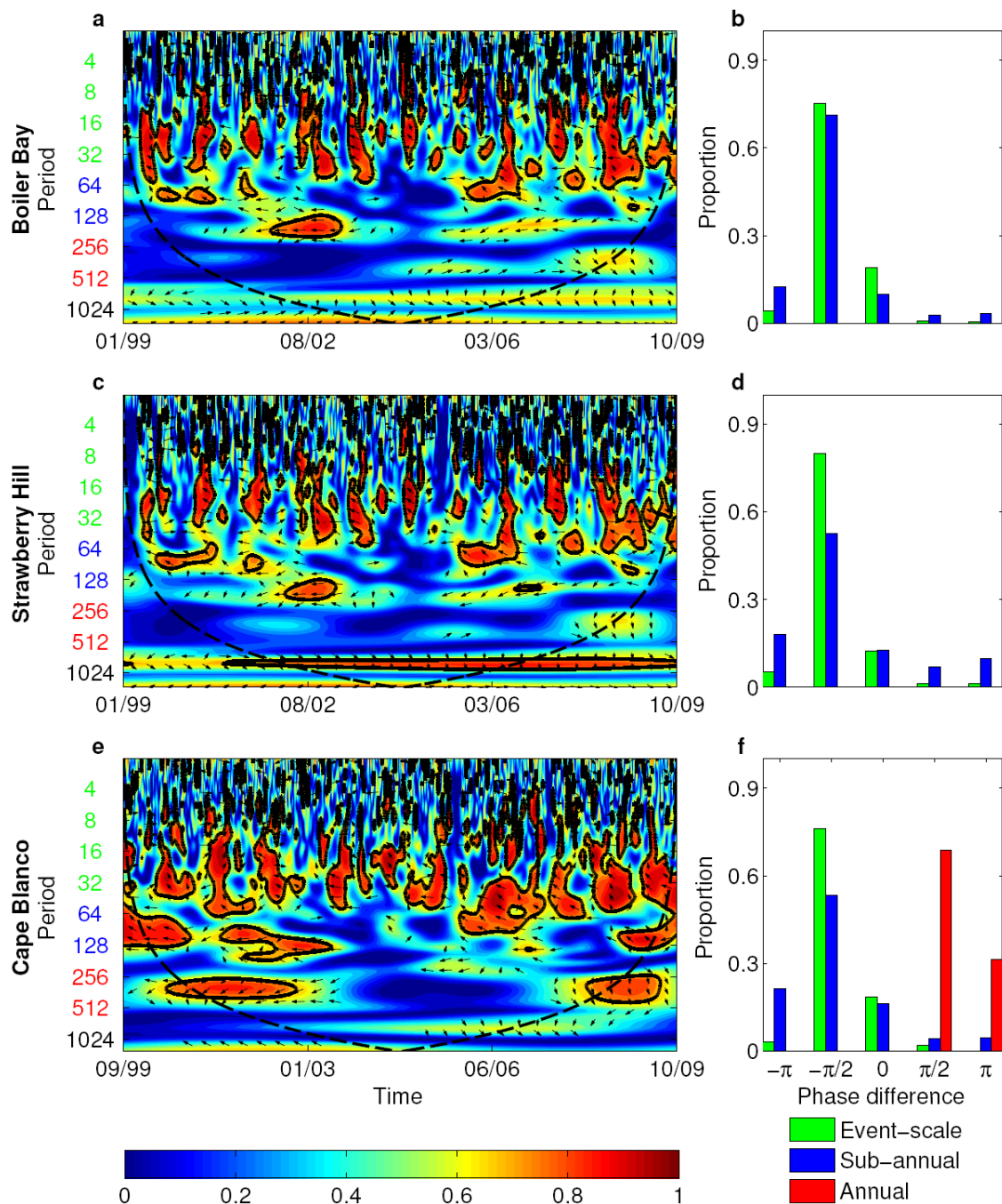
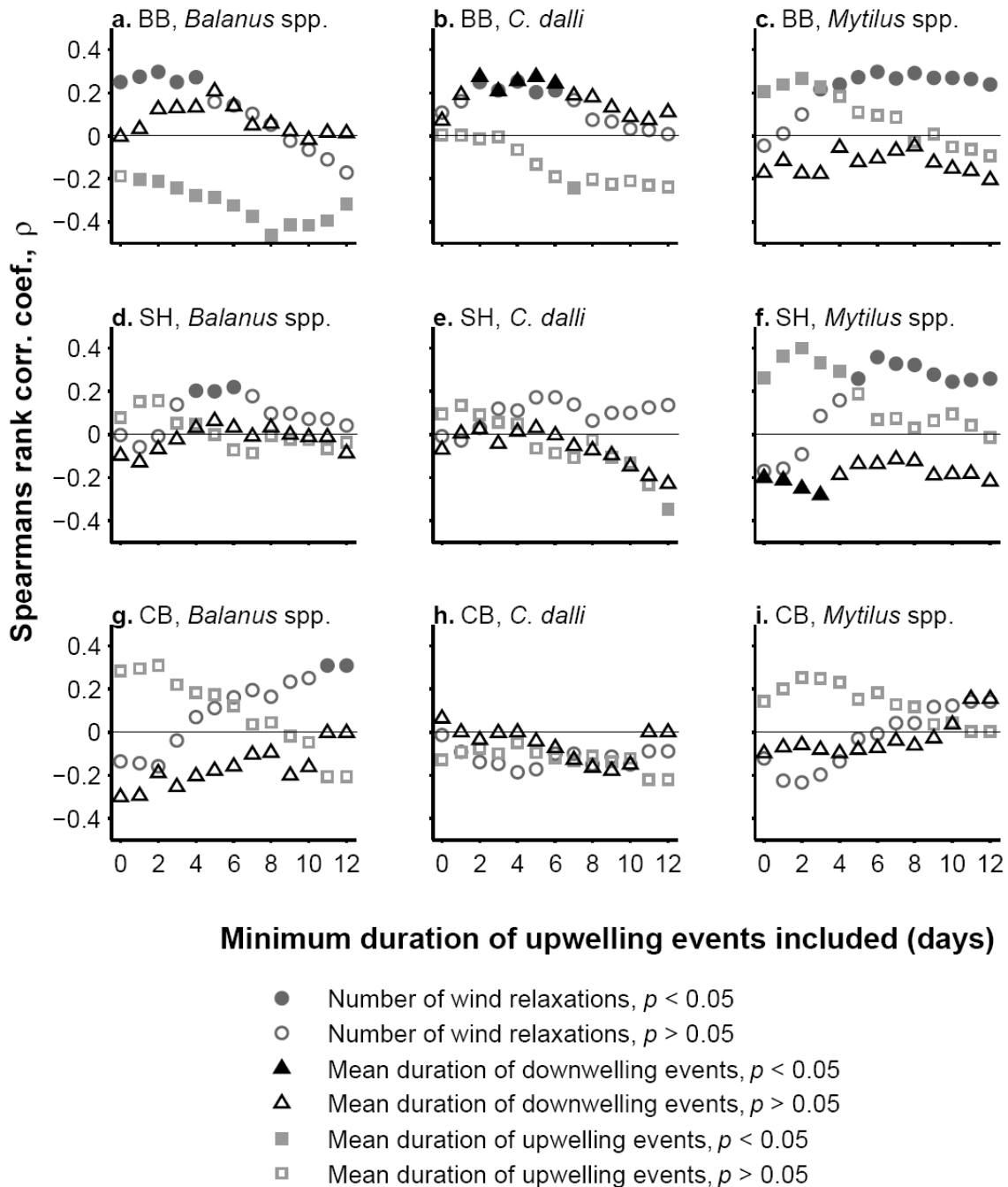


Figure 5.4

Figure 5.5 Correlation analyses of barnacle and mussel recruitment with upwelling event conditions. Plotted on the y-axis are the coefficients of the Spearman's rank correlation analyses of barnacle and mussel recruitment versus (1) the number of wind relaxations (circles), (2) the mean duration of the upwelling events that occur before (squares), and (3) the mean duration of the downwelling events that occur after those wind relaxations (triangles). The x-axis is the minimum duration of upwelling events included in the analysis, from 0 to 12 days. Correlation coefficients that account for a statistically significant proportion of the variation in the data at the $\alpha=0.05$ level are represented by closed symbols, non-significant coefficients have open symbols. Results are presented for the barnacles *Balanus* spp. (a, d, g), *Chthamalus dalli* (b, e, h), and for the mussels *Mytilus* spp. (c, f, i), at three rocky intertidal field sites: Boiler Bay (a, b, c), Strawberry Hill (d, e, f), and Cape Blanco (g, h, i).

**Figure 5.5**

CHAPTER 6: General Conclusion

My dissertation research demonstrates that the mechanistic effect of temperature on organismal performance is an important force structuring ecological communities and has potential as a tractable framework for predicting the community level effects of climate change. Ongoing, long-term changes in environmental forcing in rocky intertidal ecosystems provide an opportunity to understand how temperature shapes community structure and the ramifications of climate change (Chapter 5). The modeling exercises of Chapter 2 indicated that the bioenergetic constraints of body size and body temperature influence species persistence in communities primarily through physiological effects at the organismal level. However, local community structure also influences the effect of temperature by either limiting the flow of energy up the food web, which imposes additional energetic constraints on higher trophic species, or by mitigating the negative effects of temperature with stabilizing species interactions. The results of Chapter 3 supported the model prediction that rocky intertidal species should express declining energetic efficiencies with temperature. Finally, the effect of temperature on ingestion rates and species interaction strengths observed in the lab was also apparent under field conditions (Chapter 4).

Temperature is not the only abiotic factor affecting organismal performance, nor is it the only abiotic factor predicted to change with climate change. In rocky intertidal systems, stronger and more persistent upwelling will deliver more nutrients to the coastal photic zone, boosting primary production and fueling the base of the food web. A stronger bottom-up effect, combined with a suppressed top-down effect due to cold water temperatures limiting the ingestion rates of consumers, could contribute to the unchecked growth of phytoplankton. Since uneaten phytoplankton biomass may be the main factor causing the widespread hypoxia observed during the upwelling season along the Oregon coast since 2001, the consequences could be severe. Upwelled waters also have a low pH, which disproportionately impacts species with carbonate body parts, such as shells. In order to understand the cumulative, or synergistic, effects of many simultaneously

changing abiotic factors on ecological communities, it's important that organismal-level responses are characterized across the full range of conditions that species currently or are projected to experience.

Characterizing biological rates under the full range of typical environmental conditions is necessary to scale up physiological effects to the community level. Although the direct, physiological responses to temperature are well documented for many intertidal organisms, most investigations focus on thermal stress at the extremes of a species' tolerance and overlook temperature effects on physiology near the center of a species' thermal range (Sanford 2002). Most studies take measurements such as the LT50 (the temperature at which 50% mortality occurs), maximal habitat temperature, or the Arrhenius 'break' temperature (the temperature at which a sharp discontinuity in slope occurs in an Arrhenius plot of physiological rates). While such measurements are necessary for understanding range limits, physiological mechanisms, and energetic costs arising from *extreme* heat stress (see reviews by Somero 2002, 2011), they are not useful for defining how temperature affects performance across the range of conditions that organisms typically experience over the long-term.

The experimental design used to measure how physiological rates scale with environmental variables affects how easily organismal physiology can be integrated into community models (Angilletta & Sears 2011). Most experiments characterizing physiological responses to environmental factors use ANOVA experimental designs where continuous environmental variables are constrained to 2-5 categorical levels, with replicates at each level, resulting in estimates of the mean and variance at only those particular levels. Alternatively, an experimental regression design, such as I used in Chapter 3, characterizes the response over the full range of the predictor variable, often with superior efficiency (no need for replicates!) and statistical power, and a much improved ability to detect non-linear, threshold, or asymptotic responses (Gotelli & Ellison 2004). With multiple factors, experimental regression designs (a.k.a. response surface designs) are analyzed with multiple regression and can reveal additive or synergistic effects (Inouye 2001, Gotelli & Ellison 2004). Most importantly, the slope

and intercept parameters from regression models are much more appropriate for integrating into ecological models where predictor environmental variables vary continuously (Gotelli & Ellison 2004).

By considering how environmental factors influence species energetics and the strengths of species interactions in the context of a community network, my thesis work demonstrates the potential for using a holistic approach to understanding the consequences of environmental forcing on community structure. The development of an ecological community modeling framework that links environmental variability, organismal physiology, and species interactions will take close collaboration between ecophysiologists, community ecologists, and theoretical ecologists. Such research networks are critical for us to improve our predictive power for assessing the impact of climate change on ecological communities.

Bibliography

- Allen A.P. & Gillooly J.F. (2007). The mechanistic basis of the metabolic theory of ecology. *Oikos*, 116, 1073-1077.
- Araujo M.B., Rozenfeld A., Rahbek C. & Marquet P.A. (2011). Using species co-occurrence networks to assess the impacts of climate change. *Ecography*, 34, 897-908.
- Atlas E.L., Hager S.W., Gordon L.I. & Park P.K. (1971). A practical manual for use of the Technicon AutoAnalyzer (R) in seawater nutrient analyses, revised In. Department of Oceanography, Oregon State University, p. 49.
- Bakun A. (1990). Global climate change and intensification of coastal ocean upwelling. *Science*, 247, 198-201.
- Bakun A., Field D.B., Redondo-Rodriguez A. & Weeks S.J. (2010). Greenhouse gas, upwelling-favorable winds, and the future of coastal ocean upwelling ecosystems. *Global Change Biology*, 16, 1213-1228.
- Bakun A., McLain D.R. & Mayo F.V. (1974). Mean annual cycle of coastal upwelling off western North America as observed from surface measurements. *Fishery Bulletin*, 72, 843-844.
- Barth J.A., Pierce S.D. & Castelao R.M. (2005). Time-dependent, wind-driven flow over a shallow midshelf submarine bank. *Journal of Geophysical Research-Oceans*, 110, 20.
- Bascompte J., Melian C.J. & Sala E. (2005). Interaction strength combinations and the overfishing of a marine food web. *Proceedings of the National Academy of Sciences of the United States of America*, 102, 5443-5447.
- Berlow E.L. (1997). From canalization to contingency: Historical effects in a successional rocky intertidal community. *Ecological Monographs*, 67, 435-460.
- Berlow E.L., Dunne J.A., Martinez N.D., Stark P.B., Williams R.J. & Brose U. (2009). Simple prediction of interaction strengths in complex food webs. *Proceedings of the National Academy of Sciences of the United States of America*, 106, 187-191.
- Berlow E.L., Navarrete S.A., Briggs C.J., Power M.E. & Menge B.A. (1999). Quantifying variation in the strengths of species interactions. *Ecology*, 80, 2206-2224.
- Berlow E.L., Neutel A.M., Cohen J.E., de Ruiter P.C., Ebenman B., Emmerson M., Fox J.W., Jansen V.A.A., Jones J.I., Kokkoris G.D., Logofet D.O., McKane A.J., Montoya J.M. & Petchey O. (2004). Interaction strengths in food webs: issues and opportunities. *Journal of Animal Ecology*, 73, 585-598.
- Beveridge O.S., Humphries S. & Petchey O.L. (2010a). The interacting effects of temperature and food chain length on trophic abundance and ecosystem function. *Journal of Animal Ecology*, 79, 693-700.
- Beveridge O.S., Petchey O.L. & Humphries S. (2010b). Direct and indirect effects of temperature on the population dynamics and ecosystem functioning of aquatic microbial ecosystems. *Journal of Animal Ecology*, 79, 1324-1331.
- Broitman B.R., Blanchette C.A., Menge B.A., Lubchenco J., Krenz C., Foley M., Raimondi P.T., Lohse D. & Gaines S.D. (2008). Spatial and temporal patterns of

- invertebrate recruitment along the West Coast of the United States. *Ecological Monographs*, 78, 403-421.
- Broitman B.R., Szathmary P.L., Mislan K.A.S., Blanchette C.A. & Helmuth B. (2009). Predator-prey interactions under climate change: the importance of habitat vs body temperature. *Oikos*, 118, 219-224.
- Brose U. (2008). Complex food webs prevent competitive exclusion among producer species. *Proceedings of the Royal Society B-Biological Sciences*, 275, 2507-2514.
- Brose U., Berlow E.L. & Martinez N.D. (2005). Scaling up keystone effects from simple to complex ecological networks. *Ecology Letters*, 8, 1317-1325.
- Brose U., Jonsson T., Berlow E.L., Warren P., Banasek-Richter C., Bersier L.F., Blanchard J.L., Brey T., Carpenter S.R., Blandenier M.F.C., Cushing L., Dawah H.A., Dell T., Edwards F., Harper-Smith S., Jacob U., Ledger M.E., Martinez N.D., Memmott J., Mintenbeck K., Pinnegar J.K., Rall B.C., Rayner T.S., Reuman D.C., Ruess L., Ulrich W., Williams R.J., Woodward G. & Cohen J.E. (2006a). Consumer-resource body-size relationships in natural food webs. *Ecology*, 87, 2411-2417.
- Brose U., Williams R.J. & Martinez N.D. (2006b). Allometric scaling enhances stability in complex food webs. *Ecology Letters*, 9, 1228-1236.
- Brown J.H., Gillooly J.F., Allen A.P., Savage V.M. & West G.B. (2004). Toward a metabolic theory of ecology. *Ecology*, 85, 1771-1789.
- Burness G.P., Diamond J. & Flannery T. (2001). Dinosaurs, dragons, and dwarfs: The evolution of maximal body size. *Proceedings of the National Academy of Sciences of the United States of America*, 98, 14518-14523.
- Castelao R.M. & Barth J.A. (2005). Coastal ocean response to summer upwelling favorable winds in a region of alongshore bottom topography variations off Oregon. *Journal of Geophysical Research-Oceans*, 110, 17.
- Cazelles B., Chavez M., Berteaux D., Menard F., Vik J.O., Jenouvrier S. & Stenseth N.C. (2008). Wavelet analysis of ecological time series. *Oecologia*, 156, 287-304.
- Chan F., Barth J.A., Lubchenco J., Kirincich A., Weeks H., Peterson W.T. & Menge B.A. (2008). Emergence of anoxia in the California current large marine ecosystem. *Science*, 319, 920-920.
- Coggan N., Clissold F.J. & Simpson S.J. (2011). Locusts use dynamic thermoregulatory behaviour to optimize nutritional outcomes. *Proceedings of the Royal Society B-Biological Sciences*, 278, 2745-2752.
- Connolly S.R., Menge B.A. & Roughgarden J. (2001). A latitudinal gradient in recruitment of intertidal invertebrates in the northeast Pacific Ocean. *Ecology*, 82, 1799-1813.
- Davis A.J., Jenkinson L.S., Lawton J.H., Shorrocks B. & Wood S. (1998a). Making mistakes when predicting shifts in species range in response to global warming. *Nature*, 391, 783-786.
- Davis A.J., Lawton J.H., Shorrocks B. & Jenkinson L.S. (1998b). Individualistic species responses invalidate simple physiological models of community dynamics under global environmental change. *Journal of Animal Ecology*, 67, 600-612.

- de Ruiter P.C., Neutel A.M. & Moore J.C. (1995). Energetics, patterns of interaction strengths, and stability in real ecosystems. *Science*, 269, 1257-1260.
- Dell A.I., Pawar S. & Savage V.M. (2011). Systematic variation in the temperature dependence of physiological and ecological traits. *Proceedings of the National Academy of Sciences of the United States of America*, 108, 10591-10596.
- Denny M.W. & Harley C.D.G. (2006). Hot limpets: predicting body temperature in a conductance-mediated thermal system. *Journal of Experimental Biology*, 209, 2409-2419.
- Dorcas M.E., Peterson C.R. & Flint M.E.T. (1997). The thermal biology of digestion in rubber boas (*Charina bottae*): Physiology, behavior, and environmental constraints. *Physiol. Zool.*, 70, 292-300.
- Dudas S.E., Grantham B.A., Kirincich A.R., Menge B.A., Lubchenco J. & Barth J.A. (2009). Current reversals as determinants of intertidal recruitment on the central Oregon coast. *Ices Journal of Marine Science*, 66, 396-407.
- Dunne J.A., Williams R.J. & Martinez N.D. (2002). Network structure and biodiversity loss in food webs: robustness increases with connectance. *Ecology Letters*, 5, 558-567.
- Dunne J.A., Williams R.J. & Martinez N.D. (2004). Network structure and robustness of marine food webs. *Marine Ecology-Progress Series*, 273, 291-302.
- Emmerson M.C. & Raffaelli D. (2004). Predator-prey body size, interaction strength and the stability of a real food web. *Journal of Animal Ecology*, 73, 399-409.
- Englund G., Ohlund G., Hein C.L. & Diehl S. (2011). Temperature dependence of the functional response. *Ecology Letters*, 14, 914-921.
- Farrell T.M., Bracher D. & Roughgarden J. (1991). Cross-shelf transport causes recruitment to intertidal populations in central California. *Limnology and Oceanography*, 36, 279-288.
- Feely R.A., Sabine C.L., Hernandez-Ayon J.M., Ianson D. & Hales B. (2008). Evidence for upwelling of corrosive "acidified" water onto the continental shelf. *Science*, 320, 1490-1492.
- Fly E.K., Monaco C.J., Pincebourde S. & Tullis A. (2012). The influence of intertidal location and temperature on the metabolic cost of emersion in *Pisaster ochraceus*. *Journal of Experimental Marine Biology and Ecology*, 422, 20-28.
- Garcia-Reyes M. & Largier J. (2010). Observations of increased wind-driven coastal upwelling off central California. *Journal of Geophysical Research-Oceans*, 115.
- Gillooly J.F., Brown J.H., West G.B., Savage V.M. & Charnov E.L. (2001). Effects of size and temperature on metabolic rate. *Science*, 293, 2248-2251.
- Gilman S.E., Urban M.C., Tewksbury J., Gilchrist G.W. & Holt R.D. (2010). A framework for community interactions under climate change. *Trends in Ecology & Evolution*, 25, 325-331.
- Goudard A. & Loreau M. (2008). Nontrophic interactions, biodiversity, and ecosystem functioning: An interaction web model. *American Naturalist*, 171, 91-106.

- Grantham B.A., Chan F., Nielsen K.J., Fox D.S., Barth J.A., Huyer A., Lubchenco J. & Menge B.A. (2004). Upwelling-driven nearshore hypoxia signals ecosystem and oceanographic changes in the northeast Pacific. *Nature*, 429, 749-754.
- Grinsted A., Moore J.C. & Jevrejeva S. (2004). Application of the cross wavelet transform and wavelet coherence to geophysical time series. *Nonlinear Processes in Geophysics*, 11, 561-566.
- Hand S.C. & Kemp R.B. (1999). Chapter 9 Calorimetric approaches to animal physiology and bioenergetics. In: *Handbook of Thermal Analysis and Calorimetry*. Elsevier Science B.V., pp. 469-510.
- Harley C.D.G. & Helmuth B.S.T. (2003). Local- and regional-scale effects of wave exposure, thermal stress, and absolute versus effective shore level on patterns of intertidal zonation. *Limnology and Oceanography*, 48, 1498-1508.
- Harley C.D.G., Hughes A.R., Hultgren K.M., Miner B.G., Sorte C.J.B., Thornber C.S., Rodriguez L.F., Tomanek L. & Williams S.L. (2006). The impacts of climate change in coastal marine systems. *Ecology Letters*, 9, 228-241.
- Hauri C., Gruber N., Plattner G.K., Alin S., Feely R.A., Hales B. & Wheeler P.A. (2009). Ocean acidification in the California Current system. *Oceanography*, 22, 60-71.
- Hawkins S.J., Sugden H.E., Mieszkowska N., Moore P.J., Poloczanska E., Leaper R., Herbert R.J.H., Genner M.J., Moschella P.S., Thompson R.C., Jenkins S.R., Southward A.J. & Burrows M.T. (2009). Consequences of climate-driven biodiversity changes for ecosystem functioning of North European rocky shores. *Marine Ecology-Progress Series*, 396, 245-259.
- Hechinger R.F., Lafferty K.D., Dobson A.P., Brown J.H. & Kuris A.M. (2011). A Common Scaling Rule for Abundance, Energetics, and Production of Parasitic and Free-Living Species. *Science*, 333, 445-448.
- Heckmann L., Drossel B., Brose U. & Guill C. (2012). Interactive effects of body-size structure and adaptive foraging on food-web stability. *Ecology Letters*, 15, 243-250.
- Helmuth B., Mieszkowska N., Moore P. & Hawkins S.J. (2006). Living on the edge of two changing worlds: Forecasting the responses of rocky intertidal ecosystems to climate change. *Annual Review of Ecology Evolution and Systematics*, 37, 373-404.
- Helmuth B.S.T. (1998). Intertidal mussel microclimates: Predicting the body temperature of a sessile invertebrate. *Ecological Monographs*, 68, 51-74.
- Huey R.B. & Kingsolver J.G. (1993). Evolution of resistance to high-temperature in ectotherms. *American Naturalist*, 142, S21-S46.
- Hutchins L.W. (1947). The bases for temperature zonation in geographical distribution. *Ecological Monographs*, 17, 325-335.
- Huyer A. (1983). Coastal upwelling in the California Current system *Progress in Oceanography*, 12, 259-284.
- Iles A.C., Gouhier T.C., Menge B.A., Stewart J.S., Haupt A.J. & Lynch M.C. (2012). Climate-driven trends and ecological implications of event-scale upwelling in the California Current System. *Global Change Biology*, 18, 783-796.

- Iles A.C. & Rasmussen J.B. (2005). Indirect effects of metal contamination on energetics of yellow perch (*Perca flavescens*) resulting from food web simplification. *Freshwater Biology*, 50, 976-992.
- IPCC (2007). *Climate Change 2007: Synthesis Report. Contribution of Working Groups I, II and III to the Fourth Assessment Report of the Intergovernmental Panel on Climate Change*. IPCC, Geneva, Switzerland.
- Jorgensen C.B., Larsen P.S. & Riisgard H.U. (1990). Effects of temperature on the mussel pump. *Marine Ecology-Progress Series*, 64, 89-97.
- Karlsson P., Jonsson T. & Jonsson A. (2007). Food web structure and interaction strength pave the way for vulnerability to extinction. *Journal of Theoretical Biology*, 249, 77-92.
- Kefi S., Berlow E.L., Wieters E.A., Navarrete S.A., Petchey O.L., Wood S.A., Boit A., Joppa L.N., Lafferty K.D., Williams R.J., Martinez N.D., Menge B.A., Blanchette C.A., Iles A.C. & Brose U. (2012). More than a meal ... integrating non-feeding interactions into food webs. *Ecology Letters*, 15, 291-300.
- Keister J.E., Peterson W.T. & Pierce S.D. (2009). Zooplankton distribution and cross-shelf transfer of carbon in an area of complex mesoscale circulation in the northern California Current. *Deep-Sea Res. Part I-Oceanogr. Res. Pap.*, 56, 212-231.
- Kirincich A.R., Barth J.A., Grantham B.A., Menge B.A. & Lubchenco J. (2005). Wind-driven inner-shelf circulation off central Oregon during summer. *Journal of Geophysical Research-Oceans*, 110.
- Kittner C. & Riisgard H.U. (2005). Effect of temperature on filtration rate in the mussel *Mytilus edulis*: no evidence for temperature compensation. *Marine Ecology-Progress Series*, 305, 147-152.
- Lafferty K.D., Allesina S., Arim M., Briggs C.J., De Leo G., Dobson A.P., Dunne J.A., Johnson P.T.J., Kuris A.M., Marcogliese D.J., Martinez N.D., Memmott J., Marquet P.A., McLaughlin J.P., Mordecai E.A., Pascual M., Poulin R. & Thieltges D.W. (2008a). Parasites in food webs: the ultimate missing links. *Ecology Letters*, 11, 533-546.
- Lafferty K.D., Shaw J.C. & Kuris A.M. (2008b). Reef Fishes Have Higher Parasite Richness at Unfished Palmyra Atoll Compared to Fished Kiritimati Island. *EcoHealth*, 5, 338-345.
- Lamprecht I., Schmolz E. & Kemp R.B. (1999). Chapter 8 Calorimetry of small animals. In: *Handbook of Thermal Analysis and Calorimetry*. Elsevier Science B.V., pp. 405-467.
- Lauff R.F. & Wood C.H. (1996). Respiratory gas exchange, nitrogenous waste excretion, and fuel usage during aerobic swimming in juvenile rainbow trout. *J. Comp. Physiol. B-Biochem. Syst. Environ. Physiol.*, 166, 501-509.
- Lawrence J.M. & Lane J.M. (1982). The utilization of nutrients by post-metamorphic echinoderms. In: *Echinoderm Nutrition* (eds. Jangoux M & Lawrence JM). A. A. Balkema Rotterdam, pp. 331-371.

- Leonard G.H., Ewanchuk P.J. & Bertness M.D. (1999). How recruitment, intraspecific interactions, and predation control species borders in a tidal estuary. *Oecologia*, 118, 492-502.
- Levine S. (1980). Several measures of trophic structure applicable to complex food webs. *Journal of Theoretical Biology*, 83, 195-207.
- Lima F.P., Queiroz N., Ribeiro P.A., Hawkins S.J. & Santos A.M. (2006). Recent changes in the distribution of a marine gastropod, *Patella rustica* Linnaeus, 1758, and their relationship to unusual climatic events. *Journal of Biogeography*, 33, 812-822.
- Lopez-Urrutia A., San Martin E., Harris R.P. & Irigoien X. (2006). Scaling the metabolic balance of the oceans. *Proceedings of the National Academy of Sciences of the United States of America*, 103, 8739-8744.
- Mauzey K.P. (1966). Feeding behavior and reproductive cycles in *Pisaster Ochraceus*. *Biol. Bull.*, 131, 127-&.
- McCann K., Hastings A. & Huxel G.R. (1998). Weak trophic interactions and the balance of nature. *Nature*, 395, 794-798.
- McGregor H.V., Dima M., Fischer H.W. & Mulitza S. (2007). Rapid 20th-century increase in coastal upwelling off northwest Africa. *Science*, 315, 637-639.
- Melton C., Washburn L. & Gotschalk C. (2009). Wind relaxations and poleward flow events in a coastal upwelling system on the central California coast. *Journal of Geophysical Research-Oceans*, 114.
- Mendelssohn R. & Schwing F.B. (2002). Common and uncommon trends in SST and wind stress in the California and Peru-Chile Current Systems. *Progress in Oceanography*, 53, 141-162.
- Menge B., Hacker S.D., Freidenburg T., Lubchenco J., Craig R., Rilov G., Noble M. & Richmond E. (2011a). Potential impact of climate-related changes is buffered by differential responses to recruitment and interactions. *Ecological Monographs*, 81, 493-509.
- Menge B.A., Chan F. & Lubchenco J. (2008). Response of a rocky intertidal ecosystem engineer and community dominant to climate change. *Ecology Letters*, 11, 151-162.
- Menge B.A., Chan F., Nielsen K.J., Di Lorenzo E. & Lubchenco J. (2009). Climatic variation alters supply-side ecology: impact of climate patterns on phytoplankton and mussel recruitment. *Ecological Monographs*, 79, 379-395.
- Menge B.A., Daley B.A., Wheeler P.A., Dahlhoff E., Sanford E. & Strub P.T. (1997a). Benthic-pelagic links and rocky intertidal communities: Bottom-up effects on top-down control? *Proceedings of the National Academy of Sciences of the United States of America*, 94, 14530-14535.
- Menge B.A., Daley B.A., Wheeler P.A. & Strub P.T. (1997b). Rocky intertidal oceanography: An association between community structure and nearshore phytoplankton concentration. *Limnology and Oceanography*, 42, 57-66.
- Menge B.A., Gouhier T.C., Freidenburg T. & Lubchenco J. (2011b). Linking long-term, large-scale climatic and environmental variability to patterns of marine

- invertebrate recruitment: Toward explaining “unexplained” variation. *Journal of Experimental Marine Biology and Ecology*, 400, 236-249.
- Menge B.A., Lubchenco J., Bracken M.E.S., Chan F., Foley M.M., Freidenburg T.L., Gaines S.D., Hudson G., Krenz C., Leslie H., Menge D.N.L., Russell R. & Webster M.S. (2003). Coastal oceanography sets the pace of rocky intertidal community dynamics. *Proceedings of the National Academy of Sciences of the United States of America*, 100, 12229-12234.
- Menge B.A. & Olson A.M. (1990). Role of scale and environmental-factors in regulation of community structure. *Trends in Ecology & Evolution*, 5, 52-57.
- Moore P., Hawkins S.J. & Thompson R.C. (2007). Role of biological habitat amelioration in altering the relative responses of congeneric species to climate change. *Marine Ecology-Progress Series*, 334, 11-19.
- Morgan S.G., Fisher J.L., Miller S.H., McAfee S.T. & Largier J.L. (2009). Nearshore larval retention in a region of strong upwelling and recruitment limitation. *Ecology*, 90, 3489-3502.
- Navarrete S.A. & Berlow E.L. (2006). Variable interaction strengths stabilize marine community pattern. *Ecology Letters*, 9, 526-536.
- Noda T. (2004). Large-scale variability in recruitment of the barnacle *Semibalanus cariosus*: its cause and effects on the population density and predator. *Marine Ecology-Progress Series*, 278, 241-252.
- O'Connor M.I., Bruno J.F., Gaines S.D., Halpern B.S., Lester S.E., Kinlan B.P. & Weiss J.M. (2007). Temperature control of larval dispersal and the implications for marine ecology, evolution, and conservation. *Proceedings of the National Academy of Sciences of the United States of America*, 104, 1266-1271.
- O'Connor M.I., Gilbert B. & Brown C.J. (2011). Theoretical Predictions for How Temperature Affects the Dynamics of Interacting Herbivores and Plants. *American Naturalist*, 178, 626-638.
- O'Gorman E.J., Jacob U., Jonsson T. & Emmerson M.C. Interaction strength, food web topology and the relative importance of species in food webs. *Journal of Animal Ecology*, 79, 682-692.
- Paine R.T. & Vadas R.L. (1969). Calorific values of benthic marine algae and their postulated relation to invertebrate food preference. *Marine Biology*, 4, 79-86.
- Papastefanou K.M., Bollens S.M. & Slaughter A.M. (2006). Cross-shelf distribution of copepods and the role of event-scale winds in a northern California upwelling zone. *Deep-Sea Research Part II-Topical Studies in Oceanography*, 53, 3078-3098.
- Parmesan C. (2006). Ecological and evolutionary responses to recent climate change. In: *Annual Review of Ecology Evolution and Systematics*, pp. 637-669.
- Pauly D. & Christensen V. (1995). Primary production required to sustain global fisheries. *Nature*, 374, 255-257.
- Petchey O.L., Brose U. & Rall B.C. (2010). Predicting the effects of temperature on food web connectance. *Philosophical Transactions of the Royal Society B-Biological Sciences*, 365, 2081-2091.

- Petchey O.L., McPhearson P.T., Casey T.M. & Morin P.J. (1999). Environmental warming alters food-web structure and ecosystem function. *Nature*, 402, 69-72.
- Pincebourde S., Sanford E. & Helmuth B. (2008a). Body temperature during low tide alters the feeding performance of a top intertidal predator. *Limnology and Oceanography*, 53, 1562-1573.
- Pincebourde S., Sanford E. & Helmuth B. (2008b). Interaction between underwater and aerial body temperatures in influencing a top predator feeding rate in the intertidal. *Comparative Biochemistry and Physiology a-Molecular & Integrative Physiology*, 150, S95-S95.
- Pincebourde S., Sanford E. & Helmuth B. (2009). An Intertidal Sea Star Adjusts Thermal Inertia to Avoid Extreme Body Temperatures. *American Naturalist*, 174, 890-897.
- Poloczanska E.S., Hawkins S.J., Southward A.J. & Burrows M.T. (2008). Modeling the response of populations of competing species to climate change. *Ecology*, 89, 3138-3149.
- Pörtner H.O. & Peck M.A. (2010). Climate change effects on fishes and fisheries: towards a cause-and-effect understanding. *Journal of Fish Biology*, 77, 1745-1779.
- Rall B.C., Vucic-Pestic O., Ehnes R.B., Emmerson M. & Brose U. (2010). Temperature, predator-prey interaction strength and population stability. *Global Change Biology*, 16, 2145-2157.
- Rilov G., Dudas S.E., Menge B.A., Grantham B.A., Lubchenco J. & Schiel D.R. (2008). The surf zone: a semi-permeable barrier to onshore recruitment of invertebrate larvae? *Journal of Experimental Marine Biology and Ecology*, 361, 59-74.
- Roemmich D. & McGowan J. (1995). Climatic warming and the decline of zooplankton in the California Current. *Science*, 267, 1324-1326.
- Rooney N., McCann K., Gellner G. & Moore J.C. (2006). Structural asymmetry and the stability of diverse food webs. *Nature*, 442, 265-269.
- Roughgarden J., Pennington J.T., Stoner D., Alexander S. & Miller K. (1991). Collisions of upwelling fronts with the intertidal zone - The cause of recruitment pulses in barnacle populations of central California. *Acta Oecologica-International Journal of Ecology*, 12, 35-51.
- Samelson R., Barbour P., Barth J., Bielli S., Boyd T., Chelton D., Kosro P., Levine M., Skyllingstad E. & Wilczak J. (2002). Wind stress forcing of the Oregon coastal ocean during the 1999 upwelling season. *Journal of Geophysical Research-Oceans*, 107, 8.
- Sanford E. (1999). Regulation of keystone predation by small changes in ocean temperature. *Science*, 283, 2095-2097.
- Sanford E. (2002a). The feeding, growth, and energetics of two rocky intertidal predators (*Pisaster ochraceus* and *Nucella canaliculata*) under water temperatures simulating episodic upwelling. *Journal of Experimental Marine Biology and Ecology*, 273, 199-218.

- Sanford E. (2002b). Water temperature, predation, and the neglected role of physiological rate effects in rocky intertidal communities. *Integrative and Comparative Biology*, 42, 881-891.
- Santos A.M.P., Kazmin A.S. & Peliz A. (2005). Decadal changes in the Canary Upwelling System as revealed by satellite observations: Their impact on productivity. *Journal of Marine Research*, 63, 359-379.
- Scavia D., Field J.C., Boesch D.F., Buddemeier R.W., Burkett V., Cayan D.R., Fogarty M., Harwell M.A., Howarth R.W., Mason C., Reed D.J., Royer T.C., Sallenger A.H. & Titus J.G. (2002). Climate change impacts on US coastal and marine ecosystems. *Estuaries*, 25, 149-164.
- Scheltema R.S. (1986). On dispersal and planktonic larvae of benthic invertebrates - An electric overview and summary of problems. *Bulletin of Marine Science*, 39, 290-322.
- Schwing F.B., Bond N.A., Bograd S.J., Mitchell T., Alexander M.A. & Mantua N. (2006). Delayed coastal upwelling along the US West Coast in 2005: A historical perspective. *Geophysical Research Letters*, 33.
- Sentis A., Hemptinne J.L. & Brodeur J. (2012). Using functional response modeling to investigate the effect of temperature on predator feeding rate and energetic efficiency. *Oecologia*, 169, 1117-1125.
- Shanks A.L. (2009a). Barnacle settlement versus recruitment as indicators of larval delivery. I. Effects of post-settlement mortality and recruit density. *Marine Ecology-Progress Series*, 385, 205-216.
- Shanks A.L. (2009b). Barnacle settlement versus recruitment as indicators of larval delivery. II. Time-series analysis and hypothesized delivery mechanisms. *Marine Ecology-Progress Series*, 385, 217-226.
- Shanks A.L. & Brink L. (2005). Upwelling, downwelling, and cross-shelf transport of bivalve larvae: test of a hypothesis. *Marine Ecology-Progress Series*, 302, 1-12.
- Shanks A.L., Morgan S.G., MacMahan J. & Reniers A. (2010). Surf zone physical and morphological regime as determinants of temporal and spatial variation in larval recruitment. *Journal of Experimental Marine Biology and Ecology*, 392, 140-150.
- Shanks A.L. & Shearman R.K. (2009). Paradigm lost? Cross-shelf distributions of intertidal invertebrate larvae are unaffected by upwelling or downwelling. *Marine Ecology-Progress Series*, 385, 189-204.
- Snyder M.A., Sloan L.C., Diffenbaugh N.S. & Bell J.L. (2003). Future climate change and upwelling in the California Current. *Geophysical Research Letters*, 30.
- Somero G.N. (2002). Thermal physiology and vertical zonation of intertidal animals: Optima, limits, and costs of living. *Integrative and Comparative Biology*, 42, 780-789.
- Somero G.N. (2011). Comparative physiology: a "crystal ball" for predicting consequences of global change. *Am. J. Physiol.-Regul. Integr. Comp. Physiol.*, 301, R1-R14.
- Springer S.R., Samelson R.M., Allen J.S., Egbert G.D., Kurapov A.L., Miller R.N. & Kindle J.C. (2009). A nested grid model of the Oregon Coastal Transition Zone:

- Simulations and comparisons with observations during the 2001 upwelling season. *Journal of Geophysical Research-Oceans*, 114, 22.
- Svensson C.J., Jenkins S.R., Hawkins S.J. & Aberg P. (2005). Population resistance to climate change: modelling the effects of low recruitment in open populations. *Oecologia*, 142, 117-126.
- Szathmary P.L., Helmuth B. & Wethey D.S. (2009). Climate change in the rocky intertidal zone: predicting and measuring the body temperature of a keystone predator. *Marine Ecology-Progress Series*, 374, 43-56.
- Thebault E. & Loreau M. (2005). Trophic interactions and the relationship between species diversity and ecosystem stability. *American Naturalist*, 166, E95-E114.
- Tilman D. (1977). Resource competition between planktonic algae - Experimental and theoretical approach. *Ecology*, 58, 338-348.
- Torrence C. & Compo G.P. (1998). A practical guide to wavelet analysis. *Bulletin of the American Meteorological Society*, 79, 61-78.
- Tylianakis J.M., Didham R.K., Bascompte J. & Wardle D.A. (2008). Global change and species interactions in terrestrial ecosystems. *Ecology Letters*, 11, 1351-1363.
- Urban M.C., Holt R.D., Gilman S.E. & Tewksbury J. (2011). Heating up relations between cold fish: competition modifies responses to climate change. *Journal of Animal Ecology*, 80, 505-507.
- Vasseur D.A. & McCann K.S. (2005). A mechanistic approach for modeling temperature-dependent consumer-resource dynamics. *American Naturalist*, 166, 184-198.
- Voigt W., Perner J., Davis A.J., Eggers T., Schumacher J., Bahrmann R., Fabian B., Heinrich W., Kohler G., Lichter D., Marstaller R. & Sander F.W. (2003). Trophic levels are differentially sensitive to climate. *Ecology*, 84, 2444-2453.
- Vucic-Pestic O., Ehnes R.B., Rall B.C. & Brose U. (2011). Warming up the system: higher predator feeding rates but lower energetic efficiencies. *Global Change Biology*, 17, 1301-1310.
- Walther G.R. (2010). Community and ecosystem responses to recent climate change. *Philosophical Transactions of the Royal Society B-Biological Sciences*, 365, 2019-2024.
- Walther G.R., Post E., Convey P., Menzel A., Parmesan C., Beebee T.J.C., Fromentin J.M., Hoegh-Guldberg O. & Bairlein F. (2002). Ecological responses to recent climate change. *Nature*, 416, 389-395.
- Williams R.J. & Martinez N.D. (2000). Simple rules yield complex food webs. *Nature*, 404, 180-183.
- Williams R.J. & Martinez N.D. (2004). Limits to trophic levels and omnivory in complex food webs: Theory and data. *American Naturalist*, 163, 458-468.
- Williams R.J. & Martinez N.D. (2008). Success and its limits among structural models of complex food webs. *Journal of Animal Ecology*, 77, 512-519.
- Wood C.L., Lafferty K.D. & Micheli F. (2010). Fishing out marine parasites? Impacts of fishing on rates of parasitism in the ocean. *Ecology Letters*, 13, 761-775.

- Woodward G., Benstead J.P., Beveridge O.S., Blanchard J., Brey T., Brown L.E., Cross W.F., Friberg N., Ings T.C., Jacob U., Jennings S., Ledger M.E., Milner A.M., Montoya J.M., O'Gorman E.J., Olesen J.M., Petchey O.L., Pichler D.E., Reuman D.C., Thompson M.S.A., Van Veen F.J.F. & Yvon-Durocher G. (2010). Ecological Networks in a Changing Climate. In: *Advances in Ecological Research: Ecological Networks*, Vol 42, pp. 71-138.
- Wootton J.T. & Emmerson M. (2005). Measurement of interaction strength innature. *Annual Review of Ecology Evolution and Systematics*, 36, 419-444.
- Yamane L. & Gilman S.E. (2009). Opposite responses by an intertidal predator to increasing aquatic and aerial temperatures. *Marine Ecology-Progress Series*, 393, 27-36.
- Yee E.H. & Murray S.N. (2004). Effects of temperature on activity, food consumption rates, and gut passage times of seaweed-eating Tegula species (Trochidae) from California. *Marine Biology*, 145, 895-903.
- Yodzis P. & Innes S. (1992). Body size and consumer-resource dynamics. *American Naturalist*, 139, 1151-1175.
- Zarnetske P.L., Skelly D.K. & Urban M.C. (2012). Biotic Multipliers of Climate Change. *Science*, 336, 1516-1518.
- Zuur A.F., Ieno E.N., Walker N., Saveliev A.A. & Smith G.M. (2009). *Mixed Effects Models and Extensions in Ecology with R*. 1st edn. Springer, New York.

APPENDICES

Appendix A – An evaluation of the temperature scaling equations of Chapter 2

The joint effects of body mass, M , and temperature, T (in K), on the metabolic rate, X , and ingestion rate, Y , of ectotherms are well described by the Universal Temperature Dependence (UTD) model (Gillooly *et al.* 2001; Brown *et al.* 2004):

$$X = a_x M^{b_x} e^{-\frac{E_x}{kT}} \quad (1a)$$

$$Y = a_y M^{b_y} e^{-\frac{E_y}{kT}} \quad (1b)$$

where b is an allometric exponent, E (eV) is the activation energy, k is Boltzmann's constant (8.62×10^{-5} eV·K $^{-1}$) and a_x and a_y are normalization constants independent of body mass and temperature. By calculating the mass corrected rates and taking the natural logarithm of both sides, these equations can be linearized and the temperature scaling parameters (E_x , E_y) can easily be estimated as the slope of a least-squares linear regression line:

$$\ln(XM^{-b_x}) = -E_x \left(\frac{1}{kT} \right) + \ln(a_x) \quad (2a)$$

$$\ln(YM^{-b_y}) = -E_y \left(\frac{1}{kT} \right) + \ln(a_y) \quad (2b)$$

Because temperature is in degrees Kelvin, the intercepts ($\ln(a_x)$, $\ln(a_y)$), represent mass-corrected metabolic rates at -273.15°C , which is biologically meaningless and impossible to measure. Thus, to incorporate estimates of the normalization constants from lab measurements, it is necessary to resolve these equations at a temperature at which these rates are measured (Vasseur & McCann 2005). I will describe how this is done using the equation for metabolic rate; however the calculations for ingestion follow the same methods. First, evaluate equation 2a at a common reference temperature (T_0):

$$\ln(a_{x(T_0)}) = -E_x \left(\frac{1}{kT_0} \right) + \ln(a_{Ix}) \quad (3)$$

Where $\ln(a_{x(T_0)})$ represents the mass-corrected metabolic rate at $T = T_0$, which will be the new normalization constant where the y-axis crosses at the equivalent of 20°C instead of -273.15°C . Next, solve for the original intercept:

$$\ln(a_x) = \ln(a_{x(T_0)}) + E_x \left(\frac{1}{kT_0} \right) \quad (4)$$

Then substitute for the original intercept in equation 2a and simplify:

$$\ln(XM^{-b_x}) = -E_x \left(\frac{1}{kT} \right) + \ln(a_{x(T_0)}) + E_x \left(\frac{1}{kT_0} \right) \quad (5a)$$

$$\begin{aligned} \ln(XM^{-b_x}) &= \ln(a_{x(T_0)}) + \frac{E_x}{kT_0} - \frac{E_x}{kT} = \ln(a_{x(T_0)}) + \frac{E_x T}{kTT_0} - \frac{E_x T_0}{kTT_0} = \ln(a_{x(T_0)}) + \\ &\quad \frac{E_x(T-T_0)}{kTT_0} \end{aligned} \quad (5b)$$

$$X = a_{x(T_0)} M^{b_x} e^{\frac{E_x(T-T_0)}{kTT_0}} \quad (5c)$$

Assuming that the allometric exponent is equivalent to $\frac{3}{4}$ power scaling, then the final equation for mass-specific metabolic rate is:

$$X/M = a_{x(T_0)} M^{-0.25} e^{\left(\frac{E_x(T-T_0)}{kTT_0} \right)} \quad (6)$$

This equation is used in the ATN model using the empirical estimates of the normalization constants. Because the models are of how biomass densities (mass/area) change through time, the units of the normalization constants need to be in units of mass per time. I used empirical estimates of the normalization constants from UTD models of metabolic and ingestion rates for several rocky intertidal invertebrates (see Chapter 3). These analyses were originally analyzed in units of Joules per second but were converted to kilograms per year, assuming $6,000,000 \text{ J kg}^{-1}$ (Table A1).

Table A1 Robust linear regressions coefficients and statistics for the UTD models of the effect of body mass and water temperature on mass specific metabolic and ingestion rates ($\text{kg} \cdot \text{s}^{-1}$), using the Huber method. All the models are of the form: $\ln(y) = b \ln(M) - E \left(\frac{1}{kT} \right) + \ln(a)$, where M is body mass (kg), T is water temperature (K), and k is Boltzmann's constant ($8.62 \times 10^{-5} \text{ eV} \cdot \text{K}^{-1}$). The coefficients with the 95% confidence interval in parentheses include b , the allometric exponent; E , the activation energy (eV); and a , the normalization constant or the intercept. The model statistics include the model p-value ($\alpha < 0.05$ in bold) and the sample size, n . Also included is the normalization constant evaluated at $T_0 = 20^\circ\text{C}$, $a_{(T_0)}$, in units of $\text{kg} (\text{kg year})^{-1} \text{ kg}^{0.25}$. P value significance codes: $0 < ^{***} < 0.001 < ^{**} < 0.01 < ^{*} < 0.05 < ^{--} < 0.1$.

Species / Interaction	<i>b</i>	<i>E</i> (eV)	$\ln(a)$	$a_{(T_0)}$	<i>p</i> -value	<i>n</i>
Metabolic rate, X						
<i>M. californianus</i>	-0.34(-0.39–0.28)***	0.68(0.42–0.96)	24.89(14.53–36.26)	0.143	4.55E-12	27
<i>N. canaliculata</i>	-0.4(-0.57–0.23)**	0.6(0.29–0.88)*	20.99(9.51–32.57)-	0.069	9.66E-05	25
<i>K. tunicata</i>	-0.2(-0.3–0.08)*	0.66(0.33–0.94)**	25.16(11.55–36.54)**	0.359	4.75E-05	29
<i>N. ostrina</i>	-0.46(-0.64–0.26)**	0.92(0.58–1.28)*	33.86(19.35–48.48)*	0.085	5.37E-06	25
<i>P. ochraceus</i>	-0.54(-0.68–0.36)***	0.84(0.41–1.36)-	30.94(13.12–51.88)	0.010	2.18E-07	28
<i>M. trossulus</i>	-0.52(-0.61–0.43)***	0.76(0.54–0.99)*	26.87(18.06–36.28)*	0.042	1.31E-10	25
<i>S. purpuratus</i>	-0.47(-0.61–0.27)**	0.56(0.13–1.04)	19.7(2.65–39.18)	0.074	5.08E-07	30
Ingestion Rate, Y						
<i>N. canaliculata</i> - <i>B. glandula</i>	-1.28(-1.47–1.07)***	0.06(-0.47–0.52)	-9.6(-30.99–8.7)	6.12E-6	3.79E-14	44
<i>N. canaliculata</i> - <i>M. trossulus</i>	-0.57(-0.66–0.48)***	0.8(0.65–0.95)***	31.36(24.78–37.36)***	0.681	4.88E-21	54
<i>K. tunicata</i> - <i>S. sessilis</i>	-0.81(-1.3–0.27)*	1.06(0.04–2.16)	40.52(-2.03–85.69)	0.2271	0.00781	19
<i>N. ostrina</i> - <i>B. glandula</i>	-0.82(-0.98–0.69)***	0.57(0.36–0.76)*	15.29(6.57–23.17)	7.58E-4	4.96E-15	49
<i>N. ostrina</i> - <i>M. trossulus</i>	-0.41(-0.52–0.28)**	0.8(0.61–0.97)***	32.28(24.34–39.38)***	1.870	1.1E-14	51
<i>P. ochraceus</i> - <i>M. californianus</i>	-0.43(-0.65–0.22)*	0.39(0.02–0.77)	17.72(2.22–32.81)	8.094	0.00165	30
<i>S. purpuratus</i> - <i>S. sessilis</i>	-0.4(-0.8–0.02)	0.65(-0.26–1.52)	26.33(-12.66–61.22)	2.036	0.12	17

Appendix B – Robust linear regression analysis for the estimation of the coefficients of the UTD models from Chapter 3

In several of the universal temperature dependence (UTD) models describing the temperature and body mass dependence of metabolic rates, ingestion rates, and species interaction strengths, the residuals were non-normally distributed due to influential outliers. Because influential outliers can affect the estimation of regression parameters in least squares regression and since this was the primary objective of the study, I reanalyzed the UTD model using the Huber method for robust linear regression, which weights observations based on their residuals. The p -values of the robust regression coefficients were calculated by performing 1,000 permutations of the data and determining the proportion of permutations that yielded a coefficient that was greater than or equal to the absolute value of the one obtained with the original data. Since standard errors reported by robust linear regression rely on asymptotic approximations, and may not be trustworthy in a small sample, I used a bootstrap method, reshuffling residuals to fitted y-values 1000 times to calculate the 95% bias-corrected confidence intervals. To test for systematic differences between metabolic and ingestion rates across species, I performed a paired, two-tailed t -test and a power analysis to determine whether the t -test results were due to lack of power from the low sample size. I used R 2.13.2 (The R Foundation for Statistical Computing 2011) for all statistical analyses.

Like the linear least squares regression results, metabolic rates, ingestion rates, and the strength of species interactions tended to increase with body size and temperature in accordance with the UTD model (Fig. B1-3, Table B1). The obvious exception to this trend was the negative effect of body mass on ingestion rates and species interaction strength between *N. canaliculata* and *B. glandula* (Fig. B2-3, Table B1). This is likely due to reduced feeding rates at very high body size ratios between the large whelks and the tiny barnacle prey, which has been observed in prior feeding trials (ACI unpublished data). Although these estimates of the UTD model coefficients are more robust to

outliers, they are very similar to the estimates obtained from the least squares regression in the main paper, indicating that the outliers were not very influential on the final results.

Like the linear least squares regression results in the main paper, consumer metabolic rates tended to be more sensitive to temperature than ingestion rates, with the exception of the *N. canaliculata* – *M. trossulus* interaction, resulting in negative consumer thermal impacts (CTIs; Table B2). The paired sample t-test indicated that CTI values are more likely to be negative, $t(5) = -2.45, p = 0.058$, with an average CTI of -0.25 (95% CI ± 0.26 ; Table B2). However, due to the low number of observations ($n=6$), the power was low (power = 0.51). A power analysis ($\beta=0.9, \alpha=0.05$) indicated that a sample size of at least 13 species would be necessary to detect a significant systematic difference between the activation energies of metabolic and ingestion rates.

Table B1 Robust linear regressions coefficients and statistics for the UTD models of the effect of body mass and water temperature on metabolic rates, ingestion rates and species interaction strengths, using the Huber method. All the models are of the form $\ln(y) = b \ln(M) - E \left(\frac{1}{kT} \right) + \ln(c)$, where M is body mass (g), T is water temperature (K), and k is Boltzmann's constant (8.62×10^{-5} eV·K $^{-1}$). The coefficients with the 95% confidence interval in parentheses include b , the allometric exponent; E , the activation energy (eV); and c , the normalization constant. The model statistics include the model p -value ($\alpha < 0.05$ in bold) and the sample size, n . P value significance codes: $0 < ^{***} < 0.001 < ^{**} < 0.01 < ^{*} < 0.05 < ^{--} < 0.1$

Species / Interaction	<i>b</i>	<i>E</i> (eV)	$\ln(c)$	<i>p</i> -value	<i>n</i>
Metabolic rate					
<i>M. californianus</i>	0.66(0.61–0.71) ***	0.68(0.41–0.94)	18.68(7.84–29.27)	4.08E-18	27
<i>N. canaliculata</i>	0.6(0.42–0.78) ***	0.6(0.32–0.93)-	15.21(3.84–28.8)	5.71E-07	25
<i>K. tunicata</i>	0.8(0.69–0.92) ***	0.66(0.35–0.95)	17.95(5.3–29.49)	3.74E-13	29
<i>N. ostrina</i>	0.54(0.36–0.72) **	0.92(0.54–1.25) **	28.48(13.28–42.06)-	2.17E-06	25
<i>P. ochraceus</i>	0.46(0.31–0.6) ***	0.84(0.34–1.28)*	26.09(5.51–43.68)	3.43E-06	28
<i>M. trossulus</i>	0.48(0.4–0.58) **	0.76(0.52–0.99)*	21.87(12.28–31.14)	1.24E-10	25
<i>S. purpuratus</i>	0.53(0.34–0.69) ***	0.56(0.18–1.04)	14.35(-1.7–33.3)	4.64E-08	30
Ingestion rate					
<i>N. canaliculata</i> - <i>B. glandula</i>	-0.28(-0.46–0.07)*	0.06(-0.43–0.56)	-9.35(-29.63–10.95)	0.042	44
<i>N. canaliculata</i> - <i>M. trossulus</i>	0.43(0.34–0.52) ***	0.8(0.65–0.96) ***	26.74(20.36–33.12) **	6.3E-17	54
<i>K. tunicata</i> - <i>S. sessilis</i>	0.19(-0.3–0.67)	1.06(-0.12–2.09)-	37.54(-8.9–79.83)	0.24	19
<i>N. ostrina</i> - <i>B. glandula</i>	0.18(0.04–0.34)-	0.57(0.38–0.78) **	12.42(4.6–20.84)	4.08E-06	49
<i>N. ostrina</i> - <i>M. trossulus</i>	0.59(0.48–0.73) ***	0.8(0.64–0.99) ***	26.52(19.82–34.4) **	3.95E-16	51
<i>P. ochraceus</i> - <i>M. californianus</i>	0.57(0.33–0.79) ***	0.39(0.01–0.79)	12.14(-3.29–28.16)	0.00054	30
<i>S. purpuratus</i> - <i>S. sessilis</i>	0.6(0.18–1.01)*	0.65(-0.17–1.62)	20.53(-12.41–59.8)	0.06	17

Table B1 (Continued)

Species / Interaction	b	E (eV)	ln(c)	p-value	n
<i>Species interaction strength</i>					
<i>N. canaliculata</i> - <i>B. glandula</i>	0.14(-0.52–0.71)	-0.008(-0.01–0.002)*	0.003(-0.013–0.017)	0.047	44
<i>N. canaliculata</i> - <i>M. trossulus</i>	0.92(0.68–1.14)***	0.011(0.008–0.015)***	0.022(0.016–0.027)***	7.5E-12	54
<i>K. tunicata</i> - <i>S. sessilis</i>	0.32(-0.06–0.72)	0.003(-0.002–0.007)	0.008(-0.001–0.018)	0.15	19
<i>N. ostrina</i> - <i>B. glandula</i>	1.85(0.64–2.98)**	-0.021(-0.043–0.002)-	0.044(0.014–0.071)**	0.0034	49
<i>N. ostrina</i> - <i>M. trossulus</i>	1.12(0.82–1.47)**	0.018(0.012–0.026)***	0.026(0.019–0.035)**	1.28E-09	51
<i>P. ochraceus</i> - <i>M. californianus</i>	0.94(0.03–1.82)	0.033(0.019–0.047)***	0.026(0.004–0.048)-	0.00015	30
<i>S. purpuratus</i> - <i>S. sessilis</i>	0.36(-1.11–1.63)	0.017(-0.001–0.03)*	0.0094(-0.027–0.04)	0.015	17

Table B2 Consumer thermal impact estimates ($CTI = E_J - E_I$) calculated from robust linear regression estimates of the activation energies of metabolic rate, E_I , and ingestion rate, E_J .

Consumer	Resource	E_J	E_I	CTI
<i>M. californianus</i>	<i>Rhodomonas spp.</i>	0.33*	0.68	-0.35
<i>M. trossulus</i>	<i>Rhodomonas spp.</i>	0.33*	0.76	-0.43
<i>N. canaliculata</i>	<i>M. trossulus</i>	0.80	0.60/1.34†	0.20/-0.54†
<i>N. ostrina</i>	<i>B. glandula</i>	0.57	0.92	-0.35
<i>N. ostrina</i>	<i>M. trossulus</i>	0.80	0.92	-0.12
<i>P. ochraceus</i>	<i>M. californianus</i>	0.39	0.84	-0.45

*This value comes from a weighted average of estimates from the literature (Jorgensen *et al.* 1990; Kittner & Riisgard 2005)

†These estimates are over the range of temperatures where the relationship between temperature and metabolic rate is linear.

Figure B1 Metabolic rates as a function of water temperature (a-g) and body mass (h-n) for seven species of rocky intertidal invertebrates: *M. californianus* (a, h), *N. canaliculata* (b, i), *K. tunicata* (c, j), *N. ostrina* (d, k), *P. ochraceus* (e, l), *M. trossulus* (f, m), and *S. purpuratus* (g, n). Variables were log transformed and metabolic rates were normalized by body mass (a-g) or temperature (h-n). Statistically significant robust UTD regression models ($\alpha \leq 0.05$) are plotted in black. The grey regression line in subplot b represents a robust regression on the increasing linear subset of data (temperatures $\leq 14^{\circ}\text{C}$). The temperature axes scale inversely as $1/kT(1/\text{eV})$, where T is temperature (K) and k is Boltzmann's constant ($8.62 \times 10^{-5} \text{ eV}\cdot\text{K}^{-1}$). A transformed temperature scale in $^{\circ}\text{C}$ is on the top axis (a-g).

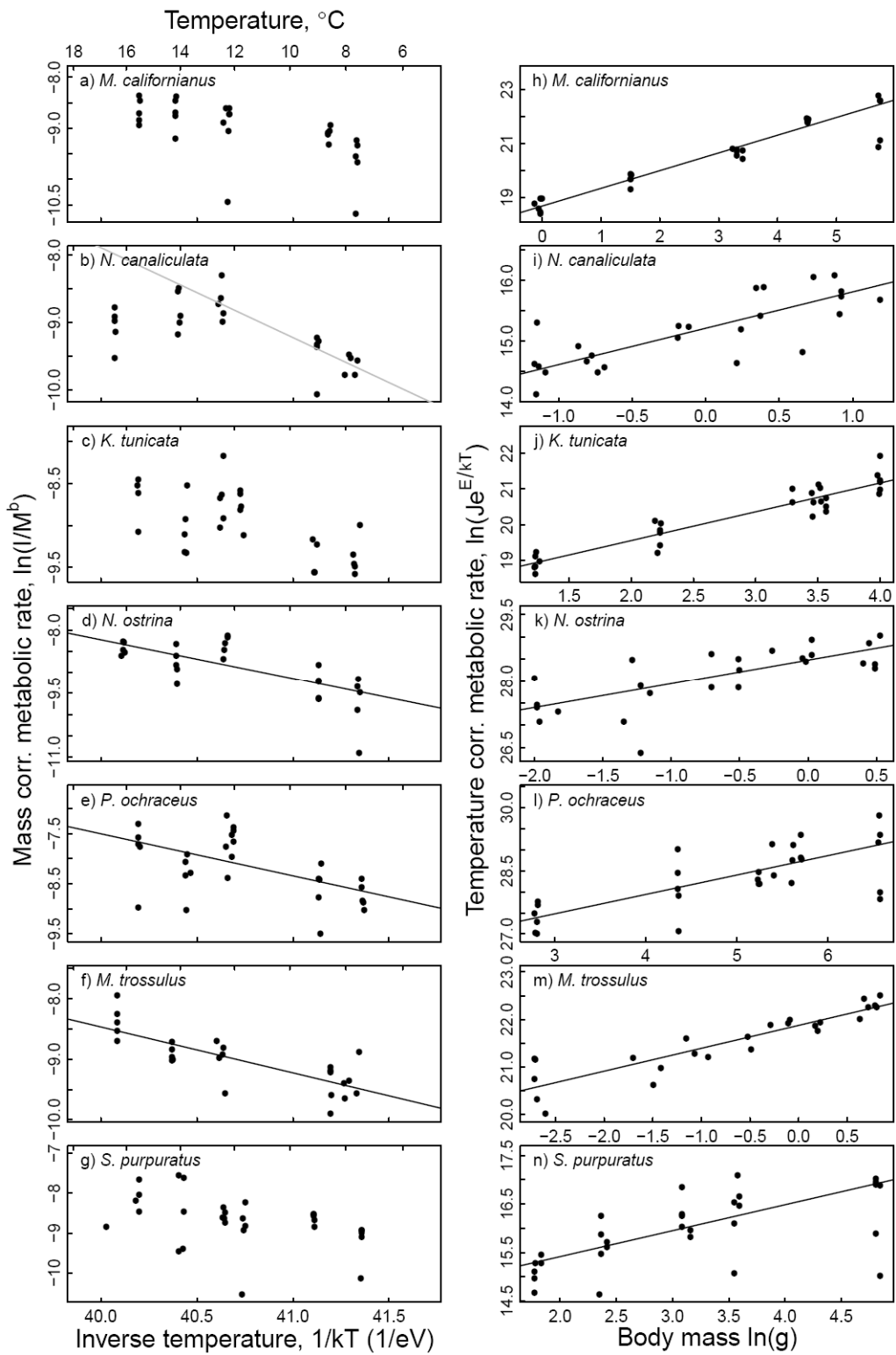
**Figure B1**

Figure B2 Ingestion rates as a function of water temperature (a-g) and body mass (h-n) for seven rocky intertidal species interactions: *N. canaliculata* - *B. glandula* (a, h), *N. canaliculata* - *M. trossulus* (b, i), *K. tunicata* - *S. sessilis* (c, j), *N. ostrina* - *B. glandula* (d, k), *N. ostrina* - *M. trossulus* (e, l), *P. ochraceus* - *M. californianus* (f, m), and *S. purpuratus* - *S. sessilis* (g, n). Variables were log transformed and ingestion rates were normalized by body mass (a-g) or temperature (h-n). Statistically significant robust UTD regression models ($\alpha \leq 0.05$) are plotted in black. The temperature axes scale inversely as $1/kT(1/eV)$, where T is temperature (K) and k is Boltzmann's constant ($8.62 \times 10^{-5} \text{ eV}\cdot\text{K}^{-1}$). A transformed temperature scale in $^{\circ}\text{C}$ is on the top axis (a-g).

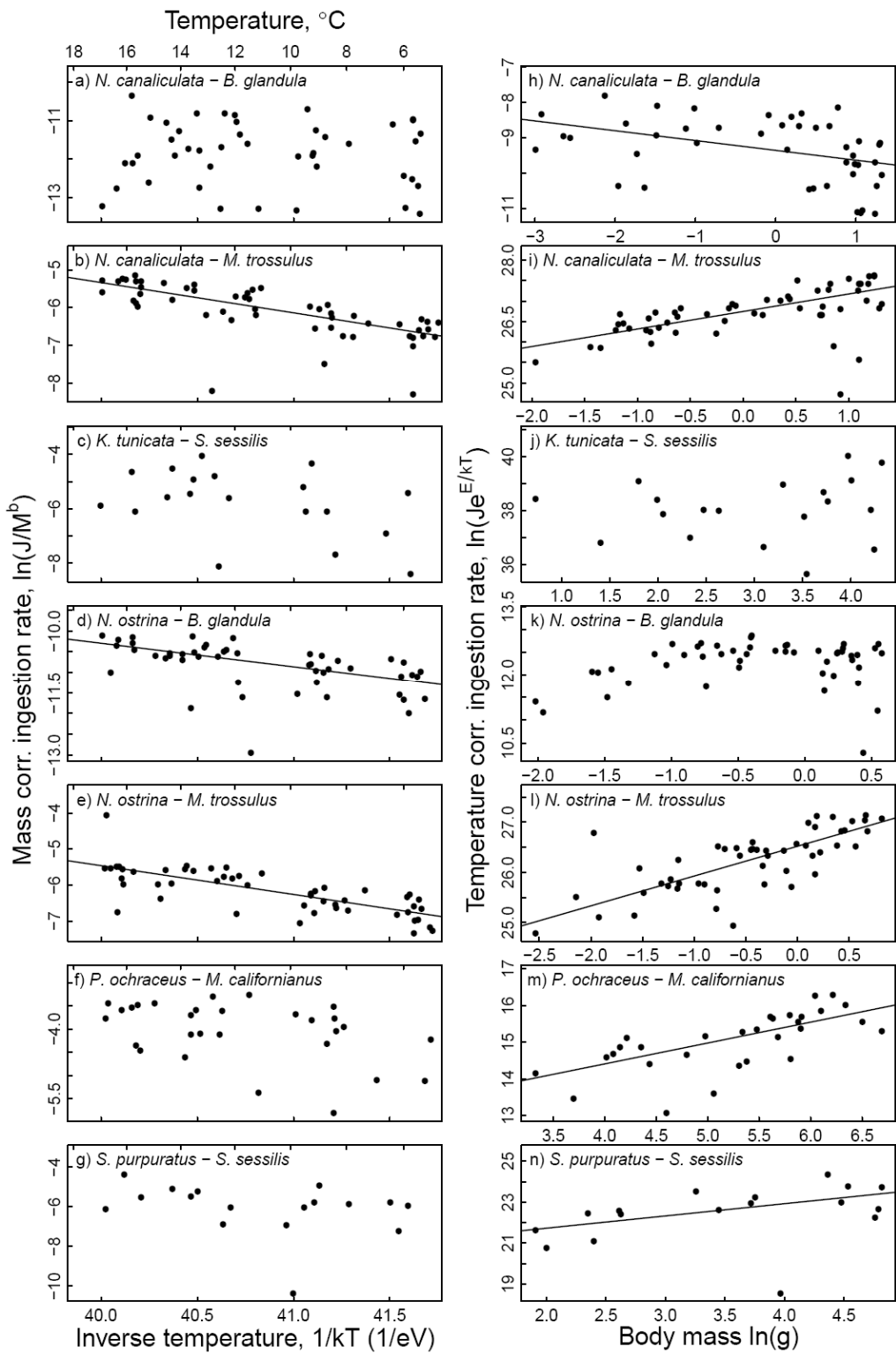
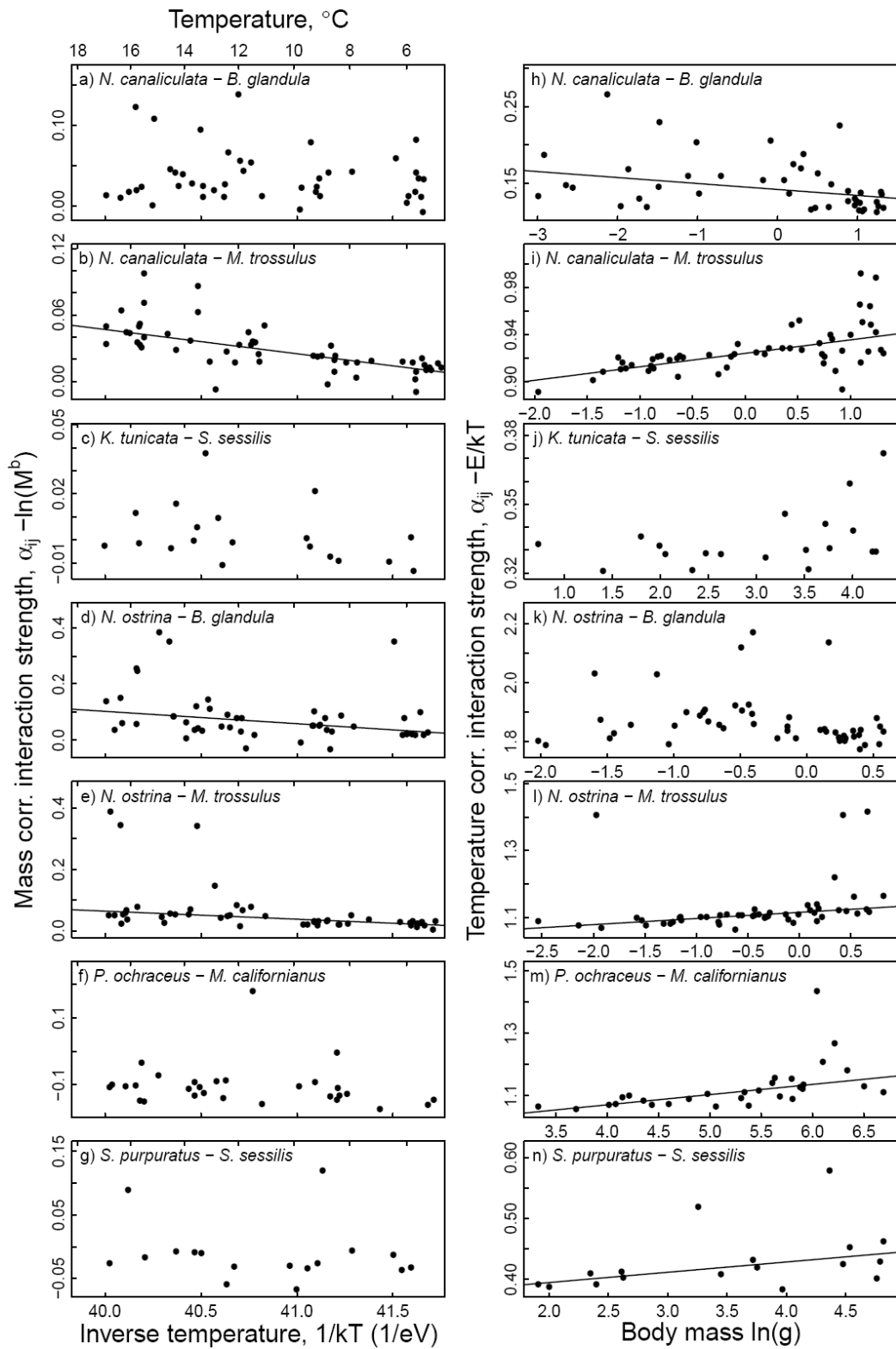
**Figure B2**

Figure B3 Log ratio interaction strength as a function of water temperature (a-g) and body mass (h-n) for seven rocky intertidal species interactions: *N. canaliculata* - *B. glandula* (a, h), *N. canaliculata* - *M. trossulus* (b, i), *K. tunicata* - *S. sessilis* (c, j), *N. ostrina* - *B. glandula* (d, k), *N. ostrina* - *M. trossulus* (e, l), *P. ochraceus* - *M. californianus* (f, m), and *S. purpuratus* - *S. sessilis* (g, n). Variables were log transformed and interaction strengths were normalized by body mass (a-g) or temperature (h-n). Statistically significant robust UTD regression models ($\alpha \leq 0.05$) are plotted in black. The temperature axes scale inversely as $1/kT$ (1/eV), where T is temperature (K) and k is Boltzmann's constant (8.62×10^{-5} eV·K $^{-1}$). A transformed temperature scale in °C is on the top axis (a-g).

**Figure B3**

Appendix C – Wavelet analysis tutorial

BACKGROUND

The variability of a time series is traditionally studied by using spectral analysis (Chatfield 1996, Cazelles et al. 2008). Spectral analysis partitions the variability (or power) in a time series into a suite of harmonic components characterized by different frequencies (or periods) (Cazelles et al. 2008). Plotting the power of each harmonic component as a function of its frequency (i.e., the power spectrum) reveals the contribution of each frequency (or period) to the variability (or power) in the time series (Fig. C1a,b). The power spectrum can thus be used to identify key temporal scales of variability (or periodicities) in a time series. Once these periodicities are detected, one can focus on processes occurring at those temporal scales to potentially uncover critical underlying mechanisms.

One important limitation of spectral analysis lies in the assumption that the moments of the time series (i.e., its mean, variance, skewness, kurtosis, etc...) do not change over time (i.e., are stationary; Torrence and Compo 1998, Cazelles et al. 2008, Rouyer et al. 2008a, 2008b). However, there is increasing evidence that many time series exhibit non-stationary variability (Rohani et al. 1999, Grenfell et al. 2001, Beninca et al. 2008, Rouyer et al. 2008a, Beninca et al. 2009, Gouhier et al. 2010). In order to analyze these types of non-stationary time series, we must turn to more complex, time-resolved methods.

Wavelet analysis provides an efficient and accurate method for describing the variability of non-stationary time series in the time-frequency domain (Fig. C1; Torrence and Compo 1998, Cazelles et al. 2008). Indeed, since wavelet analysis decomposes a time series over functions (wavelets) that can be scaled (i.e., contracted or dilated) and translated, high-frequency structures in the time series can be fit with narrow wavelets whereas low-frequency structures in the time series can be fit with wide wavelets (Fig. C2; Cazelles et al. 2008). This decomposition leads to a good trade-off for the time-scale

resolution, and a good localization in both the time and frequency domains (Cazelles et al. 2008). Hence, wavelet analysis provides an efficient way of tracking changes in time in the contribution of each frequency to the variability of a time series (Fig. C1).

Wavelet analysis can be extended to assess the relationship between two time series by calculating the cross-wavelet and the wavelet coherence. The cross-wavelet and the wavelet coherence can be thought of, respectively, as the covariance and the cross-correlation of two time series in the time-frequency domain (Cazelles et al. 2008, Rouyer et al. 2008a). Cross-wavelet and wavelet coherence thus provide ideal and complementary tools for studying the relationship between non-stationary time series. It is important to note, however, that while cross-wavelet analysis and wavelet coherence can document patterns of covariation between time series, they cannot provide definitive evidence about the mechanisms responsible for these patterns (Cazelles et al. 2008). Hence, just as with classical correlative approaches, cross-wavelet and wavelet coherence analyses must be complemented by experimental studies in order to ascribe the observed patterns of covariation to their underlying, causal mechanisms.

Applying wavelet analysis to ecological time series

Wavelet analysis is often dismissed in ecology because time series are typically short and have missing values. However, recent work has shown that wavelet analysis can be performed on short (Cazelles et al. 2008) and irregularly spaced time series (Keitt 2008). Additionally, Cazelles et al. (2008) have shown that wavelet analysis is robust to missing values, even when they occur at regular intervals. They suggest two criteria for the application of wavelet analysis: (1) the time series must have at least 30-40 data points and (2) the significant periodic components of the time series must be smaller than 20-25% of its length (Cazelles et al. 2008).

All of our daily upwelling and temperature time series fit both criteria (minimum total length of 3,945 days, main period of ~365 days). Missing values represented 0.2% of the upwelling data and 1.42% of the temperature data for Boiler Bay, 0.2% of the upwelling data and 6.4% of the temperature data for Strawberry Hill, and 0.16% of the

upwelling data and 5.3% of the temperature data for Cape Blanco. The missing values were scattered randomly across the time series and were thus unlikely to exert a strong and systematic influence on our analyses. We used linear interpolation to replace these missing values. Using cubic splines to replace the missing values yielded results that were qualitatively identical to those obtained using linear interpolation. Thus, our results are robust to the method used to replace the missing values.

In this appendix, we provide details on the wavelet, cross-wavelet and wavelet coherence analyses used in the main text. More details on these methods can be found in the reviews by Torrence and Compo (1998), Grinsted et al. (2004), Cazelles et al. (2008) and Rouyer et al. (2008b). All of our analyses were conducted with the WTC MATLAB program¹ written by A. Grinsted and the wavelet MATLAB program written by C. Torrence and G. Compo².

WAVELET THEORY

In order to conduct wavelet analysis, one must first select a “mother wavelet” function to be applied to a time series in the time-frequency domain. Wavelet functions must have zero mean and be localized in both time and frequency in order to be used in wavelet analysis (Torrence and Compo 1998). The choice of a wavelet function depends on the properties of the wavelet, the goals of the analysis and the nature of the time series. Here, because we are interested in characterizing the phase and amplitude of smoothly varying time series, we have elected to use the Morlet wavelet, which represents a sine wave modulated by a Gaussian function (Fig. C2; Torrence and Compo 1998):

$$\psi_0(t) = \pi^{-1/4} e^{i\omega_0 t} e^{-t^2/2} \quad (1)$$

¹ <http://www.pol.ac.uk/home/research/waveletcoherence/>

² <http://paos.colorado.edu/research/wavelets/>

where i is the imaginary unit, t represents nondimensional time, and $\omega_0 = 6$ is the nondimensional frequency chosen to allow the Morlet wavelet to satisfy the admissibility conditions outlined above (Torrence and Compo 1998).

The continuous wavelet transform of a discrete time series $x(t)$ with equal spacing δt and length T is defined as the convolution of $x(t)$ with a normalized Morlet wavelet (Torrence and Compo 1998, Grinsted et al. 2004):

$$W_x(s, \tau) = \sqrt{\frac{\delta t}{s}} \sum_{t=0}^{T-1} x(t) \psi_0 * \left(\frac{(t - \tau)\delta t}{s} \right) \quad (2)$$

where $*$ indicates the complex conjugate. By varying the wavelet scale s (i.e., dilating and contracting the wavelet) and translating along localized time position τ , one can calculate the wavelet coefficients $W_x(s, \tau)$, which describe the contribution of the scales s to the time series $x(t)$ at different time positions τ (Torrence and Compo 1998, Cazelles et al. 2008). Here, $\sqrt{\frac{\delta t}{s}}$ is a parameter used to normalize the Morlet wavelet function to unit variance in order to allow direct comparisons of the wavelet coefficients $W_x(s, \tau)$ across the different scales s and time positions τ (Torrence and Compo 1998, Grinsted et al. 2004). Since we used a complex Morlet wavelet, $W_x(s, \tau)$ is a complex number that can be decomposed into its amplitude $|W_x(s, \tau)|$ and its phase $\phi_x(s, \tau)$. The local (i.e., time-dependent) wavelet power spectrum is defined as $|W_x(s, \tau)|^2$. The phase varies cyclically between $-\pi$ and π , and is defined as (Cazelles et al. 2008):

$$\phi_x(s, \tau) = \tan^{-1} \left(\frac{\Im(W_x(s, \tau))}{\Re(W_x(s, \tau))} \right) \quad (3)$$

Contour plots can be used to visualize how the local wavelet power spectrum (i.e., the contribution of each frequency or period in the time series) varies in time (Grinsted et al. 2004, Cazelles et al. 2008, Rouyer et al. 2008a, 2008b, Beninca et al. 2009).

Additionally, one can quantify the global wavelet spectrum $\bar{W}_x^2(s)$ as the time-average

(i.e., over all time locations τ) of all local wavelet spectra for each scale s (Torrence and Compo 1998, Cazelles et al. 2008):

$$\bar{W}_x^2(s) = \frac{\sigma_x^2}{T} \sum_{\tau=0}^{T-1} |W_x(s, \tau)|^2 \quad (4)$$

where σ_x^2 represents the variance of the time series. Similarly, one can determine the scale-averaged wavelet power by taking the weighted sum of the wavelet power across all scale locations $j = 0, \dots, J$ for each time location τ (Torrence and Compo 1998, Cazelles et al. 2008):

$$\bar{W}_x^2(\tau) = \frac{\sigma_x^2 \delta j \delta t}{C_\delta} \sum_{j=0}^J \frac{|W_x(s_j, \tau)|^2}{s_j} \quad (5)$$

where σ_x^2 represents the variance of the time series, $C_\delta = 0.776$ is a scale-independent reconstruction constant for the Morlet wavelet, $\delta j = 1/12$ represents the number of octaves per scale and δt represents the spacing between successive time locations (Torrence and Compo 1998). These time-averaged and scale-averaged metrics can also be computed over specific time and scale bands.

The scale s of the Morlet wavelet is related to Fourier frequency f by the following equation (Maraun and Kurths 2004, Cazelles et al. 2008): $\frac{1}{f} = \frac{4\pi s}{\omega_0 + \sqrt{2 + \omega_0^2}}$. With $\omega_0 = 6$, the scale s is approximately equal to the reciprocal of the Fourier frequency f (Maraun and Kurths 2004, Cazelles et al. 2008): $s \approx \frac{1}{f}$. Hence, in all equations, the scale s can be converted to Fourier frequency $f \approx \frac{1}{s}$ or period $p = \frac{1}{f} \approx s$.

Zero-padding and the cone of influence

The continuous wavelet transform can be approximated by using (2) to compute T convolutions for each scale s (Torrence and Compo 1998). However, in practice, it is

much faster to use discrete Fourier transforms to calculate all T convolutions simultaneously (Torrence and Compo 1998):

$$\hat{x}(k) = \frac{1}{T} \sum_{\tau=0}^{T-1} x(t) e^{-2\pi i k \tau / T} \quad (6)$$

where $k = 0, \dots, T-1$ is the frequency index. The wavelet transform can then be calculated by taking the inverse Fourier transform of the product:

$$W_x(s, \tau) = \sqrt{\frac{\delta t}{s}} \sum_{k=0}^{T-1} \hat{x}(k) \hat{\psi}_0 * (s\omega(k)) e^{i\omega(k)\tau\delta t} \quad (7)$$

where $\hat{\psi}_0$ is the Fourier transform of the Morlet wavelet and where the angular frequency $\omega(k)$ is defined as (Torrence and Compo 1998):

$$\omega(k) = \begin{cases} \frac{2\pi k}{T\delta t} & k \leq \frac{T}{2} \\ -\frac{2\pi k}{T\delta t} & k > \frac{T}{2} \end{cases} \quad (8)$$

Using equation (7), one can calculate the continuous wavelet transform for each scale s at all T simultaneously (Torrence and Compo 1998).

However, since the Fourier transform used in wavelet analysis assumes that the data is cyclic or periodic, errors in the estimation of the local wavelet power spectrum will occur at the beginning and at the end of any finite-length time series (Torrence and Compo 1998, Cazelles et al. 2008). In order to limit these edge effects, the end of a time series is padded with zeros prior to taking the wavelet transform and the zeroes are then removed (Torrence and Compo 1998, Cazelles et al. 2008). Typically, enough zeros are added in order for the total length T of the time series to reach the next-higher power of two. This both limits edge effects and improves the speed of the Fourier transform analysis (Torrence and Compo 1998).

Although padding with zeros limits errors due to edge effects, it introduces artificial discontinuities at the endpoints of the data (Torrence and Compo 1998, Cazelles et al. 2008). As one gets closer to the end of the data, the local wavelet spectrum becomes increasingly affected by the discontinuity, as more zeros are included in its estimation

(Torrence and Compo 1998, Cazelles et al. 2008). The region where zero padding affects the estimation of the wavelet spectrum is called the cone of influence (COI), and is defined as the region in which the wavelet power for a discontinuity at the edge drops by a factor of e^{-2} (Torrence and Compo 1998). Here, we have excluded all regions below the cone of influence (depicted in black dashed lines) from our analyses in order to focus our interpretations on the part of the wavelet spectrum that is unaffected by edge effects.

Statistical significance testing

In order to conduct statistical significance testing on the wavelet spectrum obtained from a time series, one must first formulate an appropriate null hypothesis. Here, our null hypothesis is that the observed time series is generated by a stationary process with a given background power spectrum $P(k)$ (Torrence and Compo 1998, Grinsted et al. 2004). Since many ecological time series exhibit strong temporal autocorrelation (i.e., high power associated with low frequencies; e.g., Beninca et al. 2009, see Ruokolainen et al. 2009 for review), we used a first order autoregressive model [AR(1)] to generate a temporally autocorrelated time series or red noise, which served as our null hypothesis. Specifically, the power spectrum $P(k)$ of our red noise process was calculated with (Gilman et al. 1963):

$$P(k) = \frac{1 - \alpha^2}{1 + \alpha^2 - 2\alpha \cos(2\pi k / N)} \quad (9)$$

where the autocorrelation coefficient α at time lag 1 is estimated from the observed time series and $k = 0, \dots, N/2$ represents the frequency index. The observed wavelet spectrum can be compared to the wavelet spectrum of the red noise process by means of a chi-square test. The distribution of the local wavelet power spectrum of a red noise process is (Torrence and Compo 1998):

$$\frac{|W_x(s, \tau)|^2}{\sigma^2} \Rightarrow \frac{1}{2} P(k) \chi_2^2 \quad (10)$$

where k represents the frequency index, σ^2 represents the variance of the time series, “ \Rightarrow ” means “is distributed as”, and χ_2^2 represents the chi-square distribution with 2 degrees of freedom. The value of $P(k)$ is the mean wavelet power spectrum at frequency k that corresponds to the wavelet scale s (Torrence and Compo 1998). Here, we constructed 95% confidence contour lines by evaluating equation (10) at each scale using the 95th percentile of the chi-square distribution χ_2^2 .

BIVARIATE EXTENSIONS OF WAVELET ANALYSIS

Wavelet analysis provides critical, time-resolved information about the dominant frequencies (or periods) of a univariate time series. However, in order to determine the relationship between the time-resolved variability of pairs of time series, one needs to use the recently developed bivariate extensions of wavelet analysis (Grinsted et al. 2004). Below, we discuss both cross-wavelet and wavelet coherence, which are methods that generate complementary and time-resolved information about the relationship between pairs of time series.

Cross-wavelet analysis

In order to calculate the cross-wavelet analysis of time series $x(t)$ and $y(t)$, one first needs to take their respective wavelet transforms $W_x(s, \tau)$ and $W_y(s, \tau)$, as described in the previous section. Then, the cross-wavelet transform is computed with (Torrence and Compo 1998, Grinsted et al. 2004):

$$W_{x,y}(s, \tau) = W_x(s, \tau)W_y^*(s, \tau) \quad (11)$$

where * indicates complex conjugation. Since we use a complex wavelet (the Morlet), $W_{x,y}(s, \tau)$ is a complex number that can be decomposed into its amplitude $|W_{x,y}(s, \tau)|$ and its phase $\phi_{x,y}(s, \tau)$. $|W_{x,y}(s, \tau)|$ represents the local cross-wavelet spectrum of time series $x(t)$ and $y(t)$. The phase $\phi_{x,y}(s, \tau)$ can be interpreted as the local phase

difference between the fluctuations in the time series $x(t)$ and $y(t)$ in the time-frequency domain, and is defined as:

$$\phi_{x,y}(s, \tau) = \tan^{-1} \left(\frac{\Im(W_{x,y}(s, \tau))}{\Re(W_{x,y}(s, \tau))} \right) \quad (12)$$

The amplitude and the phase of the cross-wavelet provide complementary information about the covariation between two time series. The amplitude indicates the common strength (or power) of the fluctuations, whereas the phase indicates whether the time series vary in similar (i.e., in phase) or opposite (i.e., in anti-phase) directions. As with the local wavelet spectrum, the local cross-wavelet spectrum can be represented with contour plots that describe how the covariation between two time series varies in time. In addition, the phase of the cross-wavelet can be represented with arrows that indicate whether the two time series are moving in the same direction (i.e., in phase: arrows pointing to the right indicating a 0 degree/radian difference in the phase difference) or in opposite directions (i.e., in anti-phase: arrows pointing to the left indicating a 180 degree or π radian difference in the phase difference). Overall, the cross-wavelet can be thought of as the local or time-resolved covariance between two time series (Cazelles et al. 2008, Rouyer et al. 2008a, 2008b).

Statistical significance testing

The statistical significance of a cross-wavelet spectrum can be assessed by using a procedure that is analogous to the one described for a wavelet spectrum. We first need to determine an appropriate null hypothesis to explain the variation of both time series. As before, our null hypothesis is that both of the observed time series are generated by a stationary red noise process. Here, we generated two independent, temporally autocorrelated time series (i.e., red noise) with the same first order autocorrelation coefficients as our observed time series. Under the null hypothesis that the observed time series $x(t)$ and $y(t)$ were generated by a red noise process with power spectrum $P_x(k)$ and $P_y(k)$, the distribution of the cross-wavelet spectrum is (Torrence and Compo 1998):

$$\frac{|W_x(s, \tau)W_y^*(s, \tau)|}{\sigma_x \sigma_y} \Rightarrow \frac{Z_v(p)}{v} \sqrt{P_x(k)P_y(k)} \quad (13)$$

where σ_x and σ_y represent the standard deviations of the time series, $W_x(s, \tau)$ and $W_y(s, \tau)$ represent the wavelet transforms of the time series, $|W_x(s, \tau)W_y^*(s, \tau)|$ represents the cross-wavelet spectrum of the two time series, $Z_v(p)$ represents the confidence level associated with probability p for a probability density function defined by the square root of the product of two chi-square distributions with $v = 2$ degrees of freedom for a complex wavelet, and * indicates complex conjugation (Torrence and Compo 1998). Here, we constructed 95% confidence contours by selecting $p = 0.95$ (i.e., $Z_2(0.95) = 3.999$), and evaluating equation (13) at each scale (Torrence and Compo 1998, Grinsted et al. 2004).

Caveats and limitations

The cross-wavelet spectrum reveals areas of high common power between two time series. However, because the cross-wavelet spectrum is not normalized by the wavelet spectra of the time series, it can generate spurious associations between two time series (Maraun and Kurths 2004). Indeed, without normalization, the cross-wavelet spectrum between a wavelet spectrum exhibiting strong peaks and a wavelet spectrum that is completely flat can have pronounced peaks, despite the lack of any true association between the two time series (Maraun and Kurths 2004).

Wavelet coherence

Wavelet coherence overcomes the problems of cross-wavelet analysis by quantifying the coherence of the fluctuations between two time series. Indeed, by normalizing the square of the cross-wavelet spectrum by the wavelet spectra of each time series, wavelet coherence limits the occurrence of spurious associations between unrelated time series. Specifically, the wavelet coherence between two time series $x(t)$ and $y(t)$ with wavelet spectra $W_x(s, \tau)$ and $W_y(s, \tau)$, and cross-wavelet spectrum

$W_{x,y}(s, \tau)$ is defined as (Torrence and Webster 1998, Grinsted et al. 2004, Cazelles et al. 2008):

$$R_{x,y}^2(s, \tau) = \frac{\langle s^{-1}W_{x,y}(s, \tau) \rangle^2}{\langle s^{-1}|W_x(s, \tau)|^2 \rangle \langle s^{-1}|W_y(s, \tau)|^2 \rangle} \quad (14)$$

where $\langle \cdot \rangle$ denotes smoothing in both time τ and scale s and $0 \leq R_{x,y}^2(s, \tau) \leq 1$.

The time smoothing uses a filter given by the absolute value of the wavelet function at each scale, normalized to have a total weight of unity, which is a Gaussian function $e^{\frac{-t^2}{2s^2}}$ for the Morlet wavelet. The scale smoothing is done with a boxcar function of width 0.6, which corresponds to the decorrelation scale of the Morlet wavelet (Torrence and Webster 1998, Torrence and Compo 1998, Grinsted et al. 2004).

Since we use a complex wavelet, we can compute $\phi_{x,y}(s, \tau)$, which describes the local phase difference between the fluctuations in the time series $x(t)$ and $y(t)$ in the time-frequency domain (Torrence and Webster 1998):

$$\phi_{x,y}(s, \tau) = \tan^{-1} \left(\frac{\Im(\langle s^{-1}W_{x,y}(s, \tau) \rangle)}{\Re(\langle s^{-1}W_{x,y}(s, \tau) \rangle)} \right) \quad (15)$$

As with the cross-wavelet spectrum, the wavelet coherence can be represented with contour plots that describe how the correlation between two time series varies in time. In addition, the phase of the wavelet coherence can be represented with arrows that indicate whether the two time series are moving in the same direction (i.e., in phase: arrows pointing to the right indicating a 0 degree/radian difference in the phase difference) or in opposite directions (i.e., in anti-phase: arrows pointing to the left indicating a 180 degree or π radian difference in the phase difference). Overall, the wavelet coherence can be thought of as the local or time-resolved correlation between two time series (Cazelles et al. 2008, Rouyer et al. 2008a, 2008b).

Statistical significance testing

The statistical significance of wavelet coherence can be tested by using Monte Carlo randomization techniques (Grinsted et al. 2004). Specifically, we generated 1,000 pairs of surrogate time series with the same first order autoregressive coefficients as our observed time series. We computed the wavelet coherence for each pair of surrogate time series, thus generating a distribution of wavelet coherence. We then obtained the 95% significance level for each scale by computing the 95th percentile of the wavelet coherence distribution.

Caveats and limitations

Although wavelet coherence overcomes some of the limitations of cross-wavelet analysis, it is sensitive to the smoothing procedure, which can reduce the localization in both the time and frequency domains (Grinsted et al. 2004, Maraun and Kurths 2004). Additionally, wavelet coherence analysis will identify regions in the time-frequency domain where pairs of time series undergo common fluctuations, even if the fluctuations have low power. Hence, the relationship between pairs of time series should be assessed using both cross-wavelet and wavelet coherence methods in order to determine the robustness of the results to the specifics of the bivariate wavelet analysis (Grinsted et al. 2004).

AN EXAMPLE OF WAVELET ANALYSIS

To illustrate the use and interpretation of univariate and bivariate wavelet analyses, we construct 200-day artificial upwelling and temperature time series. Specifically, upwelling and temperature vary according to a regular sinusoidal function with a period of 40 days (frequency of 5), with upwelling lagging temperature by $\pi/2$ (i.e., a phase difference of $-\pi/2$ between upwelling and temperature). The phase difference can be converted into a temporal lag by using the following relationship:

$$\text{temporal lag} = \frac{|\text{wavelength} \cdot (\text{phase difference})|}{2\pi}. \text{ Since the period of time series is 40 days,}$$

the temporal lag = $\frac{|40 \cdot (-\pi/2)|}{2\pi} = 10$ days. Hence, in this example, there is a ten-day lag or delay between the phases (e.g., the maximum, minimum) of upwelling and temperature, with positive values of upwelling leading to a decrease in temperature and negative values of upwelling (i.e., downwelling) leading to an increase in temperature (Fig. C3a).

Although the wavelet analysis shows that both time series undergo strong and consistent (in time) variability at the same period of 40 days (Fig. C3), it cannot assess the relationship (e.g., the phase difference) between the two time series. In order to assess patterns of covariation between pairs of time series, bivariate wavelet analyses such as cross-wavelet and wavelet coherence are needed. Indeed, cross-wavelet analysis detects consistent and common high power fluctuations between upwelling and temperature at a period of 40 days with a phase difference of $-\pi/2$ (Fig. C4b). Wavelet coherence also detects consistent and coherent fluctuations between upwelling and temperature at a period of 40 days with a phase difference of $-\pi/2$ (Fig. C4c). However, because it is normalized by the wavelet spectrum of each time series, wavelet coherence also identifies coherent fluctuations between the two time series at all other periods (Fig. C4d,e). Hence, both cross-wavelet and wavelet coherence analyses identify the correct phase difference between the time series, but cross-wavelet analysis focuses on the period of common high-power fluctuations whereas wavelet coherence identifies coherent fluctuations at all periods, regardless of their power.

Figure C1 Analyzing a complex and non-stationary time series with classical power spectrum methods and wavelets. (a) The time series consists of four different 500-time step sections: (1) a sinusoidal function of frequency 5, (2) normally distributed noise with zero mean and unit variance, (3) a sinusoidal function of frequency 25 and (4) a sinusoidal function of frequency 8 with uniform random noise. (b) Classical spectral analysis using Welch's modified periodogram detects the dominant frequencies of the time series (i.e., peaks in power or variability in the time series associated with frequencies 5, 8 and 25), but cannot describe how the dominance of these frequencies changes in time. (c) Wavelet analysis describes changes in time in the contribution of different frequencies (or periods) to the power (or variance; color bar) of a time series. Black contour lines indicate regions in which the observed continuous wavelet spectra differ significantly ($\alpha=0.05$) from those obtained from a random time series whose first-order autoregressive coefficients match those of the original time series. Regions within the black dashed lines (the cone of influence) are not affected by edge effects. Here, wavelet analysis detects all key frequencies and also shows how they vary in time despite abrupt changes and the addition of stochastic noise to the last sinusoidal function. Wavelet analysis is thus an effective tool for analyzing time series that show strong and/or abrupt changes in their dominant frequencies in time, even in the presence of stochastic noise.

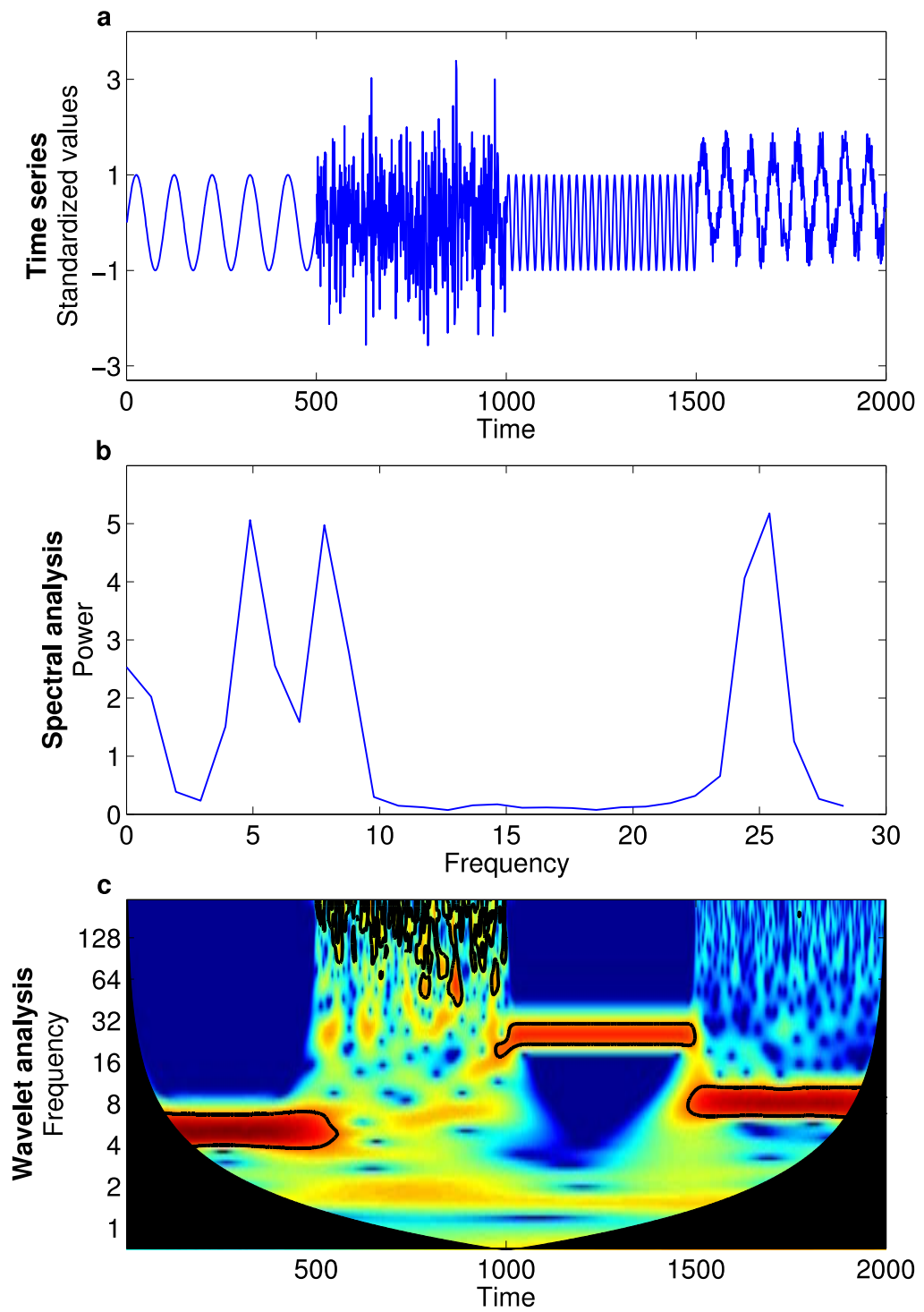


Figure C1

Figure C2 The effect of varying the scale s of the Morlet wavelet (blue curve) on its time-frequency resolution (grey box). Increasing the scale s dilates the wavelet and leads to higher resolution in the frequency domain (shorter grey boxes), but lower resolution in the time domain (wider grey boxes). Conversely, decreasing the scale s contracts the wavelet and leads to lower resolution in the frequency domain (taller grey boxes), and higher resolution in the time domain (narrower grey boxes). Hence, the wavelet must strike a balance between its resolution in the time and frequency domains. Based on Figure 1 of Cazelles et al. (2008).

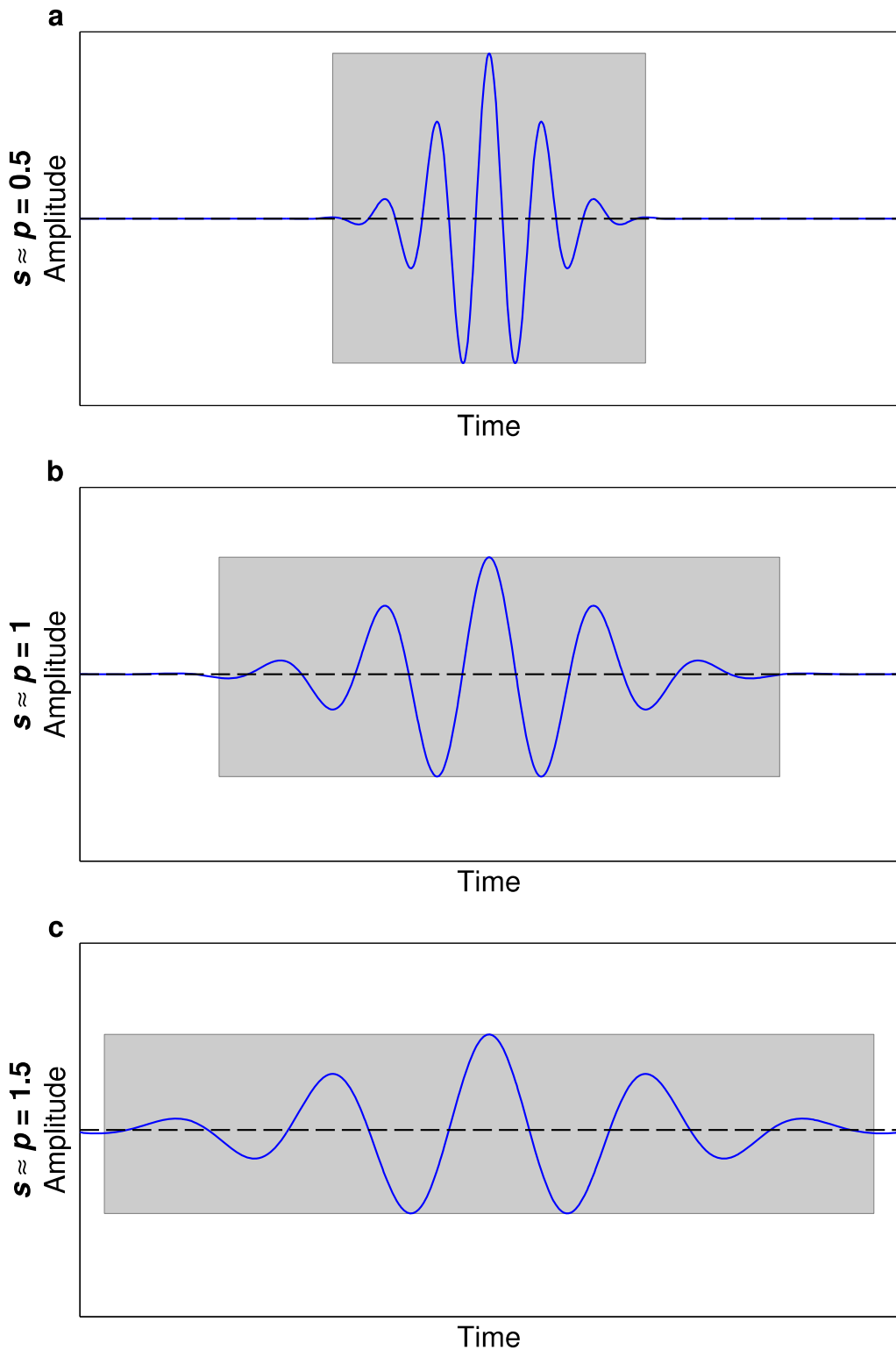


Figure C2

Figure C3 Wavelet analysis of artificial daily upwelling and temperature data. (a) Standardized values of each time series were obtained by subtracting the mean and dividing by the standard deviation. (b, d) Regions of high (low) power are represented in warm (cold) colors. Black contours represent regions of statistically significant variability at the $\alpha=0.05$ level. Period is in days and time is coded in number of days. Regions within the black dashed lines (the cone of influence) are not affected by edge effects. (c, e) Side plots represent the global wavelet spectrum for upwelling (c) and temperature (e).

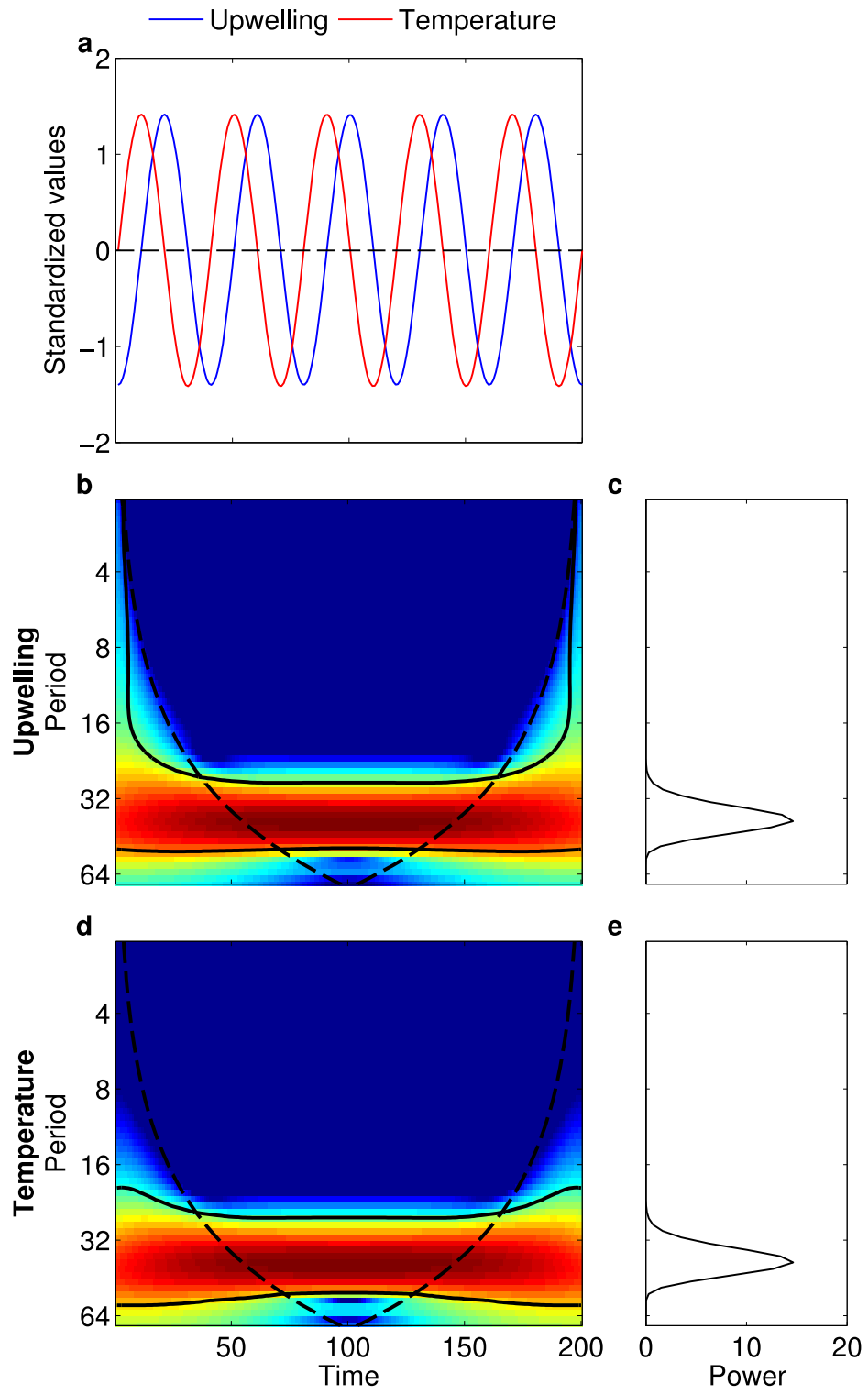
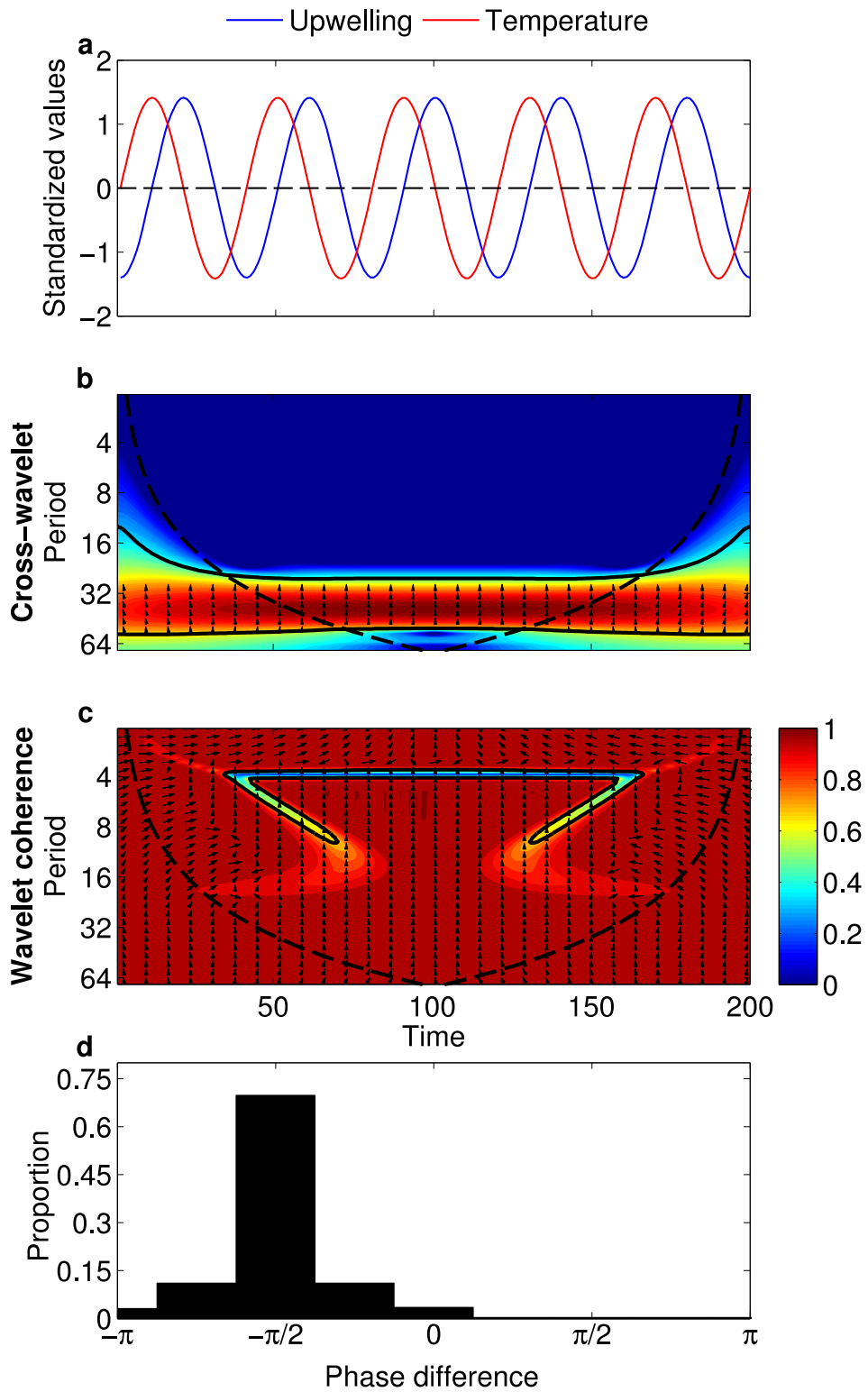


Figure C3

Figure C4 Pairwise cross-wavelet and wavelet coherence analyses of artificial daily upwelling and temperature data. (b) The cross-wavelet represents regions of high (low) common power between the time series in warm (cold) colors. (c) Wavelet coherence represents regions of high (low) common fluctuations in warm (cold) colors. Black arrows indicate the phase difference between the time series. When the time series move in the same direction (i.e., in phase), the arrows point to the right and when they move in opposite directions (i.e., anti-phase), the arrows point to the left. Arrows pointing down indicate a $\pi/2$ phase difference between the time series, with upwelling leading temperature, and arrows pointing up indicate a $-\pi/2$ phase difference between the time series, with temperature leading upwelling. Black contours represent regions of statistically significant common variability at the $\alpha=0.05$ level. Regions within the black dashed lines (the cone of influence) are not affected by edge effects. (d) Distribution of phase difference between upwelling and temperature across all significant wavelet coherence regions.

**Figure C4**

Appendix D – Wavelet analysis of temporal trends in upwelling and temperature along the California Current system

In this appendix, we use univariate wavelet analyses to characterize temporal trends in the variation of the raw 6-hour upwelling time series at all five latitudes along the California Current System. Because wavelet methods are ideal for describing the non-stationary and seasonal variability observed in the raw upwelling time series, the analyses presented in this appendix complement and augment the results based on summary statistics (i.e., mean annual duration, frequency and magnitude of upwelling) documented in the main text. Indeed, using annual summary statistics such as the mean to detect temporal trends can often conceal more complex and potentially countervailing variability within years. Because wavelet analysis decomposes the total variability of a time series into its component periodicities over time, one can track temporal trends in the relative contribution of each period to the total variability. Wavelet analysis thus provides a more complete picture of the changes in upwelling over time. We also use cross-wavelet analysis, a bivariate extension of wavelet analysis, to assess how the patterns of covariation between daily upwelling and intertidal temperature changed over time. The univariate and bivariate wavelet methods used in this appendix are described thoroughly in appendix C and reviewed by Torrence and Compo (1998), Grinsted et al. (2004) and Cazelles et al. (2008).

Temporal trends in upwelling

The univariate wavelet analyses reveal that most of the variability in upwelling is associated with annual periods (~256-512 days) at all five locations (Fig. D1). At higher periods, the temporary but strong influence of the 1982 and 1998 El Niño events can be seen (Zhang et al. 1997, McPhaden 1999), with much of the variability in upwelling shifting from annual to multi-annual periods, especially at lower latitudes (Fig. D1).

Upwelling also exhibits statistically significant variability at lower periods (<40 days) at all latitudes (Fig. D1). At northern locations (39-45°N), statistically significant

variability at lower periods occurs mainly in winter and is associated with relatively short but strong and periodic downwelling events (Fig. D1). In the summer, upwelling undergoes a shift in statistically significant variability from 4-to-40-day periods to daily periods (Fig. D1). This shift in significance to daily variability occurs because upwelling conditions in the summer do not fluctuate on a regular basis the way they do in the winter. In the summer, upwelling persists until occasional and irregular downwelling events occur. Because these downwelling events occur sporadically, upwelling variability at periods of 4-40 days is scattered across multiple periods and thus weak and not statistically significant like the regular wintertime fluctuations (Fig. D1). At southern locations ($33\text{--}36^\circ\text{N}$), summers are characterized by the same shift in statistically significant variability from 4-to-40-day periods to daily periods because upwelling is persistent and rarely interrupted by wind relaxations or downwelling events (Fig. D1).

To detect temporal trends in the variability of upwelling, we calculated the scale-averaged wavelet power for event-scale (<40 days; green), sub-annual (41-255 days; blue), annual (256-512 days; red) and super-annual (>512 days; black) periods by taking the weighted sum of the wavelet power of upwelling across each group of periods (Fig. D2). Event-scale wavelet power exhibits a statistically significant increase at 36°N but no significant change over time at other latitudes, whereas annual-scale wavelet power undergoes a statistically significant decrease at both 36°N and 33°N , but no significant change at other latitudes (Fig. D2). Super-annual wavelet power exhibits a statistically significant increase at all latitudes and sub-annual wavelet power undergoes a statistically significant increase at 45°N , 42°N , 36°N and 33°N but not 39°N (Fig. D2). Overall, these results indicate that upwelling is becoming increasingly dominated by variability at event-scale, sub-annual and super-annual periods instead of annual periods, especially at the two southernmost latitudes. These results are consistent with the notion that upwelling events are becoming stronger, more frequent and more persistent (Appendix E), and thus accounting for a greater proportion of the variance in upwelling over time.

Relating regional-scale upwelling conditions to local intertidal temperature

To determine how the relationship between regional-scale upwelling conditions and local intertidal temperature varied over time, we first performed wavelet analysis on the daily temperature time series at Boiler Bay, Strawberry Hill and Cape Blanco (Fig. D3). At all three locations, most of the variability in temperature is consistently associated with annual periods (256-512 days). However, a statistically significant proportion of the variability in temperature is also related to event-scale (<40 days) and sub-annual (41-255 days) periods during the summer (but not the winter) (Fig. D3). These seasonal patterns in temperature variability at event-scale and sub-annual periods could be explained by upwelling. Indeed, at the Oregon locations (~42-45°N), periodic upwelling events can reduce intertidal temperatures during the summer months (compare Figs. B1 and B3), whereas the strong and frequent downwelling events that occur during the winter months do not alter intertidal temperatures (compare Figs. B1 and B3).

To test this prediction, we used cross-wavelet analysis to determine patterns of covariation in the time-frequency domain between upwelling and temperature (Fig. D4). At all three Oregon locations, most of the cross-wavelet power is concentrated at annual periods (256-512 days), with upwelling leading temperature by $\pi/2$ (i.e., a temporal lag of approximately three months; Fig. D4). Upwelling peaks earlier in the year than water temperature because the sun warms the air much faster than water during the Spring months, thus generating a thermal gradient between the heated land mass and the cooler coastal ocean (Bakun 1990). The thermal gradient then produces strong alongshore winds that cause coastal upwelling to arise. This leads to a $\pi/2$ phase difference between upwelling and temperature at annual periods, with upwelling peaking in the Spring and water temperature peaking in the Summer (Fig. D5). Hence, despite the strong cross-wavelet power, there is no causal relationship between upwelling and water temperature cycles at annual periods.

At event-scale and sub-annual periods, the cross-wavelet power is relatively weak but significant during the summer months, with a phase difference of $-\pi/2$ between upwelling and temperature (Fig. D4). This phase difference means that there is a time lag between changes in upwelling conditions and water temperature, with peaks in upwelling

trailing peaks in temperature by $\pi/2$ or one quarter of a cycle. Hence, increased (decreased) upwelling leads to a lagged decrease (increase) in water temperature (see example in Appendix C, Fig. C1-3). This pattern is consistent with a causal relationship between upwelling and temperature at event-scale and sub-annual periods. The relatively weak cross-wavelet power at event-scale and sub-annual periods is due to the seasonal mismatch between the wavelet power of upwelling and temperature (Fig. D5). Indeed, the scale-averaged wavelet power of upwelling and temperature are negatively correlated to each other at all three Oregon locations ($\rho < 0$, p-value < 0.001), with upwelling power peaking in Fall-Winter and temperature power peaking in Spring-Summer (Fig. D5). This is because at sub-annual and event-scale periods, upwelling variability in Oregon is driven primarily by strong and periodic downwelling events in the Fall-Winter (Figs. D1, D5) whereas temperature variability is driven primarily by Spring-Summer temperatures (Figs. D3, D5).

Overall, our analyses show that upwelling across the California Current System is being increasingly dominated by variability at event-scale, sub-annual and super-annual periods due to the increased persistence, frequency and strength of upwelling events. Furthermore, regional-scale upwelling events have a direct effect on local intertidal temperatures during summer months. The wavelet analyses of the raw upwelling time series documented in this appendix thus augment and support the temporal trends presented in the main text using annual summary statistics.

Figure D1 Wavelet analysis of 6-hour upwelling time series from 1967 to 2010 at five locations across the California Current System. (a, c, e, g, i) Regions of high (low) power or variability are represented in warm (cold) colors. Black contours represent regions of statistically significant variability at the $\alpha=0.05$ level. Period is in days and time is coded in month/year. Regions within the black dashed lines (the cone of influence) are not affected by edge effects. (b, d, f, h, j) Side plots represent the global wavelet spectrum.

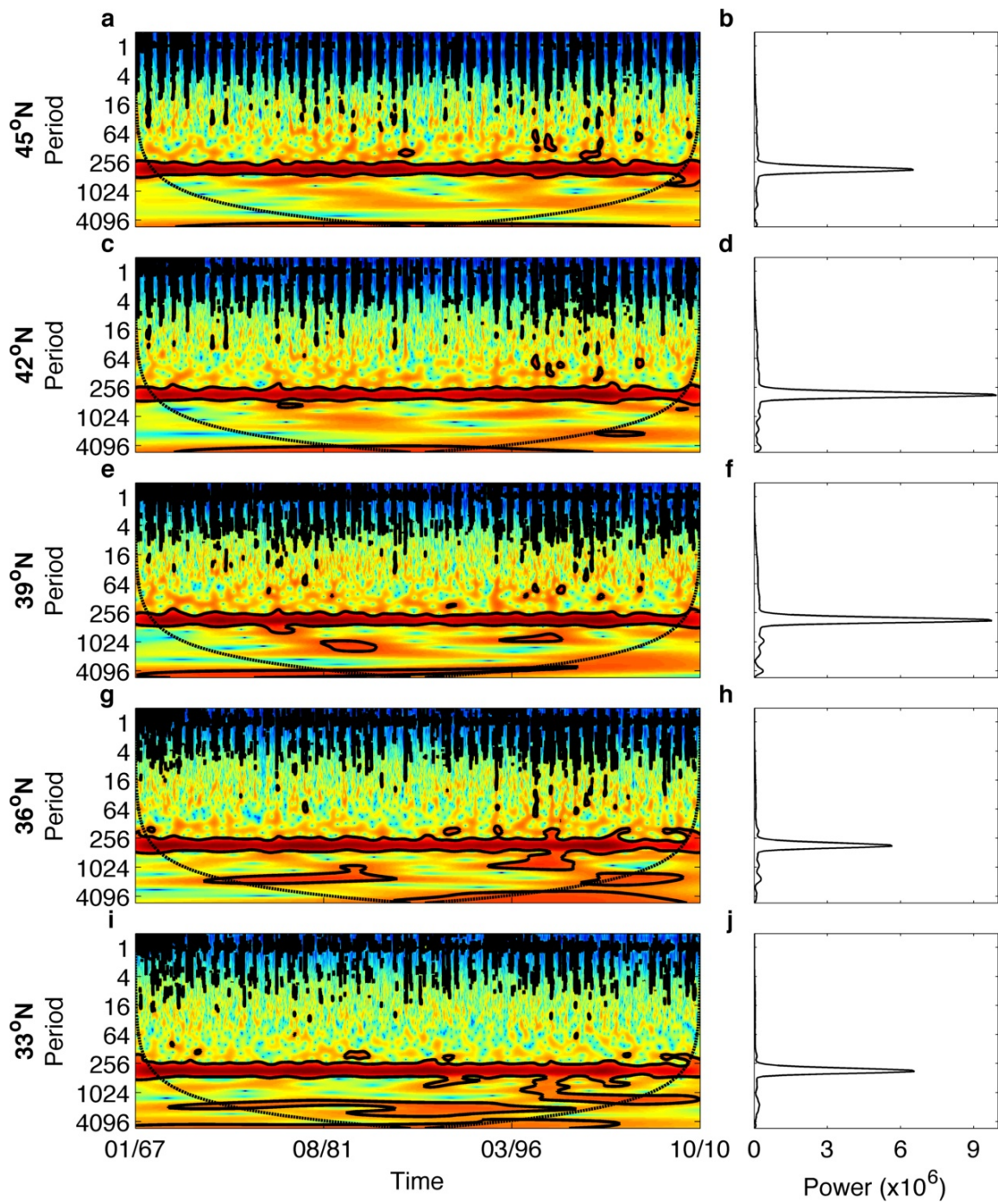
**Figure D1**

Figure D2 Temporal trends in scale-averaged wavelet power (+/- standard error bars) at event-scale (<40 days; green), sub-annual (41-255 days; blue), annual (256-512 days; red) and super-annual (>512 days; black) periodicities for 6-hour upwelling time series from 1967-2010 at five locations across the California Current System. Fitted lines represent statistically significant linear regressions (p -value < 0.05). The p -values of the regressions were calculated by performing 1,000 permutations of the data and determining the proportion of permutations that yielded a coefficient of determination that was greater than or equal to the one obtained with the original data.

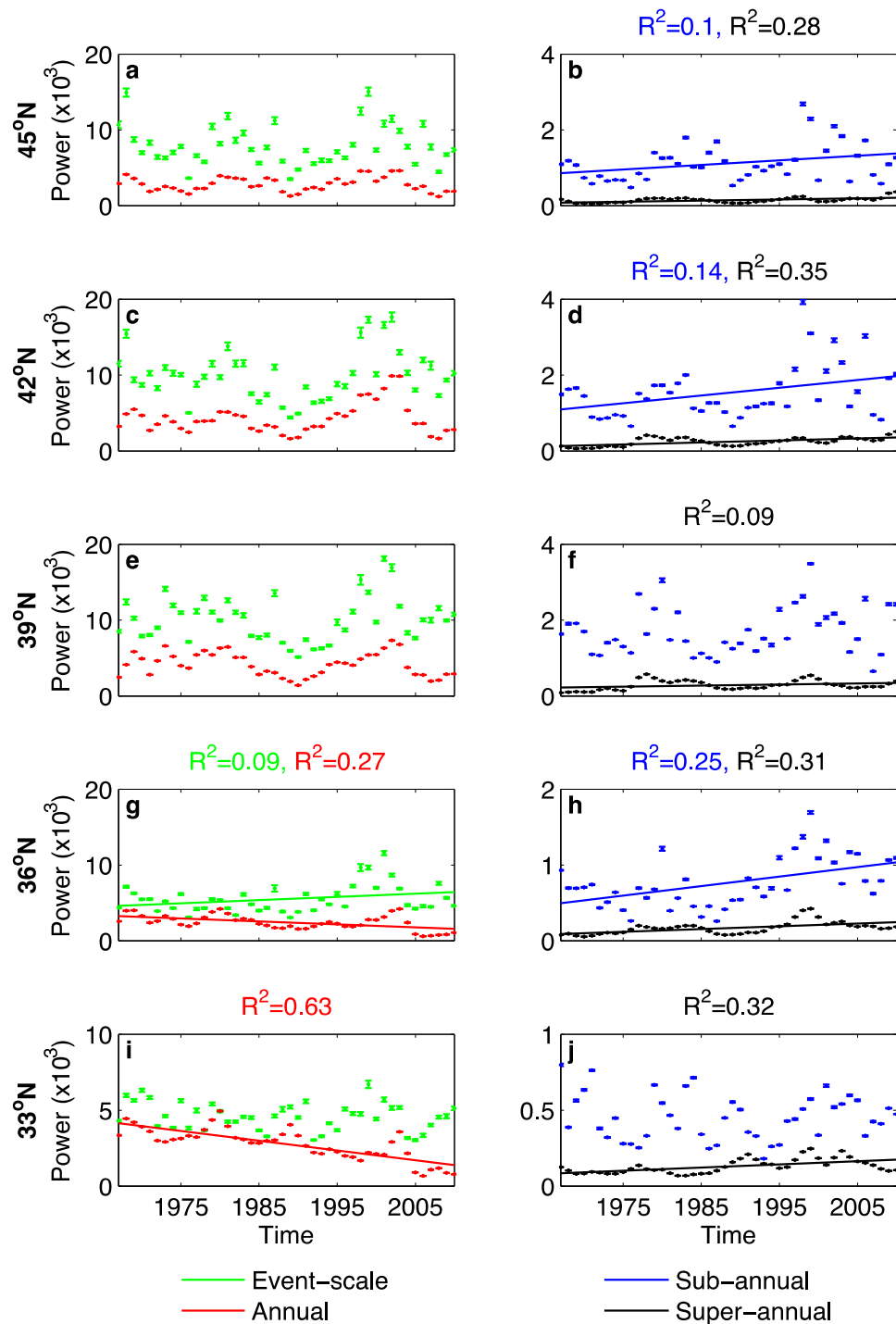
**Figure D2**

Figure D3 Wavelet analysis of daily intertidal temperature time series from 1999 to 2009 at (a, b) Boiler Bay, (c, d) Strawberry Hill and (e, f) Cape Blanco. (a, c, e) Regions of high (low) power or variability are represented in warm (cold) colors. Black contours represent regions of statistically significant variability at the $\alpha=0.05$ level. Period is in days and time is coded in month/year. Regions within the black dashed lines (the cone of influence) are not affected by edge effects. (b, d, f) Side plots represent the global wavelet spectrum.

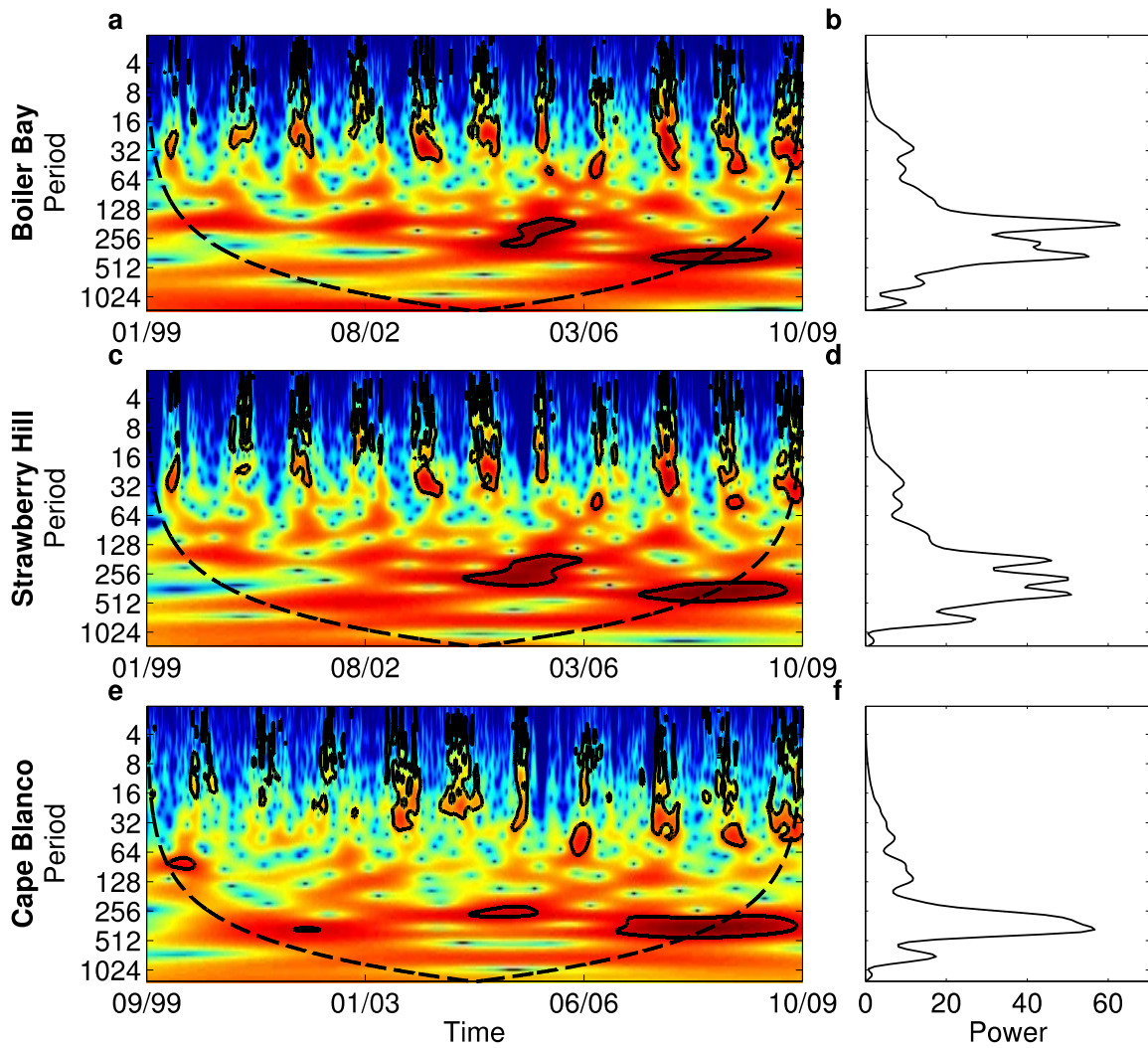


Figure D3

Figure D4 Pairwise cross-wavelet analysis of daily upwelling and temperature time series from 1999 to 2010 at (a, b) Boiler Bay, (c, d) Strawberry Hill and (e, f) Cape Blanco. (a, c, e) Regions of high (low) common power between the time series are represented in warm (cold) colors. Black arrows indicate the phase difference between the time series. When the time series move in the same direction (i.e. in phase), the arrows point to the right and when they move in opposite directions (i.e. anti-phase), the arrows point to the left. Arrows pointing down indicate a $\pi/2$ phase difference between the time series, with upwelling leading temperature, and arrows pointing up indicate a $-\pi/2$ phase difference between the time series, with temperature leading upwelling. Black contours represent regions of statistically significant common variability at the $\alpha=0.05$ level. Regions within the black dashed lines (the cone of influence) are not affected by edge effects. (b, d, f) Distribution of phase difference between upwelling and temperature across all significant cross-wavelet regions for event-scale (<40 days; green), sub-annual (41-255 days; blue) and annual (256-512 days; red) periods.

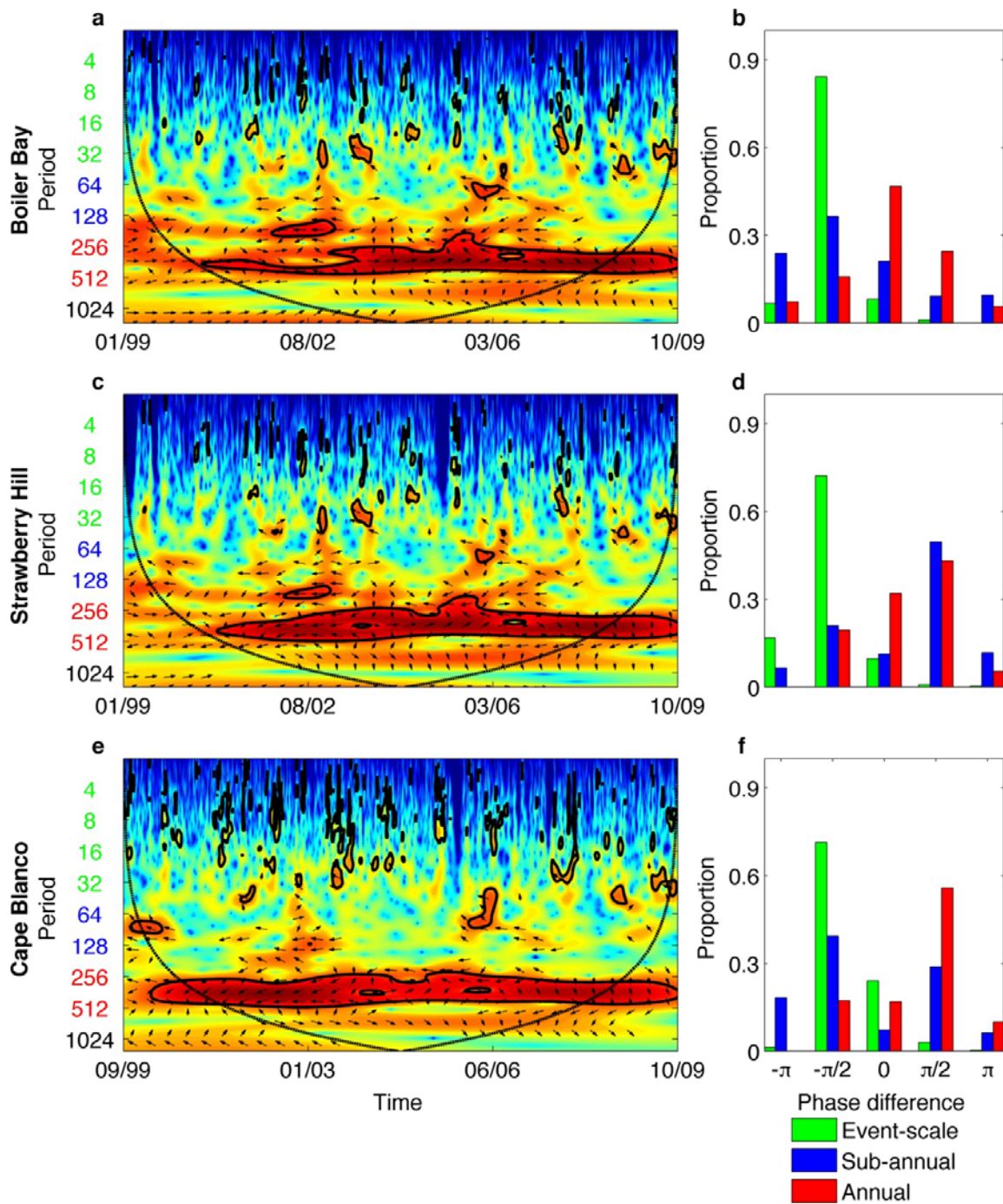
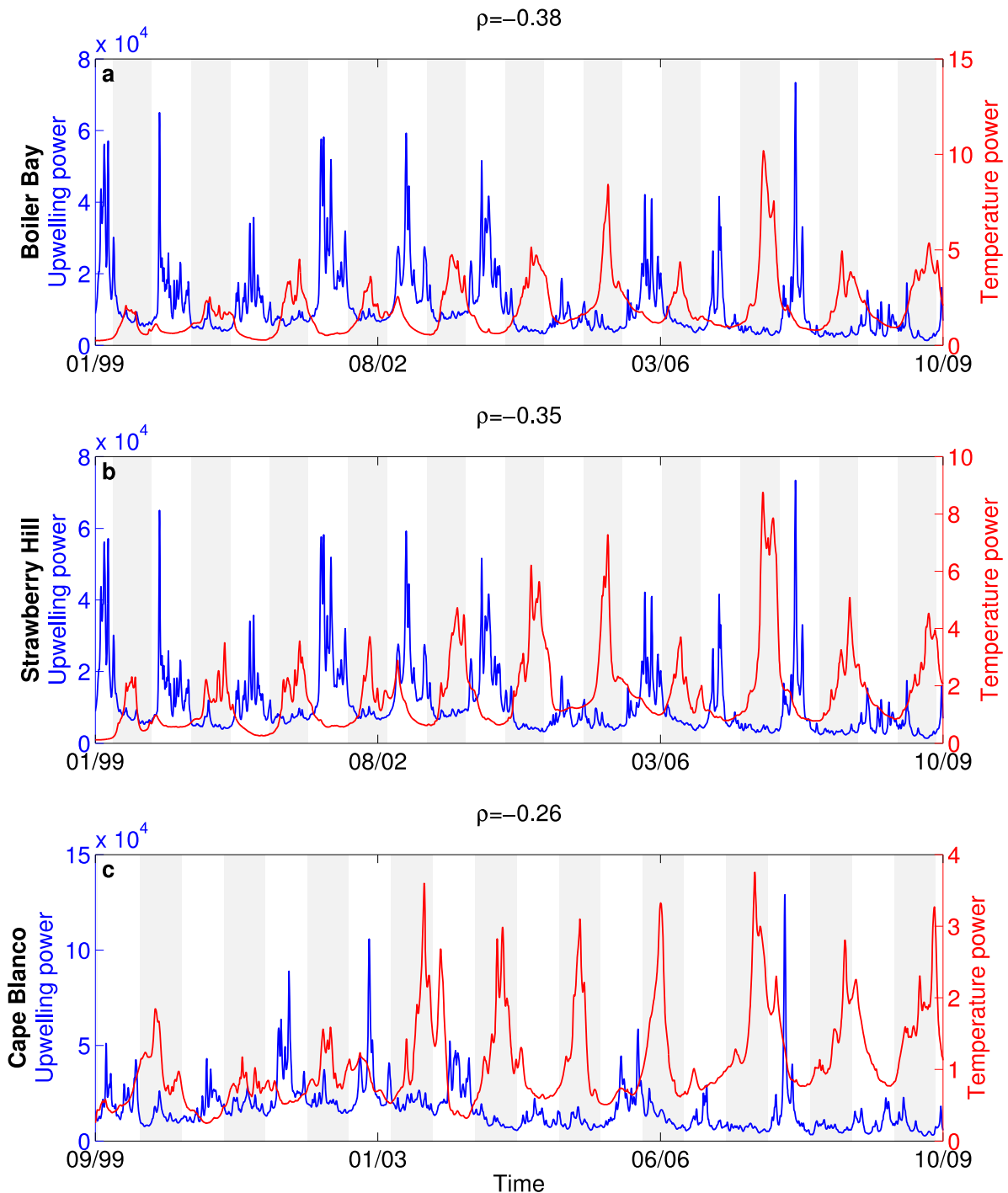


Figure D4

Figure D5 Scale-averaged wavelet power for daily upwelling (blue) and temperature (red) time series at Boiler Bay (a), Strawberry Hill (b) and Cape Blanco (c) from 1999 to 2010. The scale-averaged wavelet power of upwelling and temperature are negatively correlated at each location ($\rho < 0$, p-value < 0.001), with upwelling power peaking in Fall-Winter (white background) and temperature power peaking in Spring-Summer (gray background). The p-values of the correlations were calculated by performing 1,000 permutations of the data and determining the proportion of permutations that yielded a correlation that was greater than or equal to the one obtained with the original data. Time is coded in month/year on the x-axis.

**Figure D5**

Appendix E – Temporal trends in the annual mean and intra-annual distribution of upwelling events along the California Current system

SENSITIVITY ANALYSIS OF ANNUAL TEMPORAL TRENDS IN UPWELLING EVENTS

Number of upwelling events

When we do not impose a minimum duration of persistent upwelling for a given period to qualify as an upwelling event (i.e., minimum duration of 0 days), we find that the number of upwelling events decreases significantly over time at all five latitudes (Fig. E1). However, when we set the minimum duration of persistent upwelling to 4-6 or more days, the number of upwelling events shows little to no change at the three northernmost latitudes (i.e. slope $\beta_1 \approx 0$; Fig. E1). At the two southernmost latitudes, the number of upwelling events actually increases over time when the minimum duration is 4-6 or more days (Fig. E1). Overall, this means that the frequency of short upwelling events (<4 days) is decreasing over time at all latitudes whereas the frequency of long upwelling events (>4-6 days) is (1) not varying significantly at northernmost latitudes and (2) increasing significantly over time at southernmost latitudes.

Mean duration of upwelling events

When all periods of upwelling qualify as upwelling events regardless of their duration (i.e., minimum duration of 0 days), mean annual event duration increases significantly over time at the four southernmost latitudes but not at the northernmost latitude (Fig. E2). This significant increase in mean event duration holds for short minimum durations of 1-2 days at 33°N and 1-5 days at 36°N (Fig. E2). For intermediate minimum durations (6-9 days), mean annual upwelling event duration increases significantly at 39°N. For longer minimum durations (>5-9 days), mean annual upwelling event duration decreases over time at 36°N and 39°N, but the trends are not statistically significant (Fig. E2).

Mean magnitude of upwelling events

The mean magnitude of events is increasing over time at all five latitudes when there is no minimum duration requirement, with the trend being significant at 42°N and 36°N (Fig. E3). The trends become non-significant for intermediate minimum durations (1-4 days) at all five latitudes (Fig. E3). For long minimum durations (>5-12 days), the mean magnitude of upwelling decreases significantly over time at the two southernmost latitudes (Fig. E3). Overall, these results suggest that very short (<1 day) upwelling events are becoming stronger over time and causing an increase in the mean upwelling magnitude at 42°N and 36°N. However, excluding short upwelling events from the analysis shows that longer upwelling events (>5-12 days) are becoming weaker over time and causing a decrease in the mean magnitude of upwelling at 36°N and 33°N.

Total magnitude of upwelling events

The total magnitude of upwelling events exhibits temporal trends that are very similar to those of the mean magnitude of upwelling events (Fig. E4). Specifically, total event magnitude increases over time at all five latitudes when there is no minimum duration requirement, with the trend being significant at 42°N, 36°N and 33°N (Fig. E4). This trend remains significant for short minimum durations (1-2 days) at 36°N, but becomes non-significant at the remainder of the latitudes. For long minimum durations (>6-12 days), total magnitude decreases significantly over time at 36°N and 33°N (Fig. E4).

Overall, these results suggest that the sign and the significance of the temporal trends in the annual (i) frequency, (ii) duration, (iii) mean magnitude and (iv) total magnitude of upwelling events are highly sensitive to the minimum duration used to define an event. Indeed, our sensitivity analysis demonstrates that including short events tends to generate statistically significant positive trends in (i) the annual duration, (ii) mean magnitude and (iii) total magnitude of upwelling, whereas their exclusion typically yields statistically significant negative trends (the converse is true for the frequency of upwelling events). Hence, by using the annual mean for each event metric, we are likely underestimating the temporal trends because of the countervailing effects of short and

long upwelling events. To account for these countervailing effects, we now describe the temporal trends in the intra-annual distribution of upwelling events.

TEMPORAL TRENDS IN THE INTRA-ANNUAL DISTRIBUTION OF UPWELLING EVENTS

Mean magnitude of upwelling events

Intermediate to high quantiles of the intra-annual distribution of upwelling event mean magnitude undergo significant increases over time at 45°N, 42°N, 36°N and 33°N but not at 39°N (Fig. E5). The slopes of the quantiles typically exhibit a modal shape, indicating that intermediate quantiles of event mean magnitude are increasing at a faster rate than lower and higher quantiles (Fig. E5). At the southernmost latitude, the highest quantiles exhibit a negative slope, indicating that upwelling events of extremely high mean magnitude are decreasing over time (Fig. E5). Overall, the intra-annual distribution of upwelling event mean magnitude is shifting towards higher values over time and becoming increasingly dominated by events of intermediate to strong magnitudes.

Total magnitude of upwelling events

The slopes of the quantiles of the intra-annual distribution of upwelling event total magnitude tend to exhibit a modal shape at all latitudes, with intermediate quantiles having greater rates of increase over time than extreme quantiles (Fig. E6). Only low and intermediate quantiles at 45°N and 39°N, respectively, increase significantly over time (Fig. E6). At the other latitudes, most intermediate to high quantiles of upwelling event total magnitude undergo significant increases over time. At the northernmost latitude, the highest quantile exhibits a negative slope, indicating that upwelling events of extremely high total magnitude are decreasing over time (Fig. E6). Overall, the intra-annual distribution of upwelling event total magnitude is shifting towards higher values over time, with intermediate upwelling event magnitudes becoming increasingly dominant at most latitudes.

The results presented in this appendix demonstrate that the annual mean magnitude and total magnitude of upwelling events are increasing over time and that their

intra-annual distribution is shifting towards higher values. This indicates that upwelling is becoming increasingly dominated by stronger events over time.

Figure E1 The effect of varying the minimum duration used to define an upwelling event on temporal trends in the number of upwelling events from 1967 to 2010 at five latitudes across the California Current System. At each of the five latitudes and for each minimum duration, the number of upwelling events was related to the year via simple linear regression ($y = \beta_0 + \beta_1 x$), yielding a coefficient of determination (R^2 , left column) and a slope (β_1 , right column). Full circles indicate regressions whose p-value < 0.05.

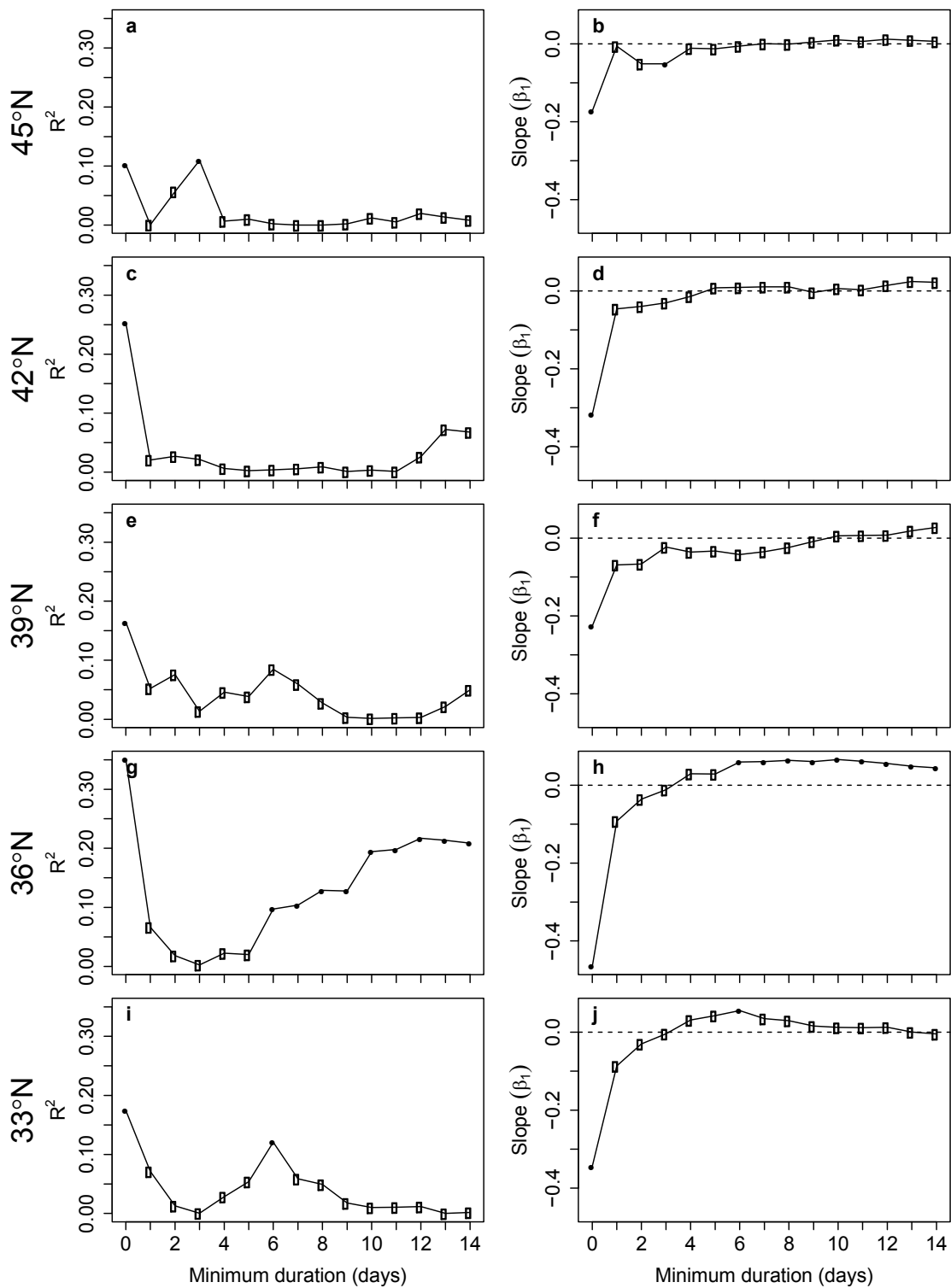
**Figure E1**

Figure E2 The effect of varying the minimum duration used to define an upwelling event on temporal trends in the mean duration of upwelling events ($\log_{10}+1$ transformed) from 1967 to 2010 at five latitudes across the California Current System. At each of the five latitudes and for each minimum duration, the mean duration of upwelling was related to the year via simple linear regression ($y = \beta_0 + \beta_1 x$), yielding a coefficient of determination (R^2 , left column) and a slope (β_1 , right column). Full circles indicate regressions whose p-value < 0.05.

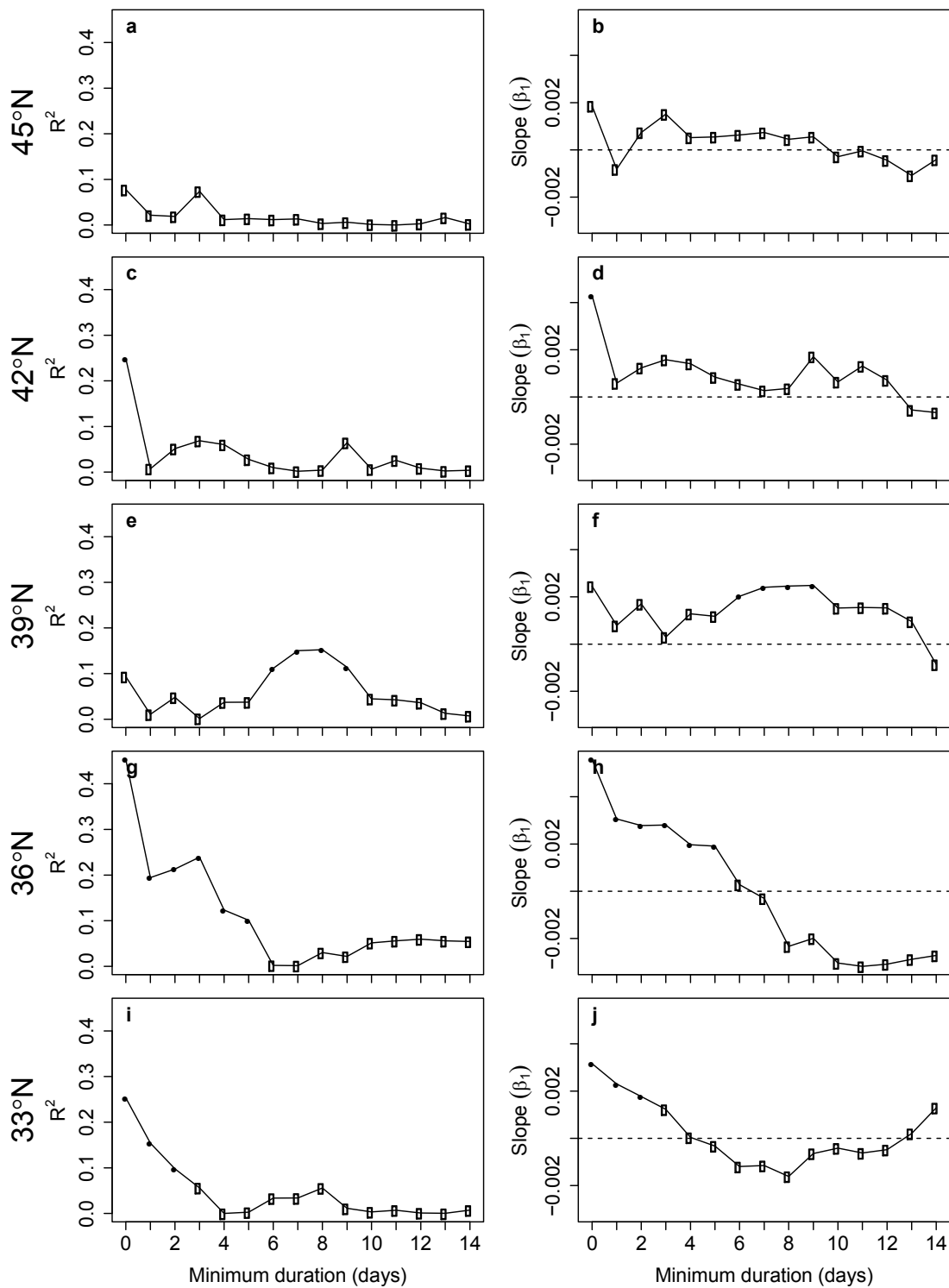
**Figure E2**

Figure E3 The effect of varying the minimum duration used to define an upwelling event on temporal trends in the mean magnitude of upwelling from 1967 to 2010 ($\log_{10}+1$ transformed) at five latitudes across the California Current System. At each of the five latitudes and for each minimum duration, the mean upwelling magnitude was related to the year via simple linear regression ($y = \beta_0 + \beta_1 x$), yielding a coefficient of determination (R^2 , left column) and a slope (β_1 , right column). Full circles indicate regressions whose p-value < 0.05.

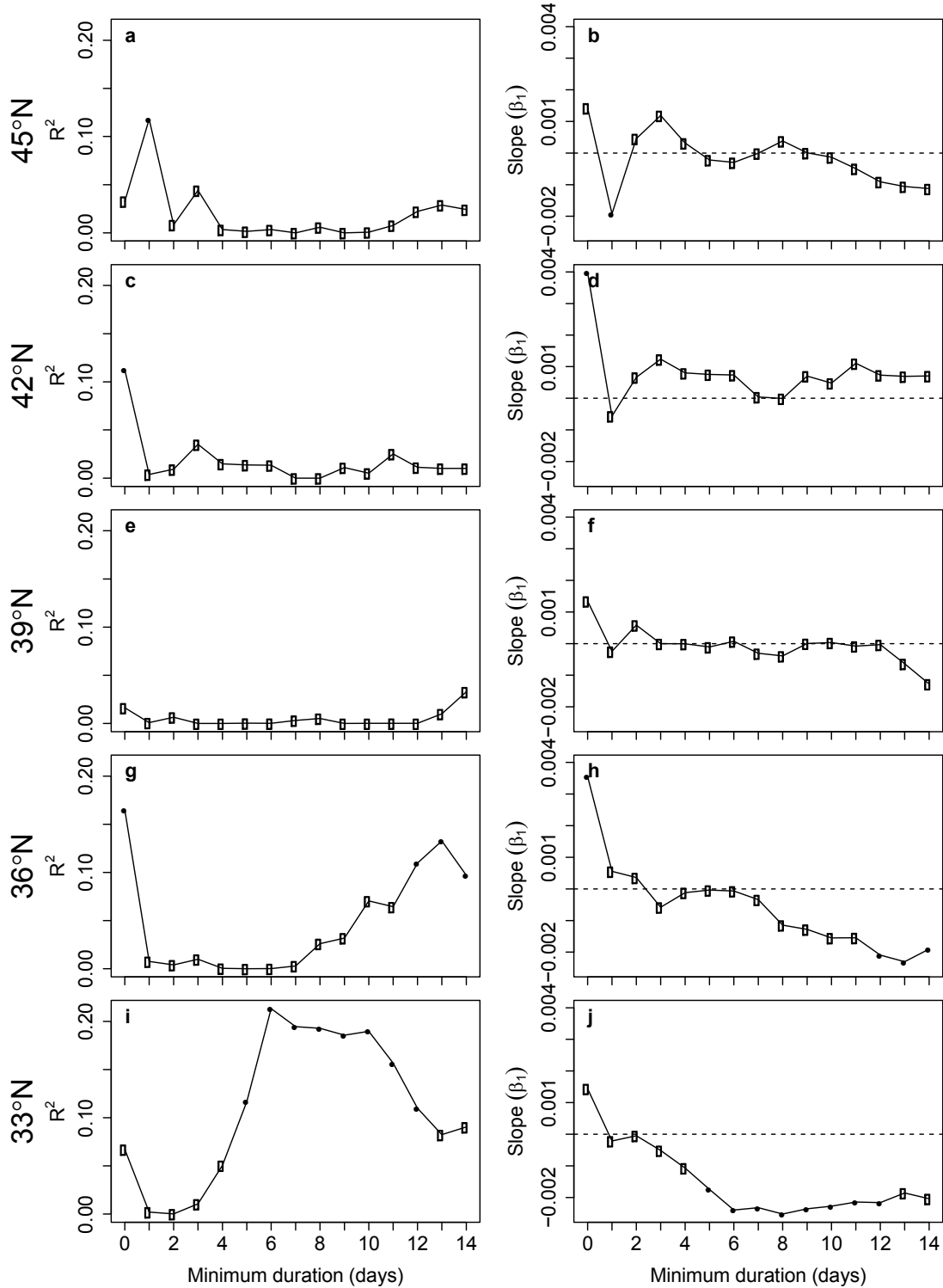
**Figure E3**

Figure E4 The effect of varying the minimum duration used to define an upwelling event on temporal trends in the total magnitude of upwelling events ($\log_{10}+1$ transformed) from 1967 to 2010 at five latitudes across the California Current System. At each of the five latitudes and for each minimum duration, the total upwelling magnitude was related to the year via simple linear regression ($y = \beta_0 + \beta_1 x$), yielding a coefficient of determination (R^2 , left column) and a slope (β_1 , right column). Full circles indicate regressions whose p-value < 0.05.

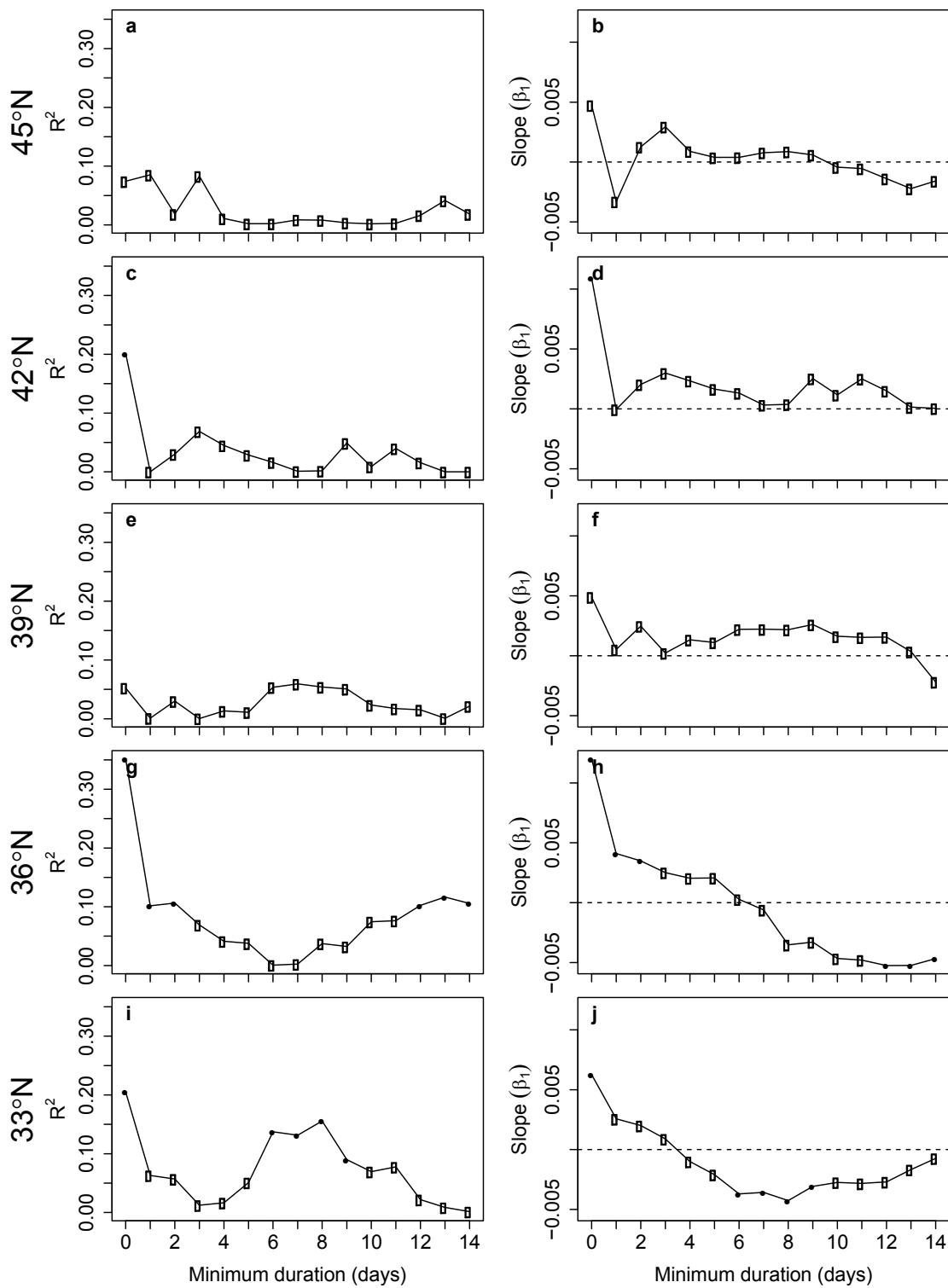
**Figure E4**

Figure E5 Regression statistics of temporal trends in the intra-annual distribution of upwelling event mean magnitude ($\log_{10}+1$ transformed) from 1967 to 2010 at five latitudes across the California Current System. Within each year, we identified the different quantiles of upwelling event mean magnitude and related them to the year via simple linear regression ($y = \beta_0 + \beta_1 x$), yielding a coefficient of determination (R^2 , left column) and a slope (β_1 , right column). Full circles dots indicate regressions whose p-value < 0.05.

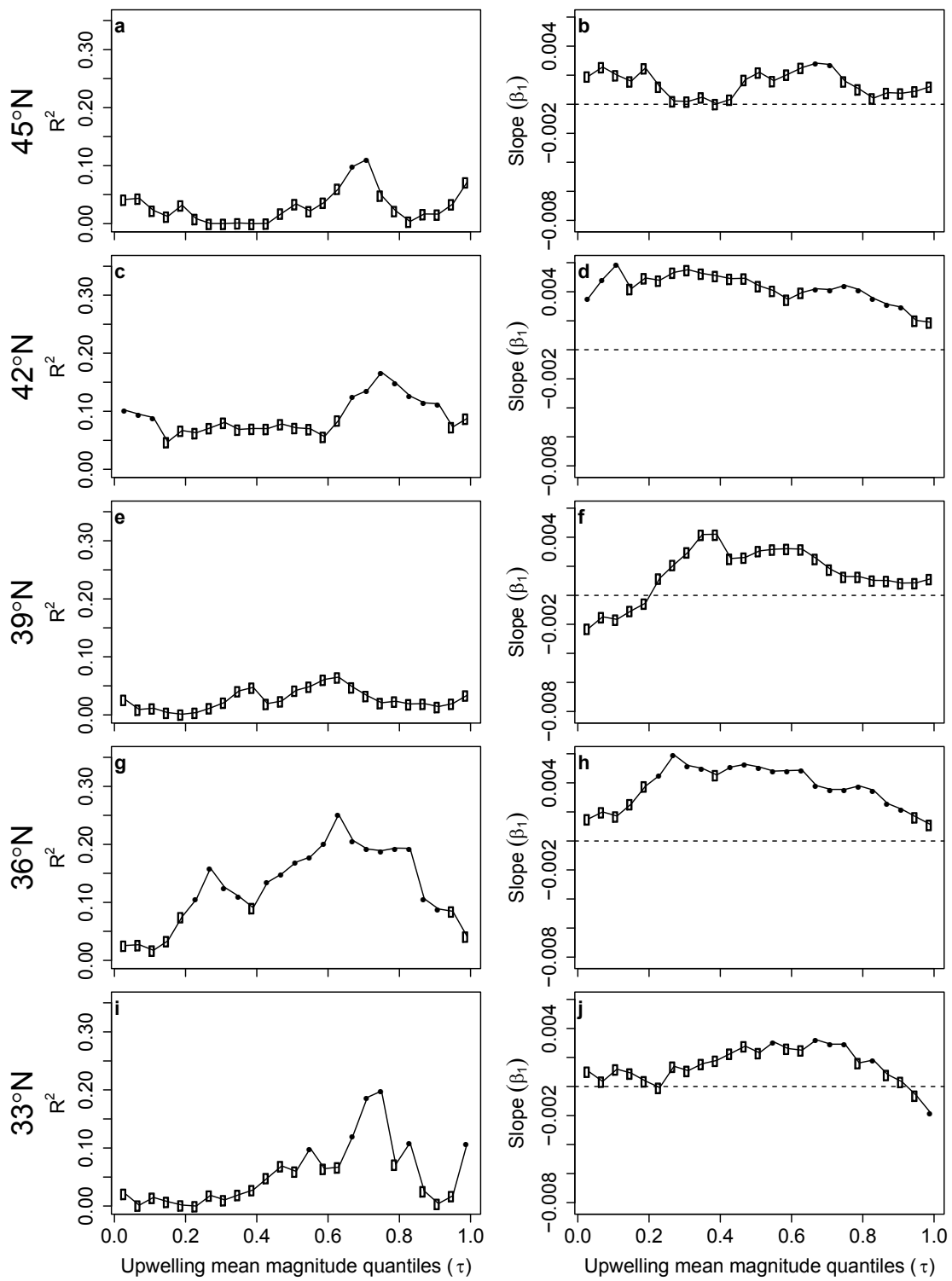
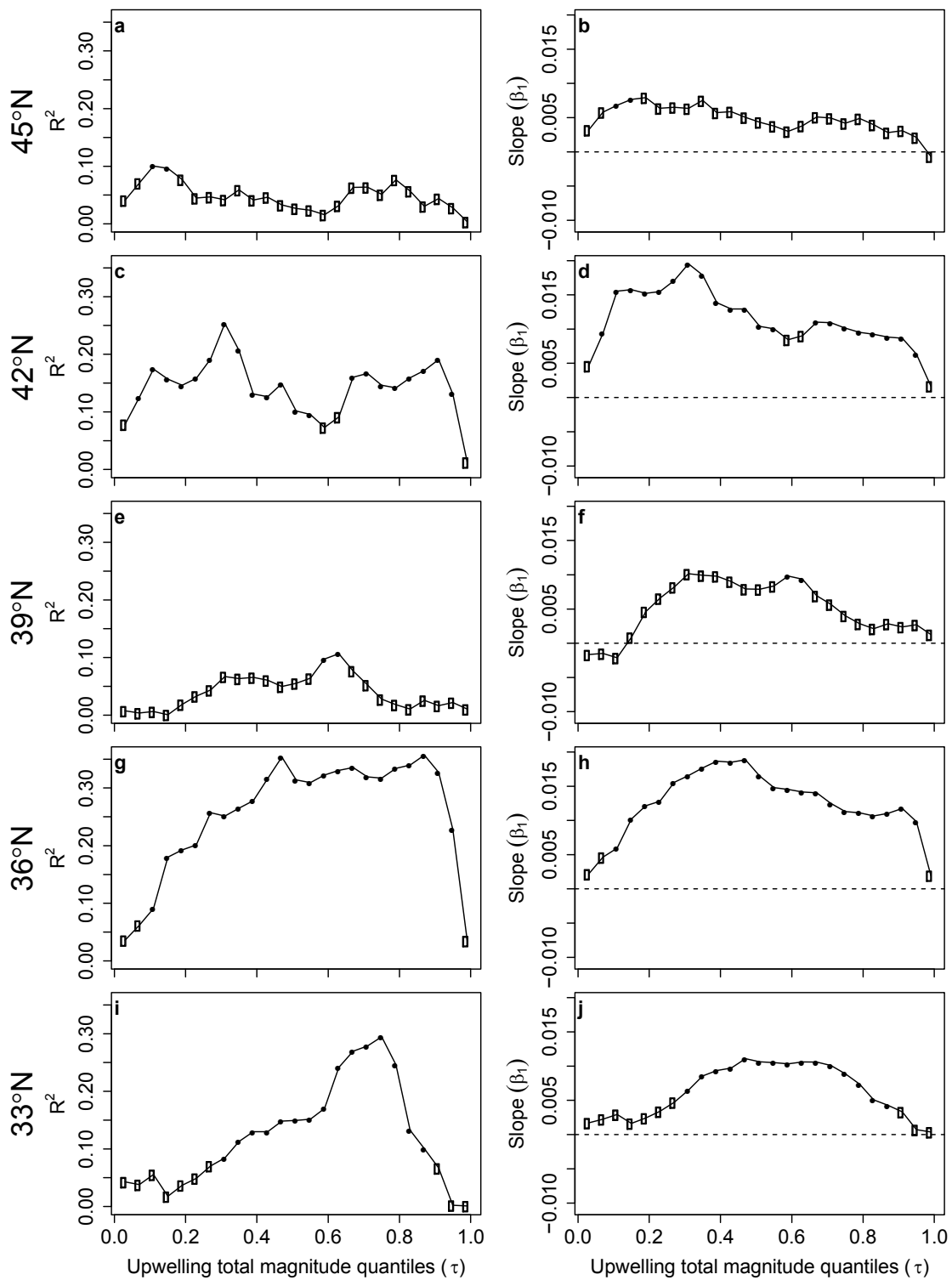
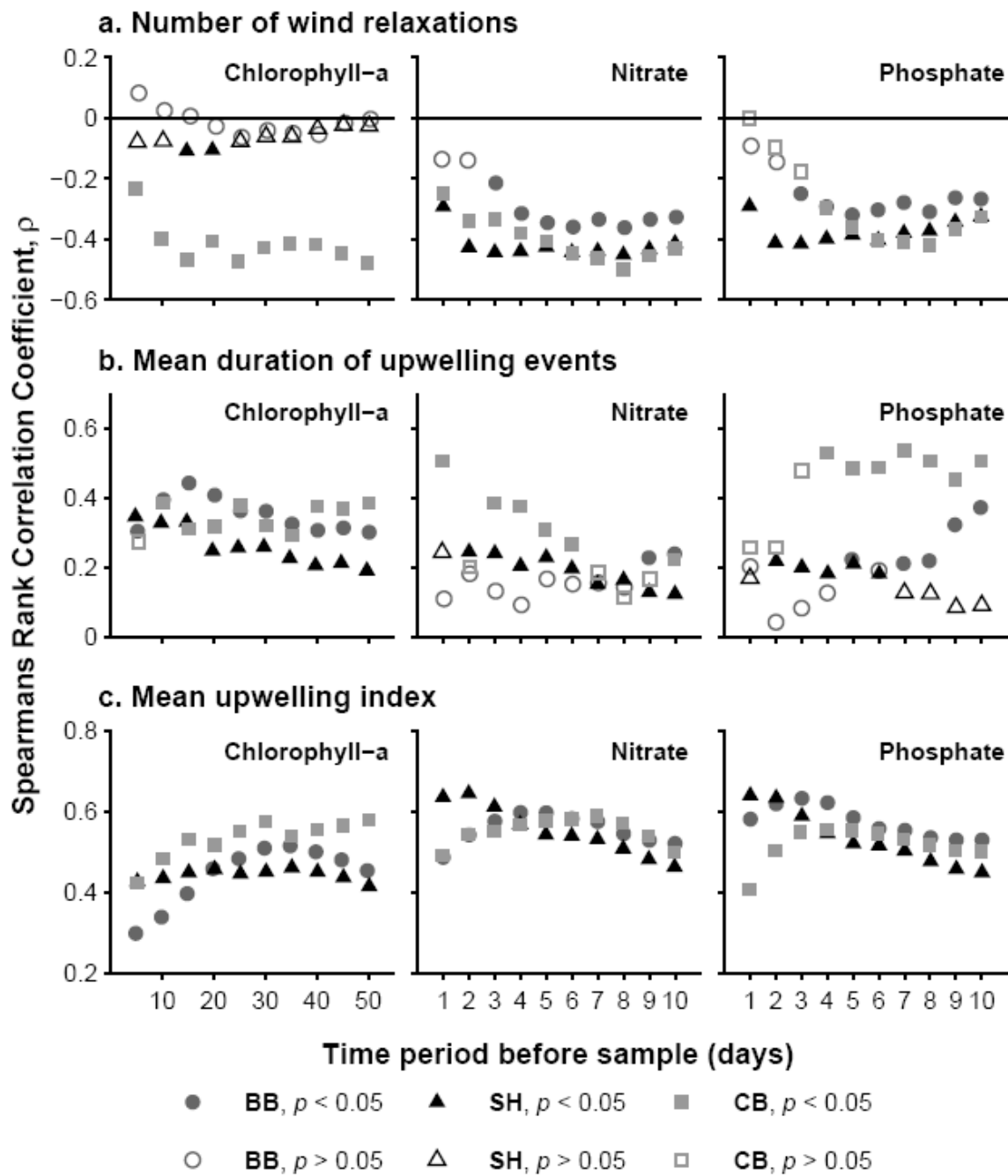
**Figure E5**

Figure E6 Regression statistics of temporal trends in the intra-annual distribution of upwelling event total magnitude ($\log_{10}+1$ transformed) from 1967 to 2010 at five latitudes across the California Current System. Within each year, we identified the different quantiles of upwelling event total magnitude and related them to the year via simple linear regression ($y = \beta_0 + \beta_1 x$), yielding a coefficient of determination (R^2 , left column) and a slope (β_1 , right column). Full circles indicate regressions whose p-value < 0.05.

**Figure E6**

Appendix F – Chlorophyll-a and nutrient analysis

Figure F1 The association between upwelling event frequency and duration of local chlorophyll-a and nutrient levels. Plotted are the coefficients of the Spearman's rank correlations between chlorophyll-a, nitrate, and phosphate concentrations and a) the number of upwelling events occurring during a certain number of days prior to each sample, b) the mean duration of those upwelling events, and c) the mean upwelling index over those days. For nutrients we examined upwelling event conditions from 1 to 10 days prior to the sample and from 5 to 50 days for chlorophyll-a. Results are plotted with dark grey circles for Boiler Bay, BB, black triangles for Strawberry Hill, SH, and light grey squares for Cape Blanco, CB. Closed symbols indicate that that relationship is statistically significant at the $\alpha=0.05$ level and open symbols are not statistically significant

**Figure F1**